A STUDY OF MICRO-MECHANICAL PUNCHING FOR THE INTERCONNECTION OF POLYMER MICROFLUIDIC DEVICES

by

Devanda Rex Lek, M.S.

A dissertation submitted to the Graduate Council of
Texas State University in partial fulfillment
of the requirements for the degree of
Doctor of Philosophy
With a Major in
Material Science, Engineering, and Commercialization
December 2018

Committee Members:

Byoung Hee You, Chair

Namwon Kim

Yoo Jae Kim

In-Hyouk Song

Vedaraman Sriraman

FAIR USE AND AUTHOR'S PERMISSION STATEMENT

Fair Use

Duplication Permission

DEDICATION

For:
My mother, Doung Malay Lek, My father, Sineth Lek
My grandmothers, Sokha Oum and Mikeang Vann
My brothers, Sovanarak Lek and Ankhara Lek

ACKNOWLEDGEMENTS

My time at Texas State has given me the opportunity to meet many people who have made a positive impact on my life and my studies. I would like to first acknowledge my advisor Dr. Byoung Hee You. I will always be grateful for the guidance and patience he has given to me. Without those, this work and the growth I have experienced would not have been possible. I would to thank my committee members Dr. In-Hyouk Song, Dr. Namwon Kim, Dr. Yoo Jae Kim, and Dr. Vedaraman Sriraman. Their feedback was greatly appreciated.

I would like to thank the faculty and staff of MSEC and Engineering Technology especially Dr. Jennifer Irvin, Dr. Andy Batey, and Karla Pizana for the support and the assistance they have given me. A special thank you to Dr. Daniel Park, Jason Guy, and Shane Arabie for their fabrication support. I would also acknowledge the Graduate College at Texas State University for partially funding my research via the Doctoral Research Support Fellowship.

I am very appreciative to Joseph Miller, Kaitlyn Solis, Goldi Makija, Dr. Juan Gomez, Sean Moore, Dr. Hyunhwan Kim, Dr. Tugba Yildiz, Dan Hatcher, Jordan Rossi and my MSEC classmates. Their assistance allowed me to accomplish my research, and their friendship made my time here even more special.

Finally, I would like to thank my parents, my brothers, and my friends for the love, support, and encouragement they have provided to me. I will always be grateful, and I look forward to spending more time with them.

TABLE OF CONTENTS

Page

LIST OF TABLES

Table **Page**

LIST OF FIGURES

Figure **Page**

ABSTRACT

The design of a microfluidic device can become encumbered when there is a desire to include multiple functional features. To avoid these complications one alternative is the modular design where independent devices are assembled into a system. To achieve this design structures that interconnect the modules are needed such as a micro- through-hole. Through-holes have been conventionally fabricated at the macroscale with mechanical punching. There has been a significant focus on the micro- mechanically punching of metallic foils and attention to polymeric foils is limited.

In this study the generation of micro-through-holes was investigated with experiments and numerical modeling. The micro- mechanical punching process was integrated with double-sided hot embossing. A pair of mold inserts were designed with features for the fabrication of through-hole, and features for a passive alignment step. Features for mechanical punching were designed to provide five levels of punch to die clearances, and a set of pins with an aspect ratio of 1:1. The mold inserts were applied to fabricate through-holes on a sheet of thermoplastic polymer. The resulting through-holes were characterized to observe the effect of the selected clearances.

The results of the experiments and the simulations showed that clearance has a significant effect on the micro-punching process. As clearance was increased it allowed more substrate material to flow into the die. When more material flowed into the die it would affect the ability to generate a fracture and its propagation through the substrate.

This would have a significant influence on the success of generating a through-hole and its subsequent dimensions and the topography of the sidewalls.

1. INTRODUCTION

1.1 Motivation

Microfluidic systems have multiple functional units to manipulate biological samples and reagents for biochemical analyses. The typical processes include separation, mixing, transporting, and sensing (Liu et al., 2011). For example, a continuous glucose monitor for a diabetic patient would require the extraction of glucose from a volume of blood, mixing the extracted glucose with a reagent, interfacing the mixture with the detection unit (Huang et al., 2010). These separate functional units for a specific analysis technique can be encapsulated into a single chip.

The encapsulated design of a single chip increases the complexity of fabricating analytical instruments. Issues may include incompatibilities between device materials, selecting fabrication processes, and achieving optimal processing conditions. An alternative could be to fabricate each functional unit as a module. A modular design overcomes the limitations of material and incompatibility of fabrication processes since the functional units are fabricated as individual components. This increases the flexibility as a variety of modules are assembled into a fully customized analytical instrument. To achieve a modular design, routes are needed to allow flow of liquids between modules.

Interconnects are structures that provide pathways for in-situ transfer of biological samples and reagents between modules. Common structures for the interconnection of microfluidic devices are micro-channels, micro-through-holes, and capillary tubing. The geometrical form of the interconnections structure will affect the result for the combined modules.

1.1.1 Interconnection of Modular Microfluidic Systems

It is common for a single device or a composition of devices to be fabricated on a single substrate. The complexity of design and fabrication increases when an attempt is made to place multiple device types on a single substrate. This requires that clear relationships between processing units must be defined, and selected fabrication techniques must be suitable to all the features and not cause interferences. To reduce complexity of integrating multiple device onto a single substrate, modularity has been suggested as a solution.

A modular design suggests that instead of integrating multiple devices into one substrate, individual devices on their own substrates can be combined to form a system of devices. To achieve a modular design, the devices must be able to transfer or receive a volume of the fluidic sample. These device modules must be designed with features that provide a path for liquids to move in and out of the the system. For modular devices, a through-hole could be a suitable interconnection structure. This could allow for transfer of volumes of fluids between different planes in an assembly of microdevices.

Yuen (2008) developed a “plug-n-play” modular microfluidic system that could be applied to biological and chemical analyses. Standard functional components such as heaters, valves, pumps, reaction chambers, detection units, and interconnections structures were miniaturized into their own modules. The functional components could be interconnected by microchannels, microgrooves, and ports which were their own individual modules. A custom microfluidic system could be assembled on a mother board. The modules were assembled using adhesives, soldering, and O-rings.

1.1.2 Fabrication of Microfluidic Interconnects

For generating a through-hole conventional material removal, non-conventional material removal and forming processes have been applied. The substrate material often factors into the selection of a processing technique. For example, soft-lithography is suitable for polydimethylsiloxane (PDMS) devices (Bobak et al., 2010; Tahk et al., 2017). Etching, electrical discharge machining, and micro ultrasonic machining are applicable to semiconductor materials and metallic alloys (Reynaerts et al., 1997; Kuppan et al., 2017). For thermoplastic polymers such as polycarbonate (PC) and poly (methyl methacrylate) (PMMA) holes have been added by post process techniques such as mechanical drilling (Horng et al., 2005), fly cutting (Grung, 2007), and laser ablation (Weindhold and Powell, 1996, Wang et al., 2006).

For microfluidic devices made from thermoplastic polymers, the addition of through-holes has been done by a secondary process such as fly cutting or mechanical drilling. It is typical to add a through-hole to a device after the main functional components have been fabricated. Puntambekar and Ahn (2002) used a mechanical drilling process to generate round, microfluidic interconnects on two layers of glass substrate. These trough-holes allowed fluidic samples to be transferred into microchannels that were fabricated by etching. A challenge of this process was to drill the through-hole simultaneously on two overlapped glass substrates while maintaining their alignment. A general issue with post processing is that they may require additional equipment and will inherently increase the cycle times. Post processing also presents a new source of defects that can be introduced to the products. For example, machining induces heat from the friction generated by the

cutting tool. The ability to generate a through-hole in conjunction with other functional features would be beneficial as it would limit the need for post processing.

Mechanical punching is a conventional manufacturing technique that produces through-holes of sheets of material at the macroscale. It has been scaled down to the micro-range however most applications focus of metallic substrates. There has been limited studies where mechanical punching was used on polymeric substrates for microdevices. This offers a significant opportunity to determine the applicability of micro-mechanical punching for the generation of polymer, microfluidic interconnection structures.

1.2 Objectives

1.2.1 Investigation of the Micro-Mechanical Punching for Modular, Polymer Microfluidic Systems

Double-sided hot embossing and mechanical punching have both been used to generate micro-scaled structures. These techniques share some similarities such as tool movement and the need of two complementing tools. Double-sided hot embossing needs two mold inserts and mechanical punching needs a punch and die. Additionally, one tool is driven vertically until the tools interact with each other. Since the tools need to be applied simultaneously their alignment must be managed during or before a processing step. One difference is that in mechanical punching the tool is retracted after a thorough-hole is formed. In double-sided hot embossing the substrate is compressed for a designated period of time. These similarities provide an opportunity for the integration of double-sided hot embossing and a micro-mechanical punching. An objective of this projects was to design two mold inserts for double-sided hot embossing with features for a passive alignment step and for micro-mechanical punching.

A critical factor for successful mechanical punching is the selection of the clearance, which is the distance between the punch and die. Clearance is known to affect the flow of the substrate during a mechanical punching step. It will inherently influence the dimensions and the quality of the profiles and edges of the mechanically punched through-hole. Understanding how clearance will impact the mechanical punching of a polymer substrate is critical. Therefore, a second objective to generate and characterize through-holes that were mechanically punched with different levels clearances.

The ability to characterize the behavior of the substrate during different stages of the mechanical punching process would lead to significant insights, however in-situ observations are limited. This means the behavior of the substrate must be inferred from characterizing samples that have been already fabricated. Computer-aided engineering (CAE) could be a stepping stone to fill this gap by constructing models of the micro-mechanical punching process. The models could consider a multitude of processing, material, and environmental conditions. This could provide understandings between the experimental design and the behavior of the substrate at different stages of the mechanical punching process. The third objective was to develop a numerical model to analyze the behavior of the substrate material during the different phases of the mechanical punching process.

1.3 Outline of the Dissertation

This dissertation will be divided into six chapters. Chapter 2 reviews literature for the investigation. It covers relevant work for fabricating microfluidic interconnections, mechanical punching, alignment processes, and polymer materials. The geometrical form of the mold inserts, the accuracy of alignment for assembly, and the hot embossing

experiments are summarized in Chapter 3. The characteristics of the mechanically punched through-holes will be discussed in Chapter 4. The behavior of the substrate will be discussed in relation to the clearance used to fabricate the through-holes. Chapter 5 will present the setup and results of the numerical analysis. It will also discuss the correlation between the experimental and numerical results. Chapter 6 will conclude the dissertation by summarizing the overall findings and suggest future work for advancement of the study.

2. LITERATURE REVIEW

2.1 Fabrication of Interconnections Structures

2.1.1 Through-holes for Interconnection of Microfluidic Devices

A through-hole is a hole that extends the entire depth of the material, with two opening diameters. The most common application of the through-hole is an inlet or outlet for fluidic samples. If microfluidic devices were stacked, through-holes would allow samples to be transported between different planes as shown in Figure 2.1. The ability to stack a set of microfluidic devices could be a foundation to realizing a modular microfluidic system.

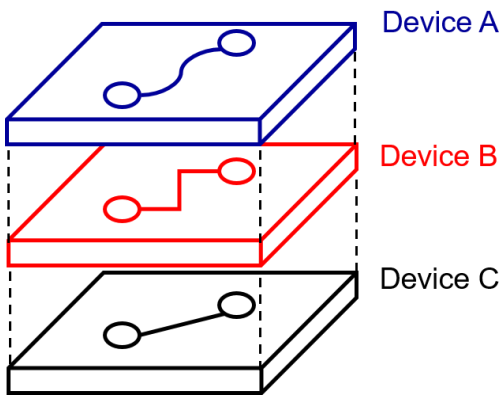

Figure 2.1. Hypothetical modular microfluidic system with three devices in a staked assembly.

2.1.2 Secondary Techniques for Adding Through-Holes

Mechanical drilling is a material removal process where a twist drill bit is used to create round holes. It is a conventional and cost effective fabrication process at both the macro- and microscale and can form a through-hole in one step. Since drill bits are standardized, the diameter of a drilled through-hole may be limited to what is commercially available (Kalpakjian and Schmid, 2014). Another challenge is that friction could heat up chips of thermoplastic polymer, which could reattach to the substrate after cooling (Evonik,

2009). Dimension issues include walking of the drill bit on the penetrating cut and splintering along the radial edges as the drill bit exits the workpiece. Walking will affect location accuracy and splintering will reduce the surface quality of the peripheral area surrounding the through-hole.

A fly cutting tool is used to face a surface with a shallow depth of cut over a broad surface area. It is comparable to a facing cut on a milling machine, but fly cutters will typically have one cutting edge while milling tools generally have two or more cutting edges (Kalpakjian and Schmid, 2014). The limited cutting edges make the fly cutting process a cost effective alternative to milling processes. To apply fly cutting, a blind-hole is fabricated where the tool does not exit the opposite side; creating a hole with only one opening diameter. The opposite diameter is therefore covered by a residual layer of substrate material. A fly cutting tool would be used to remove the remaining residual layer and thereby expose a second opening diameter (Gurung, 2007). Since a broad surface is being removed, a stable base is needed to ensure a planar, uniform surface. Since it is a machining process, heat from friction also needs to be considered for fly cutting applications.

In laser ablation, a target surface is irradiated by a focused laser beam. Energy will be transferred from the laser beam into the substrate material causing it to evaporate or sublimate thus removing material (Weindhold and Powell, 1996; Wang et al., 2006). Lenses are used to focus the laser beam to the desired diameter, and pulses are used to reduce the propagation of the heat affected zone into the surrounding material. The laser source can also be dictated by the substrate material. For example, a CO_2 laser is suitable for plastics, and crystal lasers have been applied to metals and ceramics (Dyer et al., 1997).

These three processes are suitable for fabricating through-holes but are best applied as post processing techniques. They would increase cycle times as devices would have to be transported between different equipment. Drilling or fly cutting are conventional, but heat generation could cause warpage and polymer reflow. Heat propagation can be controlled by a pulsed laser cutter, but it would require a significant investment for equipment. Avoiding the use of a post process would require through-holes to be fabricated in one step and in conjunction with other microstructures.

2.1.3 Single-Step Fabrication of a Through-Hole

Fabricating a through-hole and other micro-structures concurrently would be beneficial for reducing the cycle time. Generally, a pin is forced through the entire depth of the substrate material. This will require the pin to exit the opposite plane of the substrate material. A single-step process must protect the pin as it exits the opposite side. Hot embossing has been applied to generate through-holes in a single step (Zhu and Cui, 2010; Chou et al., 2012; Gomez, 2015). To protect the pin a buffer layer is placed below the substrate layer. As the pin exits the substrate material, the buffer layer will prevent the pin from contacting the metallic heating platens.

Zhu and Cui (2010) and Gomez (2015) used thermoplastics for the substrate material and buffer layer, and Chou et al. (2012) used an elastomer rubber as a buffer layer. The pin is forced into the substrate and it generates a blind-hole with a residual layer. The residual layer was continuously pressed into the buffer layer by the displacement of the pin. This caused indentations to form on and into the surface of the buffer layer. A tough squeeze, and friction between the sidewalls of the pin and indents would excise the residual layer (Zhu and Cui, 2010). Adhesion between the buffer layer and substrate also could have

factored in the formation of a complete through-hole (Zhu and Cui, 2010). When demolded, the substrate layer adhered to the buffer material. The force needed to separate the adhered materials could have been enough to fracture and remove the residual layer. Since a buffer layer is used, the exit side of the polymer cannot be patterned which limits the process to single side devices.

2.2 Mechanical Punching

Mechanical punching is a conventional forming technique where a punch passes through a sheet of material to form a through-hole. The main components are the punch tool, a die, and in some cases a stripper. The punch is the primary tool and will dictate the main diameter of the through-hole. The die is used to receive the punch as it passes through the material and the residual layer as it is separated from the substrate. The size of die is related to the thickness of the material and its opening diameter will have a significant effect on the punching process. The force needed for mechanical punching is estimated by applying equation 2.1, where F is the maximum force, t is the thickness of the material, L is the perimeter, and UTS is the ultimate tensile strength of the substrate material. This equation assumes that the tip of the punch has a flat geometry and does not account for friction which will increase the maximum punching force.

$$F = 0.7tL(UTS) \tag{2.1}$$

2.2.1 The Mechanical Punching Process

Shearing is the underlying phenomenon that allows the mechanical punch to remove material with minimal heat generation and no formation of metal chips (DeGarmo, 2012). The sheet of material will experience shear stress that is localized in between the edges of the punch and die. The mechanical punching process is described in four steps:

impact, penetration, fracture, and stripping as shown in Figure 2.2 (DeGarmo, 2012). During impact, a punch is forced into the top surface of the material. The impacted area will begin to plastically flow around the edges of the die and punching tool. As the punch penetrates further into the material it will flow into the die and a bulge will form on the opposite side. When the applied stress surpasses the materials shear strength, fractures will form adjacent to the punch and die edges will propagate towards each other. If the clearance value is optimal, the fractures will intersect, and the residual layer is removed. The stripping step is when punch is then retracted to eliminate contact with the punched through-hole and residual layer.

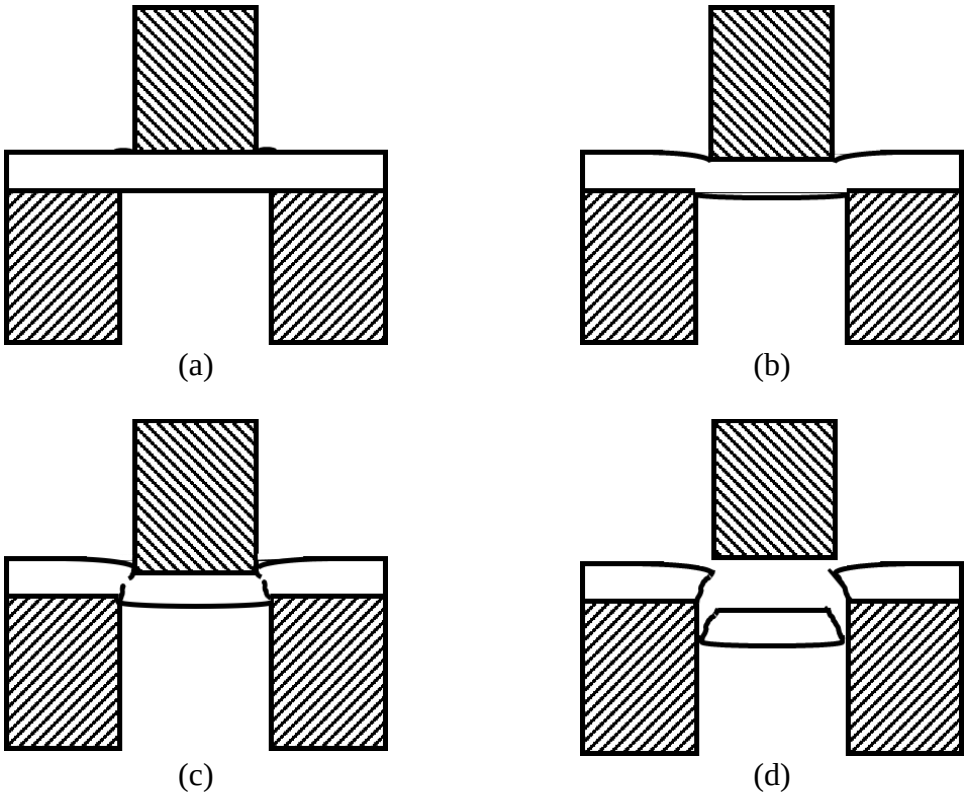

Figure 2.2. Four stages of mechanical punching (a) impact, (b) penetration, (c) fracture, and (d) stripping.

Figure 2.3 illustrates a typical profile of a mechanically punched through-hole and its terminology (Kalpakijan and Schmid, 2014; DeGarmo, 2012). This profile is typical for

holes generated on a metallic substrate at the macroscale. When the punch penetrates the surface, the material will flow with the direction of the punch. This will cause rounding along the top edge of the through-hole, which is referred to as the rollover. The depth and diameter of the rollover can be measured. As the punch progresses, the sidewall of the punch will rub against the sidewall of the through-hole. The friction between the punch and substrate will cause burnishing along the top portion of the sidewall. A fracture will form adjacent to the edge of the punch. This will separate the residual layer from the substrate and form an outward taper on the bottom portion of the through-hole. When material flows into the die causing a raised area surrounding the bottom diameter of the hole. The second fracture will occur adjacent to the edge of die and will from the burrs along the bottom diameter.

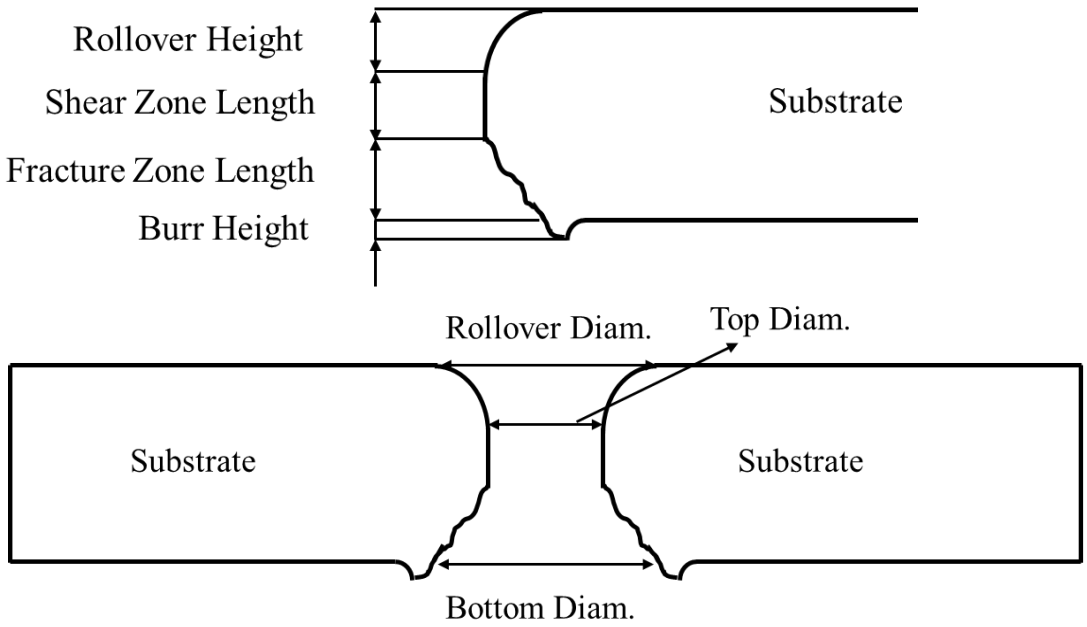

Figure 2.3. Features of a mechanically punched hole (Kalpakijan and Schmid, 2014; DeGarmo, 2012).

2.2.2 Punch-to-Die Clearances

Clearance is the distance between the sidewall of a punch and the sidewall of a die. It is a critical factor for mechanical punching. Selecting a proper clearance is known to have a significant effect on dimensional accuracy, profile characteristics, and tool life (Kalpakijan and Schmid, 2014). Normalized clearances are calculated by equation (2.1), where D_d is the diameter of die, D_p is the diameter of the punch, and t is the thickness of the substrate. The optimal clearance for sheet metals will range from 2-10% of the sheets thickness (Chern et al., 2006; Xu et al., 2012). Deviating from this range is known to reduce the quality of the part or tools.

$$\boldsymbol{C}\% = \left(\frac{\boldsymbol{D_d - D_p}}{\boldsymbol{2t}}\right) \times \mathbf{100} \tag{2.2}$$

Proper selection of clearance is important to achieve optimal part quality and tool life. In mechanical punching one common problem is the flow of material into the die, which is caused by displacement of the tool. When the size of the clearance is increased it will cause more issues as more material to flow into the die. As both fractures initiate and propagate, it will be more difficult for the cracks to converge. The residual layer is only removed if one fracture intersects the other fracture line, as opposed to if the fracture lines were to meet. This will reduce the quality of the profiles and edges of the sidewall. If the selected clearance is too small, it can also reduce tool life and require more accurate alignment (Spence-Parson, 2006).

2.2.3 Prior Work and Need for Micro-Mechanical Punching

Table 2.1 summarizes substrate materials, tool materials, hole sizes, and clearances of a set of studies on micro-mechanical punching. At the macro-scale mechanical punching

is often associated and applied to sheet metals (DeGarmo, 2012). When scaling down to the micro-range, studies also focus on metallic foils such as Copper (Cu), Titanium (Ti), Brass, and types of steels (Rhim et al. 2005; Joo et al., 2005; Chern et al., 2006; Yi et al., 2006). Studies on non-metallic substrates were varied Wang et al. (2006) examined ceramics; and Werner (2005), Mazzeo et al. (2007) and Petersen et al. (2015) studied with a polymer. Tungsten (W) or a tungsten alloy was often selected as the material for the punch tool (Joo et al., 2005; Chern et al., 2006; Xu et al., 2012; Petersen, 2015), steel was second common selection (Wang, 2006; Chern et al., 2006), aluminum has been used (Mazzeo et al., 2007) and non-metallic was least common (Rhim et al., 2005). Tungsten as a base material is quite popular for a tool due to its inherent high hardness. However, fabricating a tool from tungsten can be challenging as it requires special tools such as a diamond grinder (Joo et al., 2001) or non-conventional machining processes such as electrical discharge machining (EDM) (Yi et al., 2006; Petersen et al., 2015). The reported clearance values typically ranged from 2.5 to 15% of the thickness of the substrate (C%) (equation 2.1). The clearance of 2.5 to 15% is optimal for sheet metals at the macroscale and was transitioned to the microscale by the investigators.

Table 2.1. Summary of references for micro-mechanical punching.

Authors	Substrates	Tool	Hole Sizes	Clearances
Rhim (’01; ‘05)	Copper, Titanium	Silicon-Polymer	2-15 µm	N/A
Joo (’01;’05)	Brass, Stainless Steel	Tungsten Carbide	25 – 100 µm	5 C%
Werner (’05)	TOPAS®	Steel	200 µm	N/A
Chern (’06)	Brass, Stainless Steel	Tungsten, Steel	200 µm	5, 10, 15 C%
Wang (’06)	Ceramic	Steel	50 - 100 µm	N/A
Yi (’06)	Brass, Stainless Steel	Tungsten Carbide	15 µm	N/A
Mazzeo (’07)	PMMA	Aluminum	0.5 to 2 mm	3 – 25 µm
Xu (’12)	Brass	Tungsten Carbide	150-600 µm	2.5, 15 C%
Petersen (’15)	PLLA	Tungsten Carbide	350 µm	N/A

Edge quality was also a topic for discussion, particularly its relationship to clearance or the ratio of the hole diameter to the thickness of the target foil. When the clearance or the ratio was increased, defects such as burr height and the dimensions of the rollover increased (Joo et al., 2001; Chern et al., 2006; Wang et al., 2006; Xu et al., 2013). One challenge that was discussed by some of the investigators was the generation on an incomplete through-hole. In this scenario the residual layer was still attached to the bottom diameter.

Rhim et al. (2001; 2005) studied the micro-punching of an array of micro-holes with the diameters ranging from 2 to 15 μm on foils of copper and titanium alloy. After processing, the investigators observed that some of the residual layers were still attached to the bottom diameters of the through-holes. The residual layers were removed with a chemical etching process. Wang et al. (2006) also mentioned that residual layers were present on ceramics, incomplete holes but did not discuss any secondary processing to remove them. Werner (2005) discussed three options that could be applied. The options were vacuum pressure, a burst of gas, or a secondary pin to remove attached residual layers.

Mazzeo et al (2005) and Petersen et al. (2015) studied punching on a polymer substrtate. The feasibility of punching in a PMMA foil was established. The underlying phenomenon to cause a fracture was hypothesized to be tensile yielding (Rossen, 2008). Petersen et al. (2015) used a circular tool for a mechanical blanking of a Poly (l-lactic acid) (PLLA) structure. Mechanical blanking is analogous mechanical punching where the key difference is the residual layer is the desired part. In this study, a micro-container was fabricated from a hot embossing process on Poly (l-lactic acid) (PLLA) and the punching tool was used to separate the micro-container from the parent substrate.

Mechanical punching could be an effective technology to form through-holes on a polymer microfluidic device. Since it is a forming process it could be integrated with the various molding processes such as double-sided hot-embossing. The integration of mechanical punching with the double-sided hot embossing process could allow for the simultaneous formation of functional and interconnection structures. The design of a micro-mechanical punching tool can have some challenges. Since punching requires the pin to exit the opposite side, alignment is needed to prevent undesired contact with the die. Additionally, alignment is needed to help maintain the clearance between the punch and die.

2.2.4 Numerical Modeling the Mechanical Punching Process

Mechanical punching has been used to generate a complete, round through-hole on metallic substrates. Many numerical studies have been used to observe the behavior of metallic substrates during the punching process at macroscale. Emphasis is placed on the selection and optimization of the clearance dimension (Faura et al., 1998; Subramonian et al., 2013; Achouri et al., 2014).

Faura et al. (2007) used ANSYS to study the macro-mechanical punching of a sheet of AISI 304 steel. The simulation results were correlated to experimental results. The modeled clearances had a range of 5 to 17% of the sheet metals' thickness. The effect of clearance was analyzed by measuring the angle at which the fracture propagated and ultimately converged with the fracture generated by the punch. It was determined that a clearance that was 11 to 12% of the sheets thickness allowed the fracture lines to intersect properly. When the clearance was increased, the punch needed to displace over a larger distance before a fracture could be generated.

Subramonian et al. (2013) studied the effect on clearance or non-symmetrical punching of DP590 and the life of the tools. DEFORM 2D/3D was used to predict the effects of clearance and tool geometry. When clearance was increased the substrate tended to bend around the corner of the die. This action caused an increase in the height and diameter of the rollover. Although, lower clearance values improved part quality it was detrimental to the tools. As clearance was reduced it increased contact stress at the interface of the punch and substrate. This caused tools wear and eventually fail at a higher rate.

Achouri et al. (2014) correlated experimental and numerical punching of a high-strength low-alloy steel with respect to clearance. The punch tools had diameters that ranged from 38 to 40 mm and the clearances ranged from 7 to 31% of the sheet metal thickness. The process was modeled with ABAQUS/Explicit with an axisymmetric boundary. As clearance increased it was found to have three significant effects on the mechanical punching process. When it was increased the penetration need to initiate fracture also increased. The height and diameter of rollover were positively related to the increase in clearances. The length of the shear zone decreased, and the length of the fracture zone increased as clearances were increased. When clearance was sufficient, the model predicted a fracture would be generated by the punch and the die. These fractures would propagate into the thickness of the substrate and intersect. Once the fracture intersected the residual layer was separated from the substrate.

2.3 Alignment Techniques for Forming Processes

2.3.1 Iterative and Optical Alignment

Two common methods for aligning a pair of mold inserts for a double-sided hot embossing process are the iterative technique and optical technique. In both techniques the

location of one mold insert is fixed and the location of the secondary mold insert is adjustable. Typically, the secondary mold insert can be held on a sliding stage that can translate horizontally and rotate. By adjusting the location of the secondary mold insert, the amount of mismatch between the mold inserts can be reduced. The necessary adjustments can be inferred from previously obtained data, or the reduction of mismatch can be observed in real-time.

An iterative technique will require the fabrication of a preliminary samples with the two mold inserts in an initial position (Joo et al., 2001). The sample is then characterized to determine the misalignment between complementing features. If it is significant, the misalignment data is used to adjust the location and orientation of the secondary mold insert. A secondary sample is then molded and characterized to determine if mismatch was reduced. This process of molding, characterizing, and adjusting must be repeated until an acceptable level of mismatch is obtained. A disadvantage of this type of approach is that it will consume additional resources and increase wear on the mold inserts.

The second option is the inclusion of an optical feedback system wherein real-time images of the mold inserts can be observed. Each mold insert will have an alignment feature with a nominal dimension separating them. The location of one mold insert is adjusted and mismatch is analyzed by observing the distance between the alignment features. Adjustments can be halted once a tolerable amount of mismatch is obtained. This could reduce the excessive processing cycles and material consumption that are present in iterative alignment. Developing or obtaining an optical system can require a significant investment and become very complex. In a thermal press, high temperatures, clamping

forces, and machine elements can limit the addition of optical components or degrade their performance over time (Islam et al., 2002).

Joo et al. (2001) reported a combination of the iterative and optical alignment processes for the micro-mechanical punching of metallic foils. Image processing used a least-squares method to calculate the location of the desired die. The location of the mechanical punch was defined by indenting a sacrificial metallic foil. After that, the location of the die was adjusted until mismatch between its geometrical center and the indentation on the foil was reduced. The alignment process could be repeated as necessary. Yi et al. (2005) also used a combination of active and iterative alignment, where the die was held on an X-Y stepper. The movement of the X-Y stepper was observed with a two-way imaging optical system.

Islam et al. (2002) actively aligned a hot embossing process by integrating microscopes onto the backside of a thermal press. Alignment marks were included on the master pattern and the target substrate material. The master pattern was fixed but the target substrate was on a sliding stage. The location of the stage was adjusted and mismatch between corresponding alignment marks was observed and reduced.

2.3.2 Passive Alignment

Mechanical joints can be used to control the relative location of components as they are coupled. This can simplify the alignment process since there is no need for iterative steps or optical components. Key factors for accurate alignment include selection of joint geometries, dimensional accuracy of joints, and the number of joints applied (Slocum, 2010; Trinkle and Lee, 2011). Since adjustments are not possible, dimensional inaccuracies will stack up and affect the relative locations as bodies are assembled. The number of joints

used, and their respective geometry are important, as motion between assembled components must be constrained. An insufficient number of joints and improper geometry selection could allow for infinitesimal motions or make the assembly of joints difficult.

2.3.3 Applications of Passive Alignment

Werner (2005) and Mazzeo et al. (2007) aligned two mold inserts for the fabrication of through-holes on a thermoplastic polymer. Punches and dies were integrated on the two mold inserts and which were applied to a double-sided hot embossing process. Alignment was completed with a set of dowel pins and guide holes on the mold inserts. As the mold insert displaced it was guided by the dowel pins until it contacted the substrate material. The accuracy of alignment is significantly dependent on the dimensional and location integrity of the features for alignment and the features for punching.

One technology for passive alignment is the kinematic coupling (Slocum et al. 2010; Trinkle and Lee, 2011). A kinematic couple is a specially designed mechanical joint that controls the relative locations of parts by establishing redundant points of contacts. A unique characteristic is that kinematic couples are designed to provide an exact constraint design. An exact constraint is when all six degrees of freedom of one rigid body are constrained. This means that it cannot translate or rotate with respect to reference coordinate system.

Slocum et al. (1997) used v-grooves and spheres to align sand mold cores for a casting process. Three v-grooves are placed on the mating surfaces of the molds that will be subsequently assembled. Spherical elements are placed inside one of the sets of v-grooves. The second mold is coupled to the spherical elements by their respective v-grooves. A clamping force is applied causing indentations in the v-grooves of the molding

core which allows the cores to come into contact. The v-grooves will provide exact constraint design and prevent horizontal translations thereby precisely controlling their relative locations.

Trinkle and Lee (2011) used kinematic couplings for align a micro-contact printing for micro-scale and biochemical patterning on substrates. The substrate plate was fitting with the Kelvin Coupling elements and the stamping plate was fitted with the three spherical elements. Master stamps could be interchanged, and precise multi-layered patterns could be generated with submicron accuracy. Misalignment increased when the stamping pressure caused the Kelvin Couple to disassemble.

2.3.4 Need of Passive Alignment in Double-Sided Molding

In double-sided forming processes alignment is critical for successful for processing. Mismatch between to complementing mold masters could lead to mis-located functional features. For a mechanical punching process misalignment could lead to inconsistent clearances and unintended contact between punch and a die. A hinderance to active processes could the complexities present at the design and application level. For example, Joo et al. (2001) had to use iterations of image processing and adjustments to align a punch and die. Wang et al. (2006) needed special tools for installation and assumed alignment was reasonable. Passive alignment can avoid the complications be removing the need for feedback and adjustments therefore simplifying the alignment process. Mechanical joints can be designed so that as they are coupled, they can control their relative locations.

2.4 Hot Embossing of Microfluidic Devices

2.4.1 The Hot Embossing Processes

Hot Embossing is suitable technology for thermoforming polymer micro-structures. Characteristics include: low cycle times, flexibility of mold exchange, and medium volume production (Peng et al, 2013), The process can be described in three primary steps: molding, cooling, and demolding as shown in Figure 2.4 (Pan et al., 2008).

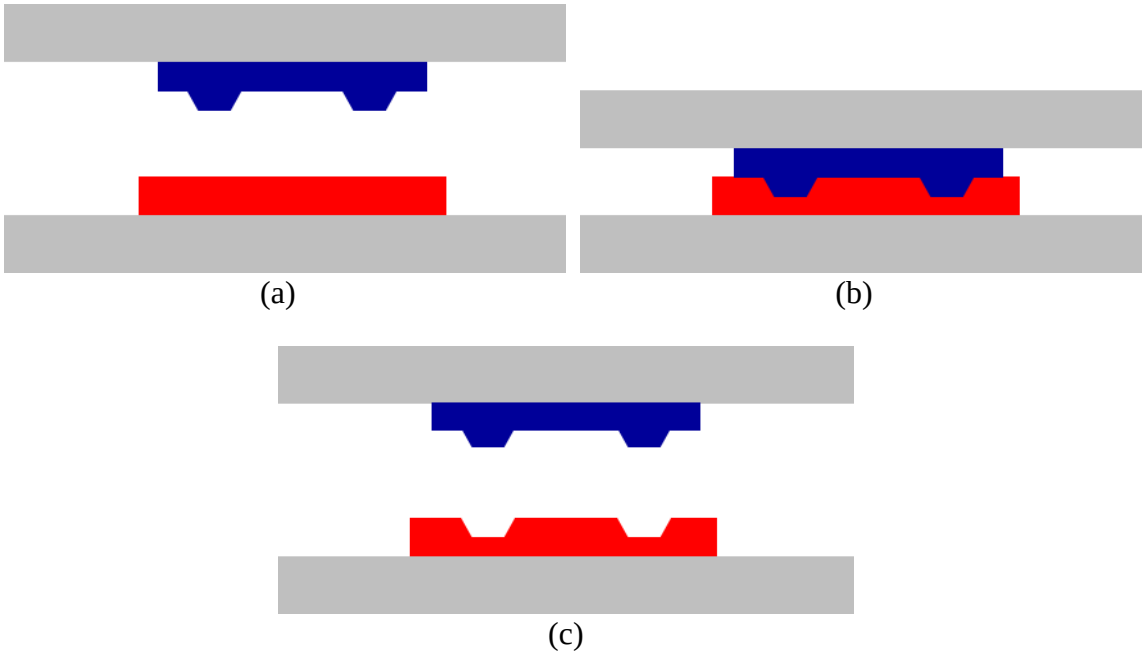

Figure 2.4. Stages of the hot embossing process (a) heating, (b) holding and cooling, and (c) demolding.

In the molding step the substrate material will be compressed by the master mold(s), both of which are heated to a specific temperature. The compression force is held on the substrate for a designated period. Adequate holding time will allow the viscous polymer to flow into the molds (Fig. 2.4(a)), allowing for transfer of geometry and dimensions. The substrate and mold inserts must be cooled while compression force is maintained. Force is maintained during cooling to prevent polymer reflow which could lead to loss of shapes.

Cooling the substrate will transition the substrate from a viscous state to a rigid-glasslike state and freeze the transferred geometries. The last step is the demolding step where the substrate is separated (Fig. 2.4(c)) from the mold inserts. Demolding is a critical steps as additional defects can be formed as the substrate is pulled away from the mold insert.

2.4.2 Thermoplastics Polymers

Thermoplastic are a common selection for thermoforming processes for microfluidic devices. At an ambient temperature a thermoplastic can often be observed as a solid-state material that is rigid and can be brittle. The mechanical properties of thermoplastic are sensitive to elevations in temperatures. Typically, as temperature increases the secondary bonds within the polymer will become weaker. The weaker bonds will cause the polymer to become more malleable and susceptible to localized forces. In this state, some thermoplastics can be thermoformed by injection molding or hot embossing. When the thermoplastic is cooled, the polymer will become rigid again and regain it hardness and strength.

For many thermoplastics, the glass transition temperature (T_g) will serve as a reference temperature for thermoforming processes. It is the temperature at which the polymer will transition between a glassy to a rubbery state and will between different types. For example, the T_g of polyester, polyethylene, and polycarbonate are 73, -125 and 150 °C, respectively (Polymer Database ®, 2018). When T_g is surpassed, the polymer will soften and progressively become for rubbery. Its viscosity will decrease, and it will become a vicious fluid. If pressure is sufficient, the viscous fluid will flow into mold master; transferring geometries and locations. The polymer is then solidified by cooling it to a

temperature below its T_g. This cycle can be repeated indefinitely but thermoplastics will degrade and age after multiple thermal cycles (Mohammadi et al., 2017).

2.4.3 Poly (methyl methacrylate)

Poly (methyl methacrylate) (PMMA) is a thermoplastic polymer that has been used as a substrate for microfluidic devices (Mathur et al., 2009; Chen et al., 2016). The mechanical properties of PMMA are summarized in Table 3.1. At room temperature, it is transparent and rigid allowing to be a substitute for silicate glass. Its transparency and low water absorption ratio (2%) make a suitable selection for microfluidic devices and biomedical prosthesis. At room temperature, PMMA has a density of 1.15 g/cm^3, a Rockwell hardness range of 63-97, Young's modulus of 3100 MPa, and a Poisson ratio of 0.40 (Kiew et al., 2009, Polymer Databases, 2018)

Table 2.2. Thermal and mechanical properties of PMMA at ambient temperature

Mechanical Properties	**Value**
Density	1.19 g/cm^3
Water Absorption	2%
Rockwall Hardness	63-97
Tensile Strength (Ultimate)	79 MPa
Young's Modulus	3100 MPa
Poisson's Ratio	0.4

PMMA can be machined by conventional or micro- machine tools such as a milling machine. However, the heat from friction can distort the workpieces and cause chips of plastic to attach to the workpiece or cutting tool (Evonik, 2009). It is brittle at room temperature and a forming process would cause the material to fracture. To avoid this, PMMA is generally formed at elevated temperatures As PMMA is heated its mechanical properties such as elastic modulus, yield stress, and ultimate tensile strength will

significantly change (Juang et al., 2002, Mohammadi et al., 2017). When above 105 °C PMMA will begin to transition from a rigid solid to a viscoelastic state.

2.4.4 Modeling of the Hot Embossing Process

Process parameter such as molding temperature and force are known to have a significant effect on the quality of replicated structures (He et al., 2008). Physical experiments of different combinations of process parameters can require extensive experiments. Numerical simulation is particularly useful for predicting the behaviors of different material during a multitude of fabrication processes. Applying numerical modeling would reduce the amount of experiments needed and allow for the selection of optimal process parameters. The behavior of PMMA during a micro-hot embossing step has been previously studied (Juang et al., 2002; Kiew et al., 2009; Gomez, 2015).

Juang et al. (2008) and Kiew et al. (2009) examined the change in physical behavior of PMMA under elevated temperatures. Theses experimental results used to define to the numerical behavior of PMMA. The relationship between the temperature and the elastic-plastic behavior of PMMA is not linear. Juang et al. (2002) defined the behavior from 25 to 105 °C. Kiew et al., (2009) defined the defined behavior from 5 to 120 °C, at 120 °C the polymer was in a semi-molten state. The heated polymer flowed along the geometry of the numerical die and filled the cavities. In both studies, the physical experiments had incomplete cavity filling and entrapped air was assumed to be the cause. When conditions were non-isothermal a weld line as heated polymer flowed back and hit cooler polymer (Juang et al., 2002).

Gomez (2015) numerically modeled the hot embossing and indentation process for fabricating interconnections structure on a PMMA layer. A model was developed for each

step of the process: molding, cooling, and demolding. For the mold step, Gomez determined that the success of generating a through-hole was dependent on the optimal selection of the molding temperature and the molding forces. Temperature affected the flow front of the viscous PMMA and allowed the pin to travel through the length. Complete through-holes were only predicted at temperature of 125 and 150 °C. During cooling it was predicted that the shrinkage of the PMMA generated stress on the brass pin which could lead to damage.

2.5 Conclusions

Interconnection structures are needed for a modular system of devices to be realized. Round microfluidic through-holes are suitable for bridging the gap between modules and allow plane to plane transfer. They can be included by a post process but would require extra equipment and increase cycle times. Mechanical punching is conventional method to producing a through-hole and is typical for sheet metal. Work is limited on punching polymers and is a significant opportunity to obtain an insight. Numerical modeling is needed to better understand the behavior of during a punching step.

3. DESIGN OF MOLD INSERTS FOR MICRO-MECHANICAL PUNCHING

3.1 Introduction

Kinematic couplings have been widely used as an underlying technology for passive alignment. This technology can eliminate the need for optical equipment and adjustments to bodies, which will simplify the alignment process (Karioja et al., 2000; Bottger et al., 2013). Kinematic couplings are particularly useful for their ability to constrain all six degrees of freedom of one rigid body (Hart et al., 2004, Slocum, 2009). Motion constraint is paramount for an accurate and repeatable alignment step. If one or more degrees of freedom were left unconstrained, infinitesimal motions could occur. This could change the relative location of the bodies and increase their misalignment.

Two complementing mold inserts were developed for a mechanical punching process via double-sided hot embossing. Mechanical joints for kinematic coupling were included on the mold inserts to provide a passive alignment step. The mold inserts were characterized to determine the dimensional and location accuracy of the structures along with the alignment between the mold inserts. Micro-punching trials were conducted on PMMA sheets. The top and bottom surfaces of the samples were analyzed to determine the level of accuracy during an embossing cycle. The accuracy of alignment during molding will be discussed in this chapter, and the qualities of the mechanically punched through-holes will be discussed in Chapter 4.

3.2 Aligning Two Complementing Mold Inserts

Kinematic couplings are made up of specially designed mechanical joints that will contact each other at specific, redundant locations. By repeating the points of contact, the relative locations of the rigid bodies can be precisely controlled during assembly. Such

joints have been integrated at the fabrication and assembly steps for macro- and micro-systems (Trinkle and Lee, 2011; Slocum, 1996). Another characteristic of kinematic couples is that they provides an exact constraint design, where the six degrees of freedom are constrained. There must be exactly six points of contact in a kinematic couple as each one pertains to one degree of freedom (Slocum, 2010).

Traditionally, kinematic couplings are arranged in an equilateral triangle where the features are separated by an angle of 120°. The *Maxwell Couple* is a common embodiment that has been readily applied for passive alignment (Slocum, 2010). One side of this couple has three v-grooves while the opposing body will have three spherical surfaces. The geometry and location of the v-grooves and spheres are symmetrical; this simplifies the fabrication process. A different embodiment is called the *Kelvin Couple*. The key difference is the types of joint uses a flat plate, and a tetrahedral groove which replaces two of the v-grooves. This design still satisfies the six points of contact, but it is not symmetrical and is more difficult to fabricate.

3.2.1 V-Groove and Hemisphere Tipped Post for a Kinematic Joint

The hemisphere tipped post to a v-groove is classic type of kinematic pair. The hemisphere of the post will contact both sidewalls of the v-groove at a single point or along a single line segment as shown in Figure 3.1. Assuming the location of the v-groove is fixed, and contact is constant, the available motions of the post are describable. As the hemisphere stays in contact with the sidewalls of the v-groove, it will have four unconstrained degrees of freedoms, and two constrained degrees of freedom. The hemisphere tipped post would be able to translate along the Z-Axis, and rotate about the

X- Y, and Z-Axes. The constant contact with the sidewalls of the v-groove would prevent the post from translating along the X- and Y-Axes.

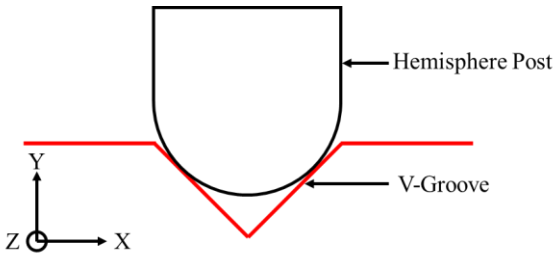

Figure 3.1. Kinematic joint consisting of v-groove and hemisphere tipped post.

The desired double-sided hot embossing process required that a substrate be clamped between two separate mold inserts. A hemisphere tipped post is typically a permanent, positive feature. It would interfere with a hot embossing process. When designing a kinematic couple, a gap is expected to exist between the planes of the bodies. This means the post will have to extend beyond the planes of the primary surface. During a molding step, the tip of the post would contact the substrate first and it would prevent the patterned surface from contacting the substrate material. This would render the mold insert useless for double-sided hot embossing. For this issue the geometry and embodiment of this kinematic pair should be altered to be suitable for a double-sided molding process. The ability to disassemble the hemisphere tipped post from the primary body could be useful and allow it to be applied to double-sided hot embossing.

3.2.2 V-Groove, Dimple, and Sphere for a Kinematic Joint

A modification was suggested where a sphere coupled with a dimple replaced the hemisphere tipped post. The motion of the joint can be described by examining Figure 3.2. It is assumed that the dimple is at a fixed location and contact with the sphere is constant in Figure 3.2 (a). At the interface of the sphere and dimple there is a surface contact where

three degrees of freedom are unconstrained and three are constrained. While contacting the dimple, the sphere can rotate about the X-, Y-, and Z-Axes but it cannot translate along any of the three axes. By constraining the sphere's translation, its location is controlled. Since the sphere is homogenous, any change in its orientation will not alter its location. Figure 3.2(b) shows the sphere in a v-groove. The sphere can rotate about the X-, Y-, and Z-Axes, and translate along the Z-Axes. Since contact is assumed to be constant the sphere cannot translate along X- and Y-Axes. The behavior of this geometry is comparable to the hemisphere to a v-groove joint.

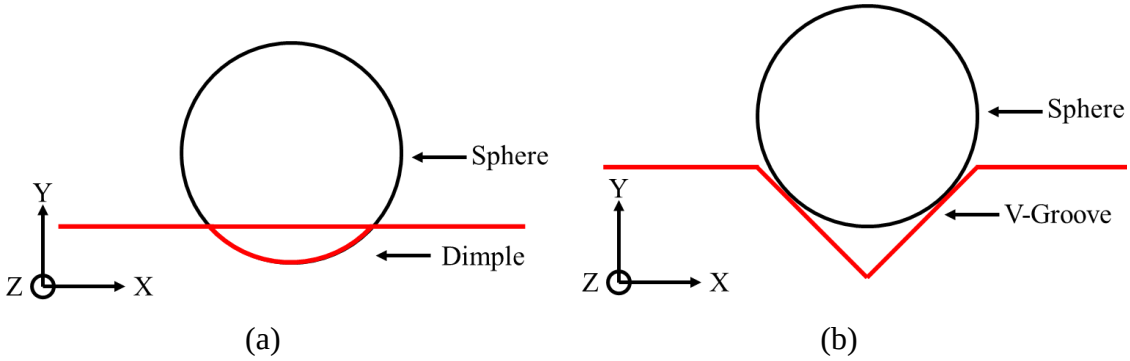

Figure 3.2. Proposed mechanical joint consisting of sphere contacting a dimple (a) and sphere contacting a v-groove (b).

Figure 3.3 shows the proposed kinematic joint; it consists of a: v-groove, sphere, and a dimple. The sphere is resting in the dimple and contacting the sidewalls of the v-groove. It is assumed that the v-groove is at a fixed location while contact between the sphere and dimple is constant, and the sphere and dimple will move in unison. The sphere-dimple would behave similarly to the hemisphere-tipped post, where it would have two constrained degrees of freedom, and four are unconstrained. In this scenario, the sphere and dimple could translate along the Z-Axis and rotate about the X-, Y-, and Z-Axes with

respect to the v-groove. It cannot translate along the X- or Y-Axes of the v-groove. It also satisfies the six points of contact criteria for providing exact constraint design.

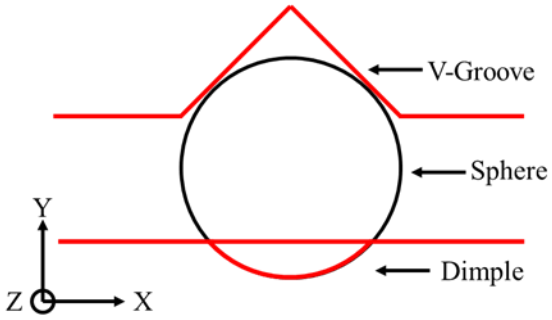

Figure 3.3. Coupled mechanical joint consisting of sphere, v-groove, and sphere.

An additional benefit of this design is each sphere are detachable from a dimple. When applied to an embossing step there will be no positive features that could interfere with a molding process. This design could be an alternative to the hemisphere tipped post. The proposed design was to add three v-grooves to the primary mold insert and on the complementing mold insert three dimples were added. The molds could be assembled with three spheres as shown in the render of the two proposed mold inserts in Figure 3.4.

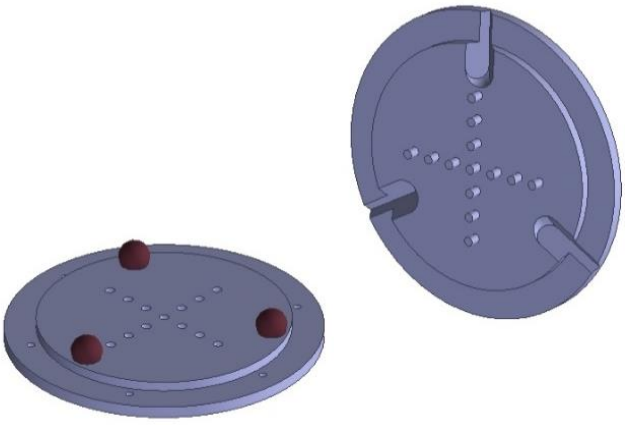

Figure 3.4. A 3D render of proposed mold inserts to be passively aligned by proposed mechanical joints.

3.3 Double-Sided Hot Embossing

Hot embossing is commonly applied with a single master mold insert that will only pattern one side of the substrate. A benefit of single-sided hot embossing is the simplicity of the setup as there is only a need to align the substrate to the master mold. Microstructures will only exist on one side of the substrate and its opposing side will have no patterns. Adding a second mold insert would allow both sides of one substrate to be processed simultaneously. Micro-structures would be fabricated on the opposite planes of the substrate, or it would act as a receptacle for protruding mold structures. It would become a more challenging process as the alignment between the mold inserts must be managed. A mold insert that is misaligned could lead to a microstructure being fabricated in the wrong location. This would cause the device to be less reliable or possibly defective.

Alignment for mechanical punching is critical to maintain the clearance between a punch and die. When misalignment is present, then clearance will be inconsistent, or it could lead to an interference contact. Contact that is undesired could lead to excessive wear or damage to the structures. Commercially available thermal and mechanical presses use iterations to manage the misalignment between complementing mold inserts (Rhim et al., 2005; Joo et al., 2005; Chern., 2006). Adjustment to the relative locations of the mold inserts are made based off data from a preliminary sample or from machine vision. Cycles of forming, characterization, and adjustments are repetitive, tedious, and will decrease the life of the mold inserts. If tooling is damaged, the relative locations of the microstructures changes and therefore alter alignment. The application of passive alignment for double-sided hot embossing would be a significant benefit. The proposed design would not require

iterations or optical feedback. Instead, the alignment process is reduced to a smaller number of assembly steps.

3.3.1 Designed Dimension and Location of Mold Structures

Two mold inserts were designed for a micro-mechanical punching process via double-sided hot embossing. The two molds were designed with features for kinematic joints and mechanical punching. The primary mold insert was fabricated to have thirteen cylindrical pins and a set of three v-grooves. The cylindrical pins served as the punch features for the mechanical punching process. They had a 1:1 aspect ratio where height and diameter was 800 µm and were set along the X- and Y-Axis locations of 10, 20, and 30 mm, as shown in Figure 3.5. One cylindrical pin was located at 0 mm. The v-grooves had a width of 7.4 mm, and a depth of 3.7 mm. They were displaced from the center of the mold by 50 mm and the angular spacing between them was 120°.

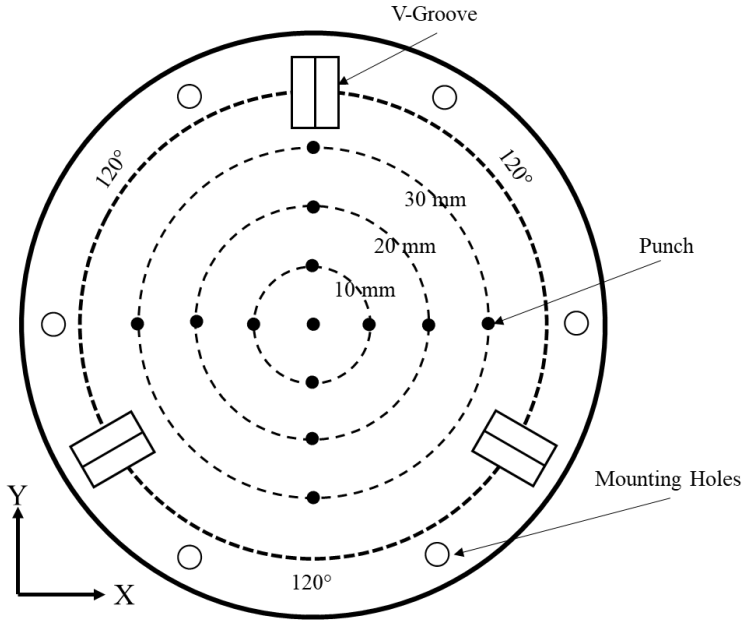

Figure 3.5. Layout of primary mold inserts, showing locations of cylindrical pins and v-grooves.

Thirteen through-holes and three dimples were included on the complementary mold insert. The through-holes served as dies for mechanical punching; five different diameters of 0.90, 1.0, 1.2, 1.4, and 1.6 mm were selected. They were set along the X- and Y-Axes at locations of 10, 20, and 30 mm and one through-hole was located at 0 mm, as shown in Figure 3.6. The diameter of the dimple was 5.3 mm and its depth was 1 mm. They were located 55 mm from the center of the mold and were separated by an angle of 120°. On the bottom of the complementary mold insert a pocket with a diameter of 74 mm and a depth of 5 mm was added. The pocket was included to assist with characterizing the alignment of the mold inserts. Six countersunk bolting holes were included.

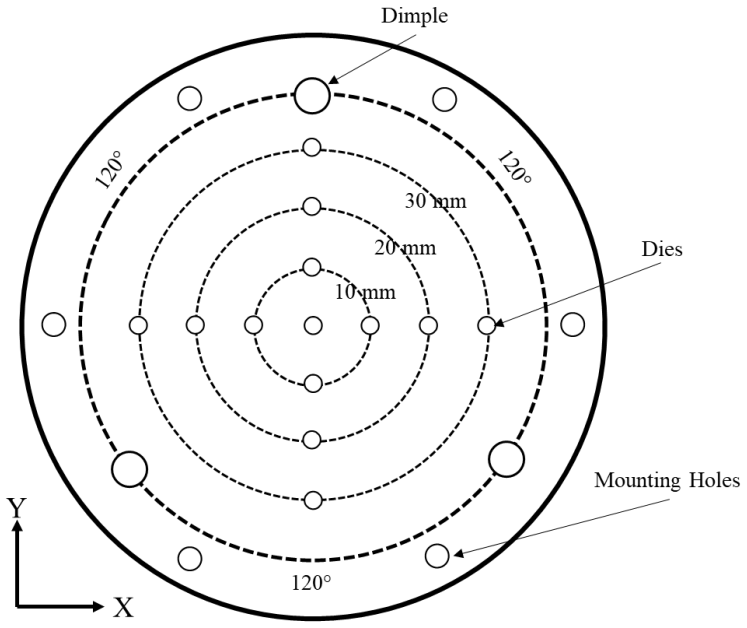

Figure 3.6. Layout of complementary mold inserts, showing locations of through-holes and dimples.

3.3.2 Fabrication of Mold Inserts

The dimensions and locations of both mold inserts were drafted on AutoCAD 2016 (Autodesk, Inc., San Rafael, CA) and were translated into toolpaths with GIBBS

CAM/CAD (GibbsCAM 2018, Moorpark, CA). The mold inserts were fabricated on a KERN MMP high precision micro-milling and drilling machine (KERN Micro- und Feinwerktechnik GmbH & Co. KG, Germany). The accuracy of the micro-milling and drilling machine is in the order of ±1 μm. The mold inserts were fabricated on blanks of brass alloy 353 (McMaster-Carr, Atlanta, GA, USA) with an initial thickness of 10 mm and a diameter of 120 mm.

3.3.3 Hot Embossing Machine

An Auto Series NE Automatic Hydraulic Press 4NE18 (Carver, Inc. Wabash, IN, USA) was used to conduct micro-mechanical punching as shown in Figure 3.7. The main components are two steel heating/cooling platens, a hydraulic ram, a control unit, and a cooling system. The working area of the steel platens was 305 x 305 mm and the maximum temperature was 343 °C. Blind-holes were added to the steel platens and then they were threaded. This allowed for the interchanging of aluminum platens. The hydraulic ram has a maximum clamping force of 134 kN and a stroke of 152 mm. The press was cooled by an oil transfer pump (Hydraulic Power Unit -85-HPS, Amatrol Inc., Jefferson, IL) and a heat exchanger. The oil pump has minimum flow of 9.5 liters per minute (2.5 gpm) and a maximum flow pressure of 3450 kPa. The heating/cooling fluid was Paratherm MR Heat Transfer Fluid (Paratherm, King of Prussia, PA, USA). The fluid is rated for heating or cooling with a temperature range of 2 to 291 °C (36 to 550 °F). Two aluminum platens (McMastet-Carr, Atlanta, GA, USA) that were 305 x 305 x 10 mm, and a vacuum pump (DOA-P704-AA, Gast Mfg Inc., Benton Harbor, MI, USA) were also used. A vacuum channel and vacuum line was machined on one aluminum platen. On the other aluminum

platen, six holes were drilled and threaded to fit M3 screws. The vacuum pump has 1/8 hp motor, and can provide maximum vacuum pressure of 150 mbar abs.

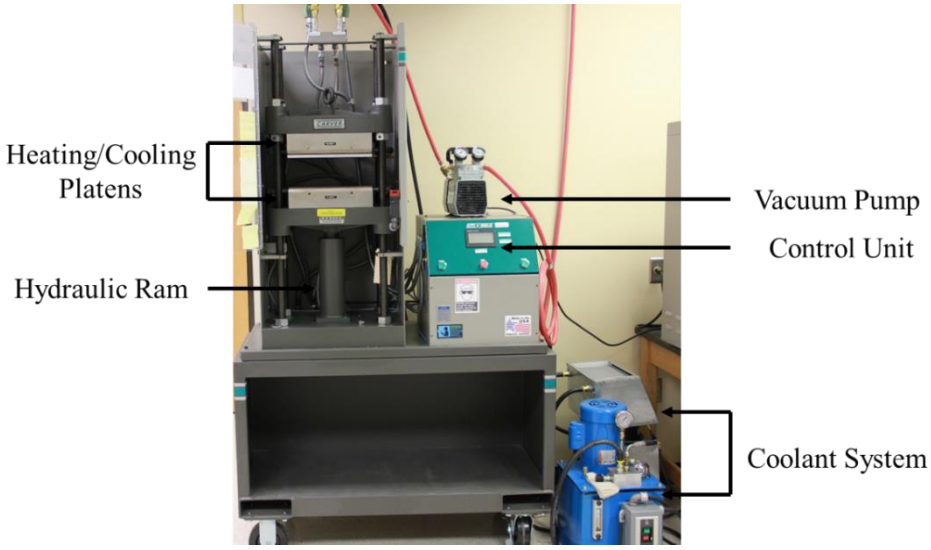

Figure 3.7. Carver 4NE automatic hydraulic press with supporting vacuum pump and cooling systems.

3.3.4 Double-Sided Hot Embossing for Micro-Mechanical Punching

The alignment process for a double-sided hot embossing step is shown in Figure 3.8. The first step was to mechanically fasten the complementary mold to the bottom aluminum platen with six M3 screws (Fig 3.8(a)). By fastening the complementary mold insert its motion was constrained and it fixed its location. Three stainless spheres with a diameter of 8 mm were set inside the dimples (Fig 3.8(b)). The alignment step was completed by locating and contacting the three v-grooves to their corresponding sphere (Fig 3.8 (c) and (d)). The bottom platen was driven vertically until the blank side of the primary mold insert contacted the vacuum channel on the top aluminum platen (Fig 3.8 (e)). When contact was observed the press was opened and the primary mold was held by the vacuum (Fig 3.8(f)). At this stage, the thermal press was heated to the molding temperature of 120 °C.

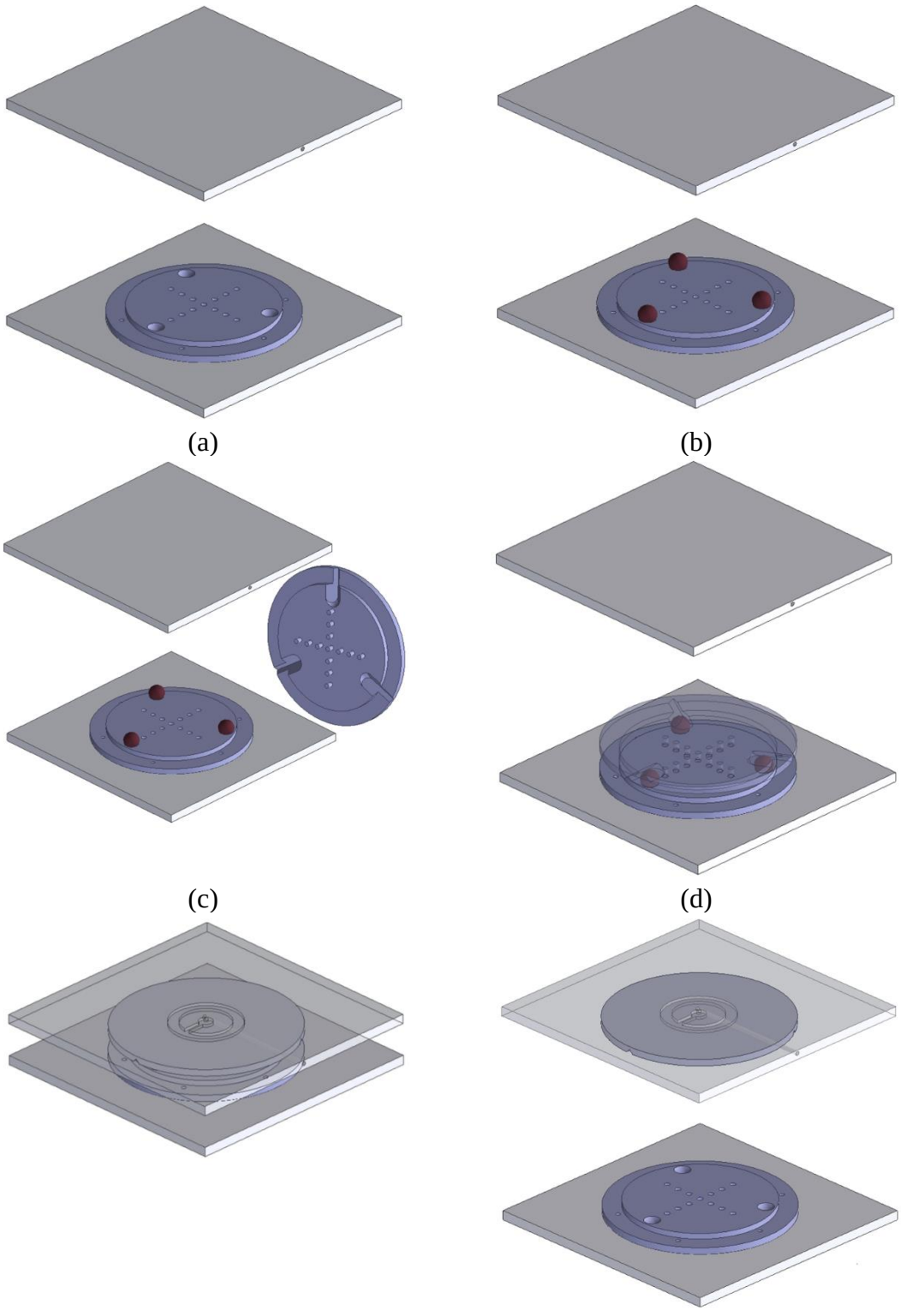

Figure 3.8. The complementary mold is fastened to aluminum platen (a), three stainless steel sphere are located in the dimples (b), the primary mold is aligned to the complementary mold and coupled by the v-grooves (c-d), the bottom aluminum platen is driven to contact the top aluminum platen (e), the thermal press is opened and the primary mold is held by a vacuum (f).

Micro-punching trials were conducted on sheets of PMMA with a thickness of 0.5 mm (CLAREX ®, Nitto Jushi Kogyo Co., Ltd., Tokyo, JPN). PMMA is known to absorb moisture from the environment so the samples had to be dried in a convection oven (31-350ER-1 Quincy Lab Inc., Chicago, IL, USA) for four hours at 80 °C (Erikson et al., 2015). Particulates on the surfaces of the substrate were removed with a stream of nitrogen gas (Airgas, Austin, TX, USA). A mold release agent (Mold Wiz, F-57N, Axel Plastics Research Laboratory Inc., Woodside, NY) was applied to the heated mold inserts. The PMMA was set on top of the complementary mold insert for a period of ten minutes. This allowed the PMMA to reach thermal equilibrium with the mold inserts. After ten minutes, the hot embossing cycle was initiated, and the sample was clamped between the mold inserts. The embossing force of 20 kN was held for two minutes. After the holding time, the system was cooled to the demolding temperature of 85 °C. Cooling to the demolding temperature took approximately ten minutes. This allowed the PMMA to transition from a viscoelastic state to a solid state. The embossing force was released, and the sample was demolded.

Conventionally, mechanical punching is often conducted at an ambient temperature which allows for an elastic behavior of the material. The elevated temperature, force, and holding time were selected to replicate an environment that is suitable for a micro- hot embossing process. In this environment the PMMA behaves as a viscoelastic material which allows the PMMA to flow. This could allow for the formation of a through-hole and other micro-structures such as microchannels to be formed simultaneously. The process parameters for double-sided hot embossing are summarized in Table 3.1.

Table 3.1. Process parameters for processing PMMA sheets.

Embossing Temperature (°C)	120 ± 3
Demolding Temperature (°C)	85 ± 3
Embossing Force (kN)	20 ± 0.1
Hold Time (min)	2 ± 0.1

3.4 Results of Micromachining of Mold Inserts

3.4.1 Characterization of Micro-Machined Mold Inserts

A stereoscope image (a) and measurescope image (b) of a typical cylindrical pin and a through-hole with a diameter of 0.9 mm are shown in Figure 3.9. Accurate passive alignment is dependent on the dimensional quality of the kinematic joints (Fischer, 2011). This is because parts in a kinematic couple are designed to contact at a specific, repeatable location. Variation is inherent in machining; the dimensions and locations of the structures will differ from their nominal values. These innate variations will alter relative locations of the mold inserts as they are assembled, causing misalignment.

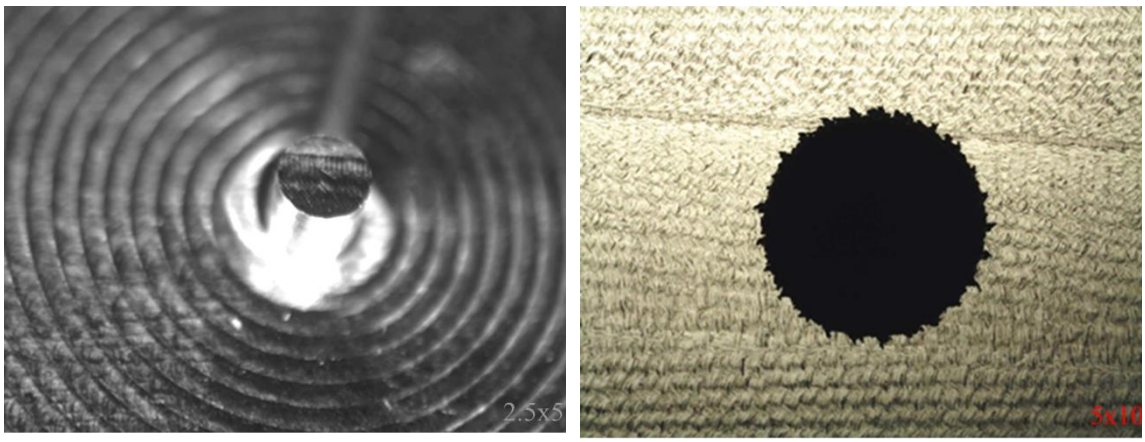

(a) (b)

Figure 3.9. Micrographs of a typical cylindrical pin (a) at 2.5x5 and a typical mechanically drilled through hole (b) at 5x10.

The primary and complementary mold inserts were characterized using a measurescope at a 10x10 magnification (MM-800, Nikon Corp. Kawasaki, Japan) and a Quadra-Check Digital Readout (DRO) (Heidenhain Corp., Traunreut, Germany). A description of the performance of the measurescope is offered in Appendix A. A focus-defocus method and the DRO were used to measure the heights of the structures. This technique tracked the change in focal length when focus is changed between different planes (Xiong and Shafer, 1993). The locations and diameters of the pins and through-holes were characterized by selecting three sets of coordinate points along their circumferences with respect to a reference coordinate system. This method was applicable to the v-grooves since the milling tool left a half-circle at one end of each v-groove. A circle was fitted to the three coordinate points which expressed the geometrical center point and the radius (Lay et al., 2005). Location of a structure was determined by comparing its calculated center point to a center-point of the pin or hole located at 0 mm.

3.4.2 Characterization of Alignment Accuracy of Assembled Mold Inserts

The alignment accuracy of the assembled mold inserts was analyzed by measuring the relative locations of the pins and through-holes. Three stainless steel spheres with a diameter of 8 mm were set in the dimples on the complementary mold insert. The primary mold was coupled to the complementary mold insert using the method described in section 3.3.4. A horizontal force was applied by hand to the top mold insert along its circumference. The primary mold did not translate or rotate; the assembly was stable. The assembly inverted so that complementary mold was on top, and the circular pocket was visible as shown in Figure 3.10. This allowed the bottom openings of the drilled through-

holes to be visible during characterization. Sets of three coordinate points were selected on the bottom edges of each through-hole. It was assumed that the holes were straight, and the center points of the top and bottom diameters were aligned. Next, the complementary mold insert was removed, and the primary mold insert was left in the same location. Sets of three coordinate points were selected along the top circumferences of each pin as shown in Figure 3.11.

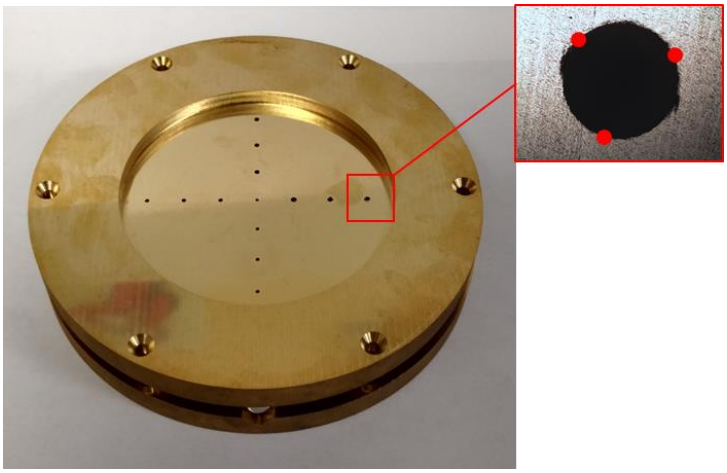

Figure 3.10. Inverted assembly of the coupled primary and complementary mold inserts show the milled pocket.

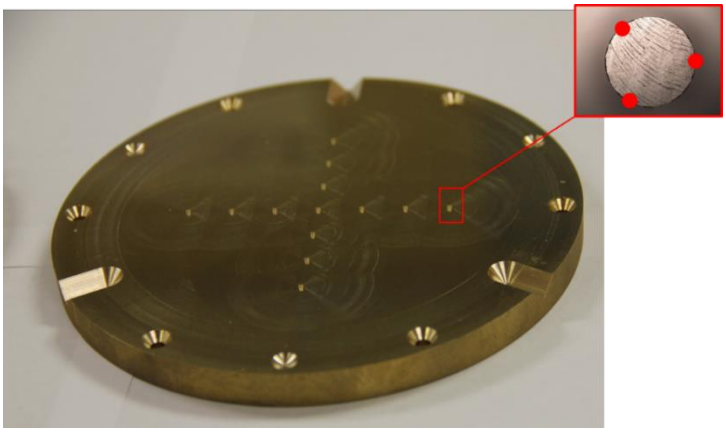

Figure 3.11. Characterizing alignment of primary mold inserts.

All coordinate points were selected at a 10x10 magnification and the measurements were triplicated. A circle was fitted to the sets of coordinate points of the pins and through-holes (Conner, et al., 2014). This yielded the coordinates of each center point. The pairs of pins and holes were divided into two groups: features on the X-Axis, and features on the Y-Axis (Fig 3.4 and 3.5).

3.4.3 Dimensional and Location Accuracy of Micro-Machined Structures

Table 3.2 compares the designed dimensions versus the average height and diameter of the thirteen pins. The diameter typically ranged from 0.801 to 0.809 mm, and their height ranged from 0.803 to 0.807 mm. Both the height and diameter were accurate within 0.63% of one micron.

Table 3.2. The average diameter and heights of the micro-milled cylindrical pins with the 95% confidence interval and percent variance.

Dimension	Designed size (μm)	Calculated (μm)	%Variance
Diameter	800	805 ± 4	0.63
Height	800	805 ± 2	0.63

Table 3.3 shows the designed diameters of the through-holes compared to the measured diameters. Considering all the designed dimensions, the diameters of the through-holes varied by 0.020 to 0.060 mm or from 2% to 5% of their intended size. The level of variation of the through-holes is more significant compared to the cylindrical pins. Fractures along the top circumferences were observed and could have affected the selection of coordinate points. This is a common defect in the mechanical drilling process. It can be caused by walking of the drill bit, tool quality, and machining parameters (Arlon Electronic Materials, 2012).

Table 3.3. The average diameter of the micro-drilled through-holes with the 95% confidence interval and percent variance.

Designed diameter (mm)	Calculated (mm)	%Variance
0.90	0.92 ± 0.02	2
1.00	1.04 ± 0.02	4
1.20	1.27 ± 0.03	6
1.40	1.43 ± 0.01	2
1.60	1.66 ± 0.01	4

The measured widths and depths of the v-grooves are summarized in Table 3.4. The average width was approximately 0.5 mm wider than the design value of 7.4 mm, while their depths only varied by ± 0.01 mm. When designing the v-groove it was assumed that the bottom of each groove would have a sharp, pointed tip (Fig. 3.1). The v-grooves that were fabricated did not have a sharp point at their bottom section. The variation in width which was related to the geometry of the milling tool used to fabricate the v-grooves. The discrepancy happened since the milling tool had a flat tip, and the width of the machined v-groove is controlled by the depth of cut. During machining, the depth of cut for the milling tool was set to 3.7 mm. This was observed since the average depth of the grooves was 3.70 mm and varied by ± 0.01 mm. Since the tool had a flat tip it plunged beyond the designed depth, thus increasing the width.

Table 3.4. The average width and depth of the micro-milled v-grooves with the 95% confidence interval and percent variance.

Dimension	Designed size (mm)	Calculated (mm)	%Variance
Width	7.4	7.90 ± 0.01	8
Depth	3.7	3.70 ± 0.01	0.5

The width and depth of the dimples only varied by ± 0.002 mm and ± 0.01 mm, respectively. The variation was less significant due to the compatibility between the designed geometry of the dimple and geometry of the milling tool. A sphere with a diameter

of 8 mm was the basis of the designed dimensions of the dimple. It was fabricated by a ball end mill that had a diameter of 8 mm, and it was plunged with a depth of cut of 1 mm. The geometry and dimensions of the ball end mill could effectively mimic the surface of an 8 mm sphere and accurately produce the dimples.

Table 3.5. The average diameter and depth of the micro-milled dimples with the 95% confidence interval and percent variance.

Dimension	Designed size (mm)	Calculated (mm)	%Variance
Diameter	5.3	5.300 ± 0.002	.2
Depth	1	0.98 ± 0.01	2

Table 3.7 shows the variation of location for the pins and through-holes. The cylindrical pins located at 10 mm showed a variation at ± 0.001 mm and pins located at 20 mm and 30 mm showed variation of ± 0.002 mm. On the complementary mold insert, through-holes located at 10 mm had the most variation at ± 0.02 mm while through-holes at 20 mm and 30 mm varied only by ± 0.003 µmm. A source of this error could be the mechanical drilling process. As previously discussed, the mechanical drilling process can create two separate diameters at the top portion of the holes. It is likely that coordinate points were selected along an inconsistent circumference.

Table 3.6. The average location of the cylindrical pins and through-holes with the 95% confidence interval.

	Calculated location (mm)	
Designed location (mm)	**Pin**	**Hole**
10	10 ± 0.001	10 ± 0.020
20	20 ± 0.002	20 ± 0.003
30	30 ± 0.002	30 ± 0.003

The location the v-grooves and dimples were compared to the pin and through-hole located at 0 mm, respectively. The average location is shown in Table 3.7. Both features

varied from the designed location by an additional 0.69 mm; progressing away from the center of the mold insert.

Table 3.7. The average location of the v-grooves and dimples with the 95% confidence interval and percent variance.

Feature	Designed (mm)	Calculated (mm)	%Variance
V-Grooves	50	50.690 ± 0.004	1.38
Dimples	55	55.680 ± 0.008	1.23

The centroid of the v-grooves and dimples were compared to the center-point of pin and through-hole locate at 0 mm. The centroid is defined as the point where the centerlines of the v-grooves and dimples will intersect with each other. To calculate the centroid, a circle was fitted to the location of the v-grooves and dimples. The average mismatch between a centroid and the feature at 0 mm is shown in Table 3.8. The cylindrical pin and through-hole located at 0 mm of both mold inserts was the center of the mold. The centroid of the v-grooves was displaced from the punch-center-point in the X- and Y-direction by 1 and 4 μm, respectively. The centroid of the recesses was displaced from the punch center point in the X- and Y-direction by 4 and 3 μm, respectively.

Table 3.8. Misalignment between feature centroid and central punch and die with the 95% confidence interval.

	ΔX (μm)	ΔY (μm)
Centroid Displacement from Punch	1 ± 1	6 ± 8
Centroid Displacement from Die	4 ± 11	3 ± 6

3.4.4 Alignment Accuracy of the Assembled Mold Inserts

Figure 3.12 shows alignment between a punch and die at their nominal locations along the X-Axis and Y-Axis. For features on the X-Axis, the misalignment ranged from 2 to 7 um in the X-direction, and 7 to 16 μm in the Y-Direction. On the Y-Axis, the

variation in the X- and Y-Direction ranged from 1 to 4 µm, and 5 to 7 µm, respectively. Alignment was controlled within 15 µm by the mechanical joints that was proposed.

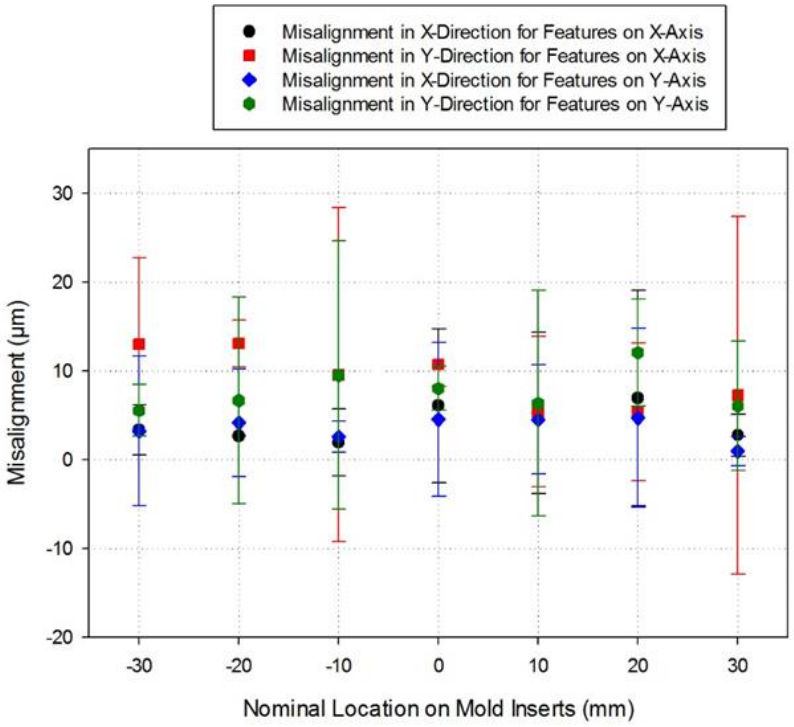

Figure 3.12. Alignment between cylindrical pins and through-holes with respect to designated axes and nominal locations.

The mold inserts could be aligned with limited assembly steps. Therefore, no adjustment or optical feedback was needed to correct or monitor misalignment. As the primary mold insert was coupled to the complementary mold insert, the sphere would contact the v-grooves at known locations and generate the six points of contacts. Since its six degrees of freedom were constrained, the relative location of the primary mold insert could be precisely controlled. The coupling that was proposed was confirmed to be capable of providing alignment for assembly that was accurate and repeatable.

3.4.5 Characterization of Experimental Results

After mounting the primary mold insert to the vacuum platen the kinematic couple was disassembled and the spheres were removed from the dimples. The primary mold was able to regain a limited amount of degrees of freedom. It is possible that the mold insert moved during mounting or an embossing step. If it experienced an infinitesimal motion, its relative location would have changed. Therefore, it necessary to measure the micro-punched samples to characterize the inherent misalignment. The double-sided hot embossing process generated artifacts on the top and bottom surfaces of the PMMA substrate. These structures were used to locate the surfaces of the top and bottom. Images of the through-holes were captured with a Scanning Electron Microscope (SEM) (JSM–6010 PLUS/LA, JEOL, Ltd., Akishima, Tokyo, JPN) to show the artifacts from both of the surfaces. The samples were coated in a 2 nm layer of iridium by a sputter coater (EMS150T ES, Electron Microscopy Sciences, Hatfield, PA, USA).

Figure 3.13 shows SEM images the top (a) and bottom diameter (b) of a through-hole that was fabricated with a clearance of 100 μm. The top diameter of the through-hole can be seen in Fig. 3.13(a) and it was used as a reference feature to locate the topside of the sample. On the bottom side (Fig. 3.13(b)), the top diameter and was enveloped by the bottom diameter. The diameters were offset from each other; indicating that their center-points were misaligned. The circumference of the bottom diameter was used to locate the bottom of the PMMA samples. Three coordinate points were selected along the circumference of the top diameter of the through-hole with the measurescope at a 10x10 magnification. The focal distance on the measurescope was decreased until the bottom diameter was visible, and three coordinate points were selected along its circumference.

Radii and center points were mathematically extracted from the sets of coordinate points. The center point of a bottom diameter was compared to the center points of a top diameter to determine mismatch. The average misalignment between the assembled pins and through-holes was displayed with the 95% Confidence Interval.

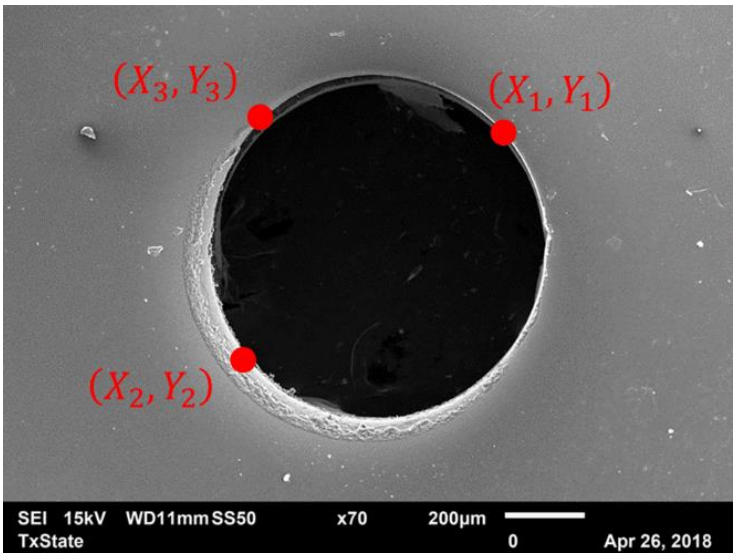

(a)

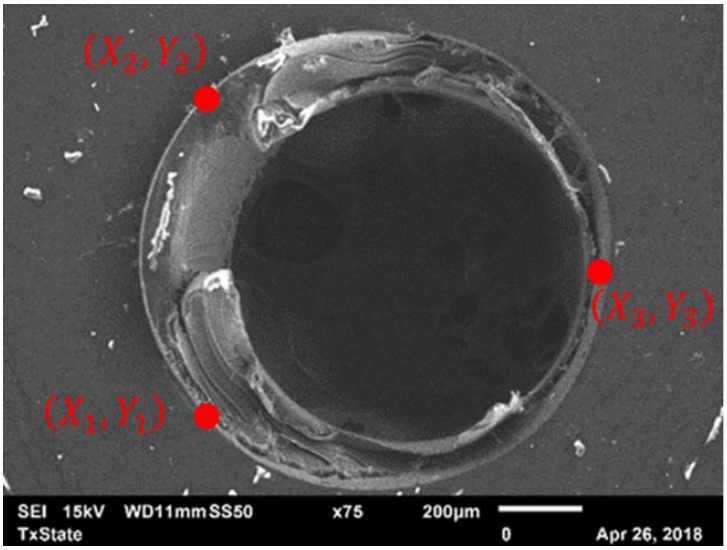

(b)

Figure 3.13. SEM image of the top (a) and bottom (b) diameter of an iridium coated through-hole fabricated with a 100 µm clearance located at 10 mm.

3.4.6 Results of Micro-Mechanically Punched Through-Holes

Figure 3.14 shows the mean misalignment of the micro-punched PMMA samples. The artifacts on the X-Axis had misalignment that ranged from 12 to 82 µm and 32 to 72 µm in the X- and Y-direction, respectively. The misalignment ranges for artifacts on the Y-Axis in both the X- and Y-direction were 11 to 71 µm and 32 to 70 µm, respectively. The results indicate that the relative location of the primary mold insert was altered.

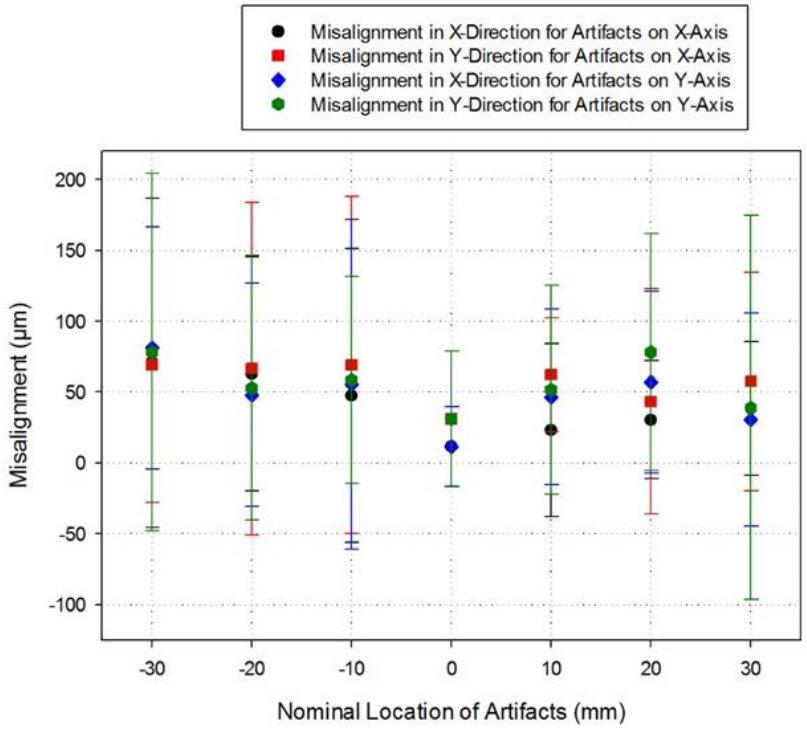

Figure 3.14. Alignment between top and bottom of the micro- mechanically punched samples with respect to designated axes and nominal locations.

The physical consequences suggest that the primary mold insert experienced an infinitesimal motion. This could have happened during the mounting process of the primary mold insert or the hot embossing step. Suction from the vacuum pump was the only force used to hold the primary mold insert to the top aluminum platen. This created an under-

constrained situation where the primary mold could translate or rotate along the platen. An illustration of the primary mold insert mounted by a vacuum seen in Figure 3.15.

By examining the image, it is observable that the contact between the primary mold insert and platen will prevent translation along the Z-Axis and rotations about the X- and Y-Axis. However, translation along the X- and Y-axis, and rotations about the Z-axis are available. The non-planar surfaces of the vacuum platen and the blank side of the primary mold insert also prevented a maximum vacuum pressure. A sufficient force could have been applied that caused the primary mold insert to translate or rotate along the surface of the platen.

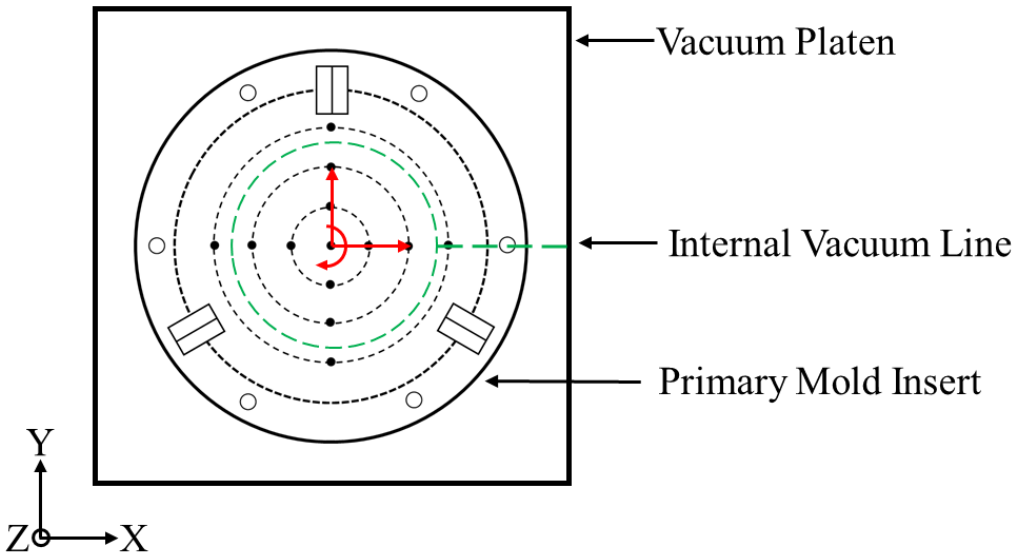

Figure 3.15. Diagram of vacuum-mounted primary mold insert that could translate along the X- and Y-Axis and rotate about the Z-Axis.

During the contact step of the alignment process (Fig. 3.6(e)) the thermal press would apply a reduced load on to the assembled mold inserts. Since the mold inserts were made from brass and the spheres were made from hardened stainless steel, the force from the press caused the spheres to leave indentations on the sidewalls of the v-grooves. This compressive force and indentation could have allowed for an infinitesimal motion of the

primary mold insert. These indentations could have changed the locations of the points of contact. Trinkle and Lee (2011) also observed a similar behavior where contact pressures could interfere with the assembly of a kinematic coupling.

During demolding the embossing force was released when the thermal press was opened. There was adhesion between the PMMA substrate and mold inserts. It was significant, and it separated the primary mold from the vacuum platen when the thermal press was opened. The primary mold had to be aligned and mounted before every hot embossing trial. A consequence of this could be a reduction in repeatability of the alignment process. The location of the primary mold on the top aluminum platen could have been different during each micro-punching experiment.

3.5 Conclusion

Two mold inserts were designed with sets of features for passive alignment and a micro punching process. They were fabricated with a micro milling and drilling machine. The mold inserts were measured to determine the integrity of the dimensions and locations. With respect to their designed values, the dimensions and locations of the structures varied from 0.2 to 4% and 0.2 to 2%, respectively. These variations are innate and will inherently induce alignment when the mold inserts were coupled. When the primary and complementary mold inserts were assembled no motions were observed. The misalignment between a punch and die was measured and it was below 20 μm in the both X- and Y-Direction.

The misalignment between artifacts left on the top and bottom surface of the PMMA was measured. It ranged 12 to 82 μm and 32 to 72 in the X- and Y-Direction, respectively. An under-constrained situation was present when the primary mold insert was

held only by a vacuum. Three degrees of freedom were unconstrained, and the primary mold could have translated and rotated with the application of a force. Any motion would have changed its relative location and increased misalignment. The compressive force applied to the mold inserts during mounting left indentations in the v-grooves. This changed the contact points which is an issue for passive alignment. The characteristics of the mechanically punched through-holes will be discussed in the next chapter.

4. MICRO-MECHANICALLY PUNCHED THROUGH-HOLES

4.1 Introduction

A double-sided hot embossing process was used to micro-mechanically punch through-holes on sheets of PMMA that had a thickness of 0.5 mm. Through-holes were mechanically punched with clearances of 50, 100, 200, 300, and 400 μm. The experiments yielded through-holes that were either completed, partially completed, or incomplete. The top diameter, bottom diameter, rollover diameter, and rollover height were measured to quantify their accuracy and observe the effect of the clearances. The through-holes were bisected to allow for imaging of their sidewalls. These images could be used to infer the behavior of the PMMA during punching and establish the qualities of the through-holes.

4.2 Clearances for Micro-Mechanical Punching

Thirteen cylindrical pins with a height and diameter of 800 μm were placed on the primary mold insert and served as the punch tool. Thirteen mechanically drilled through-holes were included on the complementary mold insert with five levels of diameter as summarized in Table 4.1. Only one through-hole, located at 0 mm, was drilled with a diameter of 0.9 mm which provided a clearance of 50 μm. The remaining twelve dies had diameters of 1.0, 1.2, 1.4, and 1.6 mm and were fabricated in sets of three at locations of 10, 20, and 30 mm. These dies provided clearances of 100, 200, 300, and 400 μm.

Table 4.1. Dimensions, clearance, and locations of dies.

Die Diameter (mm)	Clearance (μm)	Locations (mm)
0.9	50	0
1.0	100	10, 20, 30
1.2	200	10, 20, 30
1.4	300	10, 20, 30
1.6	400	10, 20, 30

4.3 Results of Mechanically Punched Through-Holes

Figure 4.1 shows a photograph and micrographs of the top plane of a typical PMMA substrate after micro-punching. On the top surface of the samples two types of artifacts were present: the top diameter of the through-holes, and machining marks that were transferred from the primary mold insert. The top diameter of a complete or incomplete through-hole indicated the point of contact between the pin and the substrate. The transfer of machining marks is typical in hot embossing and has been used to assess the filling of a mold insert (Pan et al., 2007; Henann et al., 2009) The machine marks created by the primary mold insert had a spiral pattern that encircled the top diameter of the through-holes. The distribution of the transferred machining marks was not consistent over the top surface of the sample. There were sections of the top surface where machining marks were not present or began to diminish over a length.

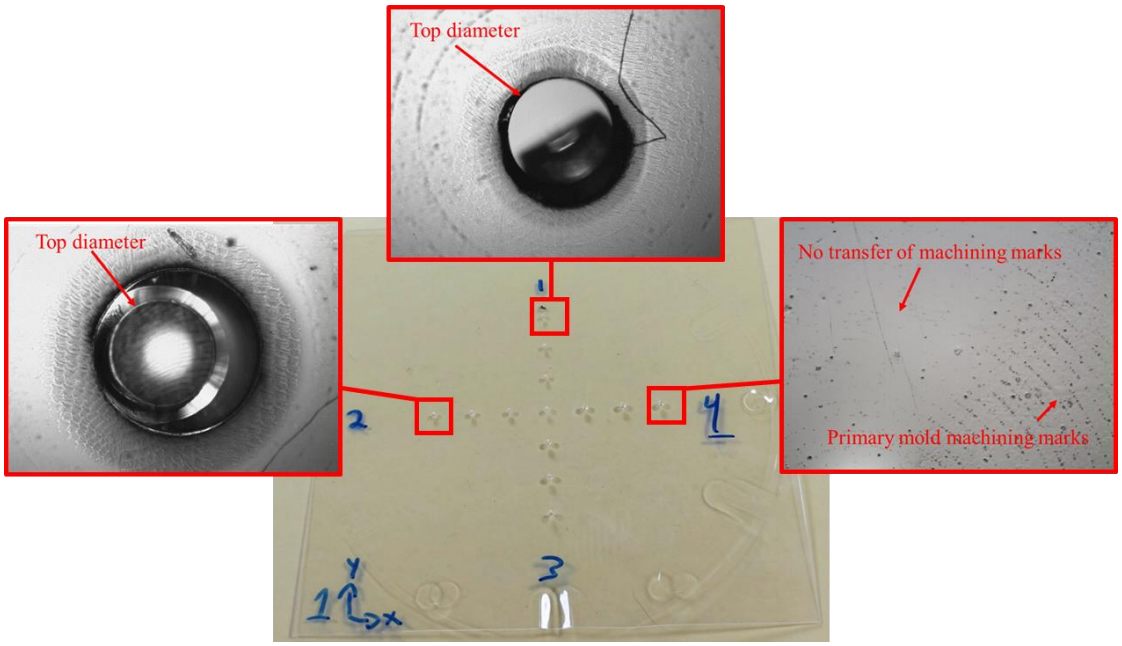

Figure 4.1. A photograph of the top surface of a typical PMMA sample and micrographs of the artifacts that were present on the top surface.

A photograph and micrographs of the bottom surface of a typical micro-punched PMMA substrate are shown in Figure 4.2. On the bottom surface of the PMMA sample three types of artifacts were present: the bottom diameter of a through-hole, the residual layer on an incomplete or partial through-hole, and machining marks that were transferred from the complementary mold insert. Directly after a micro-punching step, a through-hole could be classified as one of the following: completed, partially completed, or incomplete. A completed through-hole was when the bottom diameter was un-obstructed, and the residual layer was removed. A partial through-hole was when the bottom diameter was partly obstructed by the residual layer that was attached to the bottom surface. When the bottom diameter of the through-hole was fully obstructed it was classified as incomplete. The amount of types of through-holes directly after mechanical punching is summarized in Table 4.2.

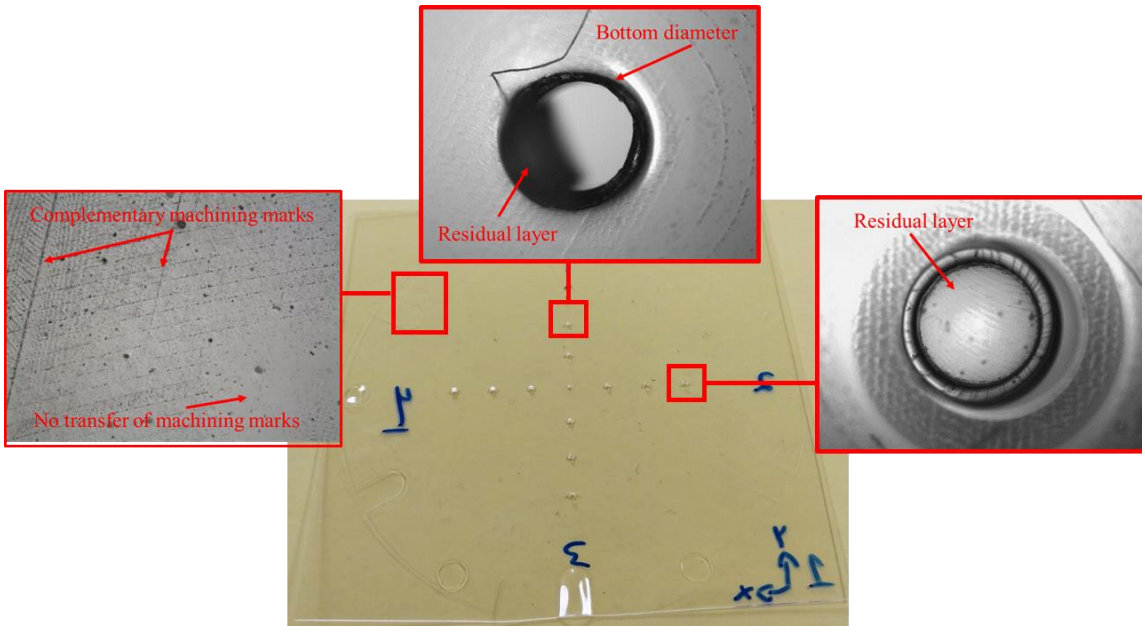

Figure 4.2. A photograph of the bottom surface of a typical PMMA sample and micrographs of the artifacts that were present on the bottom surface.

Machining marks that were transferred from the complementary mold insert to the bottom side of the PMMA could be described as equally spaced lines that were parallel and separated by a granular texture. Similar to the top surface, the presence machining marks on the bottom surface were inconsistent. The machining marks were predominantly on the areas that were adjacent to the bottom diameters and residual layers. There were segments of the bottom surface that did not have any machining marks.

Table 4.2. The number of through-holes produced directly after processing.

Clearance (μm)	Possible	Complete	Partial	Incomplete
50	12	10	2	0
100	36	2	34	0
200	36	0	14	22
300	36	0	2	34
400	36	0	3	33

Partial through-holes were described by having the residual layer partly attached to the bottom diameter of the through-hole by a fragment that was brittle. Wang et al., (2006) reported through-holes where the residual layer was partly attached to the bottom diameter but did not remove them. Using a Kimwipe^{TM} (Delicate Task Wiper, Kimberly-Clark Corp., Irving, TX, USA), the residual layer could be removed by applying a swiping pressure by hand. With this non-invasive post process, partial through-holes were converted into complete through-holes. The removal of burrs or fragments of the residual layer is common for mechanical punching and it has been done as a post process. However, these processes can be invasive and require dedicated equipment. For example, metallic burrs on sheet metals have been removed by chemical etching, abrasives, or rollerball deburring tools (Biermann and Heilmann, 2010, Schnabl, 2010). At the micro-scale, Chowdhury (2010) used KOH to wet etch mechanical burrs from through-holes made from

liquid crystal polymer. Rhim et al. (2006) used isotropic wet etching to remove the partially attached residual layers from micro-mechanically punched through-holes on a titanium and copper foils.

All of the partial through-holes that were generated with a clearance of 50 and 100 µm were converted into complete through-holes. When clearance was 200 µm, fourteen partial through-holes were processed into complete-through-holes. On some incomplete through-holes fractures on the residual layers were observed but the residual layers were too rigid to be removed by swiping. At clearances 300 and 400 um, the residual layers were mostly rigid and could not be removed with a Kimwipe^{TM}. Only two and three partial through-holes could be generated at the clearances of 300 and 400 µm, respectively. For the rigid, intact residual layers an invasive post processing step would be needed to complete the through-hole. For example, a machine tool with a fly cutter or end mill would be needed to remove the residual layer and generate the bottom diameter of the through-hole.

Table 4.3. The number of through-holes produced after post processing.

Clearance (µm)	Possible	Complete	Partial	Incomplete
50	12	12	0	0
100	36	36	0	0
200	36	14	0	22
300	36	2	0	34
400	36	3	0	33

4.3.1 Results with a Clearance 50 µm

Optical micrographs of the through-hole punched with a clearance of 50 µm located at 0 mm is shown in Figure 4.3. The residual layer was absent and the diameters of the top (a) and bottom (b) were not obstructed. The primary mold insert transferred machine marks

that were concentric circles. They were observable on the top surface of the PMMA but they did not fully encircle the through-hole. Their presence began to dissipate when progressing away from the through-hole. On the surface of the bottom side of the PMMA, the machine marks from the complementary mold insert were transferred to the areas that were adjacent to the circumference of the bottom diameter. Their texture was granular, and their presence was inconsistent when moving away from the through-hole.

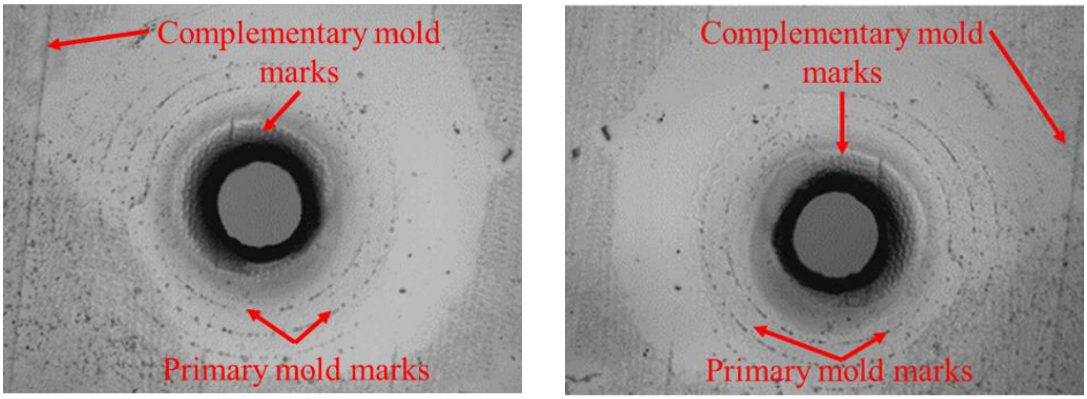

(a) (b)

Figure 4.3. Optical micrographs at 2.5x10 of the top diameter (a) and the bottom diameter (b) of a complete through-hole that was fabricated with a clearance of 50 µm.

SEM images of the top and bottom diameters of a typical completed through-hole punched with a clearance of 50 µm are shown in Figure 4.4. The topography, the top and bottom diameters as well as the adjacent surface areas are distinct. The top diameter of the through-hole is observed in Figure 4.4(a). It was uniform along its circumference and it had an opening diameter of 837 µm. The edge was rounded, and this depression extended into the surface areas that surrounded the through-hole. At the top-left quadrant of the top diameter, there were defects visible on the surface. These defects could have been caused by the demolding process. Progressing to the bottom of the through-hole, fragments of the residual layer were still visibly attached to the sidewall of the through-hole.

When observing the bottom side of the sample, the top and bottom diameter of the through-hole are visible Figure 4.4(b). The roundness of the bottom diameter was not uniform along its circumference. Its diameter was approximately 911 µm; which was 74 µm larger than the top diameter. A fragment of the residual layer is seen on the top-right quadrant of the bottom diameter. On the surface near the bottom-left quadrant, transferred machining marks were present. These marks were transferred from the complementary mold insert and had a pattern that was comparable to the machining marks seen on a drilled through-hole.

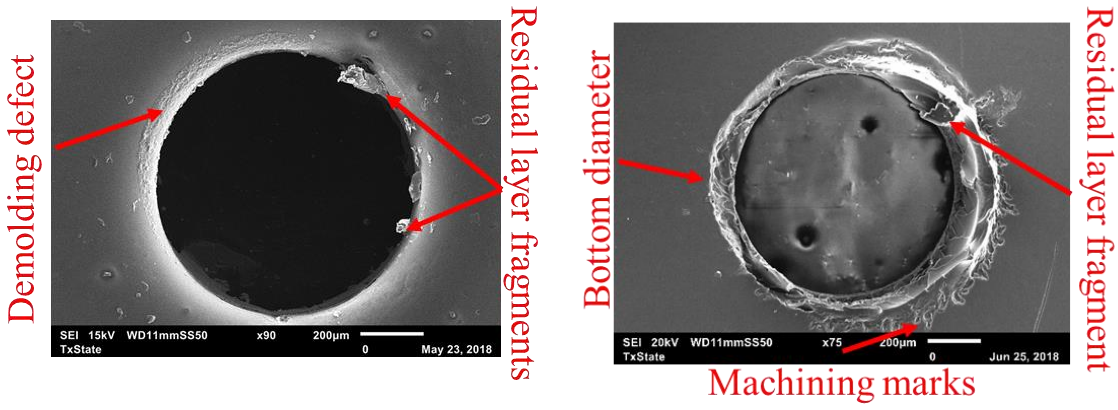

(a) (b)

Figure 4.4. SEM images of the top diameter (a) and the bottom diameter (b) of a complete through-hole that was fabricated with a clearance of 50 µm.

The through-hole was bisected so that a portion of the sidewall could be imaged by the SEM as shown in Figure 4.5. It had a top diameter of 837 µm and rollover was present, which caused the profile to be rounded. The depth and diameter of the rollover were 130 and 1346 µm, respectively. The rollover then transitioned into the sidewall of the through-hole. Striations and reliefs were present on the sidewall and extended the surface for 403 µm. Along the bottom of the through-hole two distinct artifacts were present: a fragment of the residual layer and the bottom diameter of the through-hole. The fragment was on the

left side, and the bottom diameter was visible on the right side of. The fragment protruded by 170 µm from the bottom surface.

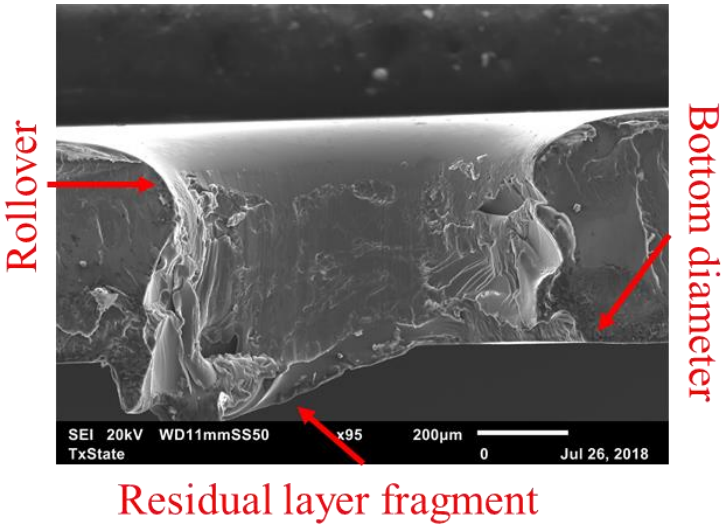

Figure 4.5. SEM images of a portion of the sidewall of a complete through-hole that was fabricated with a clearance of 50 µm.

4.3.2 Results with a Clearance 100 µm

Optical micrographs at 2.5x10 of the top diameters of partially completed through-holes are shown in Figure 4.6. They were mechanically punched with a clearance of 100 µm at locations of 10, 20, and 30 mm. The residual layers were visibly attached; they obstructed a portion of the bottom diameter of the through-holes. Machining marks from both of the mold inserts were inconsistent with respect to the location of the through-holes at 10 (a), 20 (b), and 30 (c) mm. Machining marks from the primary mold insert were prominent on the surface area that surrounded the through-hole at 30 mm. The partial through-hole at locations of 10 and 20 mm had machining marks that did not fully encircle the partial through-holes. Machining marks from the complementary mold insert were visible from a top view of the sample. They were mainly present at the areas that were adjacent and encircled the attached residual layer.

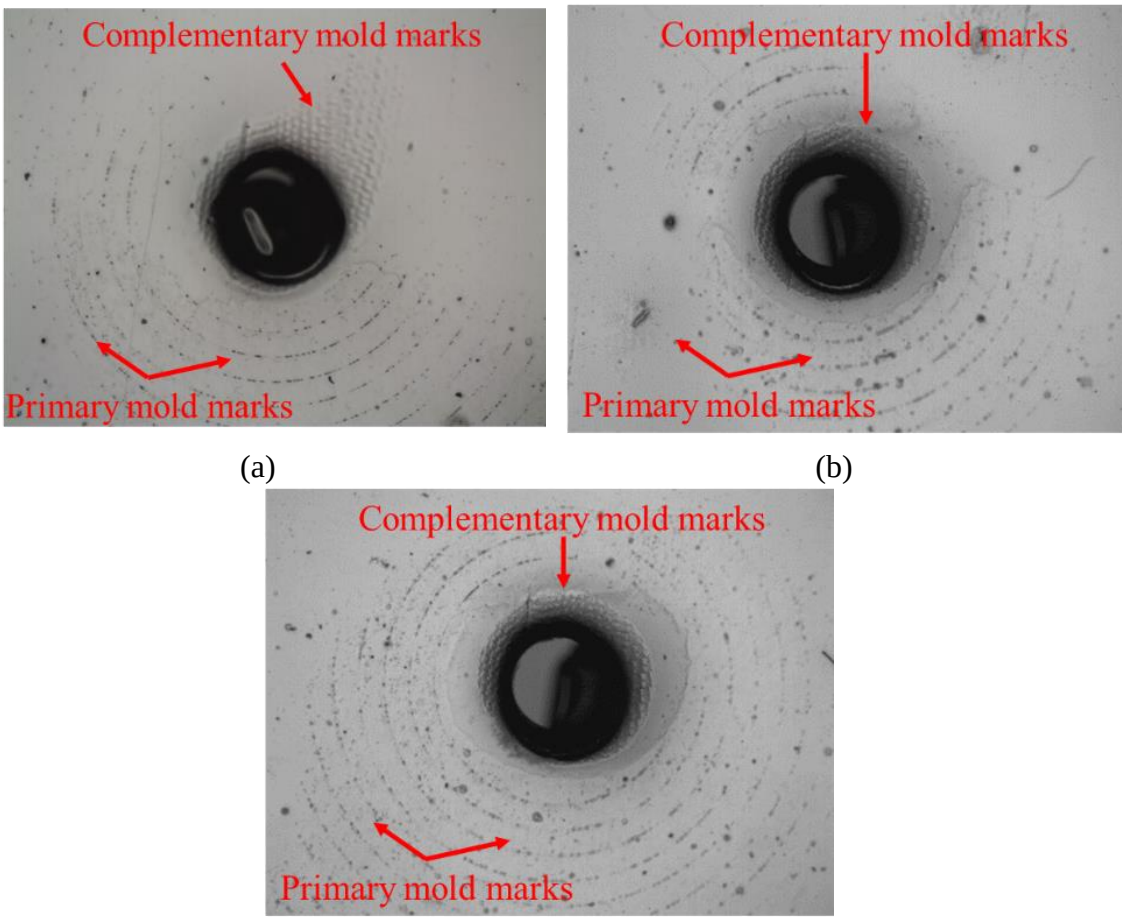

Figure 4.6. Optical micrographs at 2.5x10 of the top diameter of a partially complete through-hole that was fabricated with a clearance of 100 µm at locations of 10 (a), 20 (b), and 30 (c) mm.

An SEM image of a through-hole that was completed by excising the residual layer is shown in Figure 4.7. It was punched with a clearance of 100 µm at a location of 10 mm. Defects caused by the demolding of the substrate were present on the bottom-left quadrant of the top diameter (Fig. 4.7(a)). The remaining segment of the top diameter was uniform with minimal defects present on the edge and adjacent surface area. The dimension of the top diameter was 823 µm. When observing the bottom side, both the top and bottom diameters can be seen in Figure 4.7(b). The misalignment between the punch and die can

be inferred; since the location of the top diameter is biased towards the left side of the bottom diameter. In the area between the top and bottom diameters, the fractures that were generated when the residual layer was removed are visible. A significant defect is that a fragment of the residual layer is still present at the bottom-left quadrant of the bottom diameter. The size of the bottom diameter was 1066 µm, which is 243 µm larger than the top diameter.

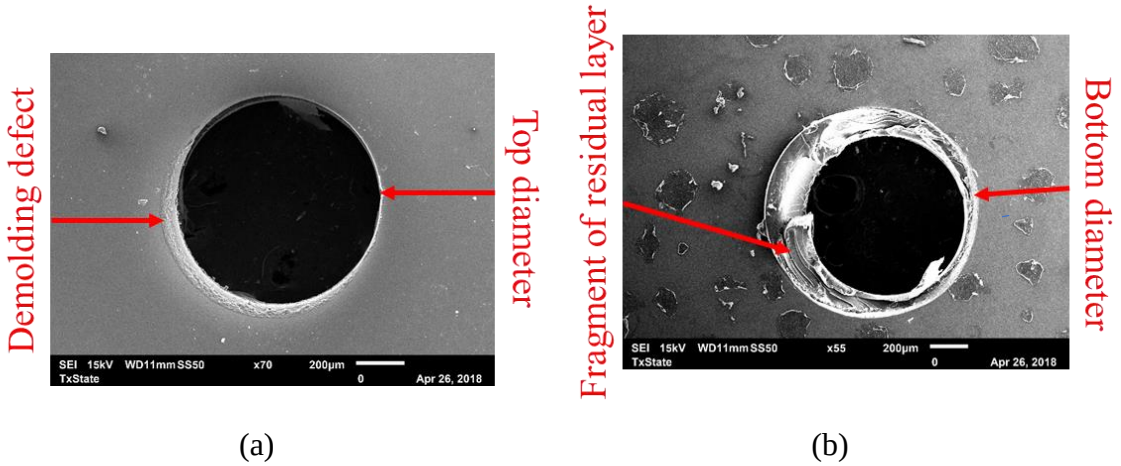

(a) (b)

Figure 4.7. SEM images of the top diameter (a) and the bottom diameter (b) of a complete through-hole fabricated with a clearance of 100 µm at 10 mm.

A typical partial through-hole with an attached residual layer that was bisected with scissors can be seen in Figure 4.8(a). It was punched with a clearance of 100 µm at a location of 20 mm. A rollover was present along the circumference of the top diameter, its depth was 128 µm and its diameter 1297 µm. The rollover then transitioned into the burnish zone, which was caused by friction between the sidewalls of the punch and substrate material. The height of the rollover and the length of the burnish zone were not consistent along the sidewall. On the right-side of the partial through-the burnish zone was diminutive

and directly transitioned into a fracture. On the left-side the burnish zone was protracted, and it separated the rollover and the fracture.

The opposite side of the partial through-hole that was bisected is shown in Figure 4.8(b). The depth of the burnish zone varied along the circumference of the top diameter. The length of the top fracture was approximately 307 µm. It transitioned to a fracture zone where the sidewall began to peel away from the substrate. Portions of the peeled sidewalls remained intact and formed a ridge that spanned the sidewall. Below the ridge, the sidewall transitioned to a coarse topography that terminated at the bottom diameter which was exposed by the removal of the residual layer.

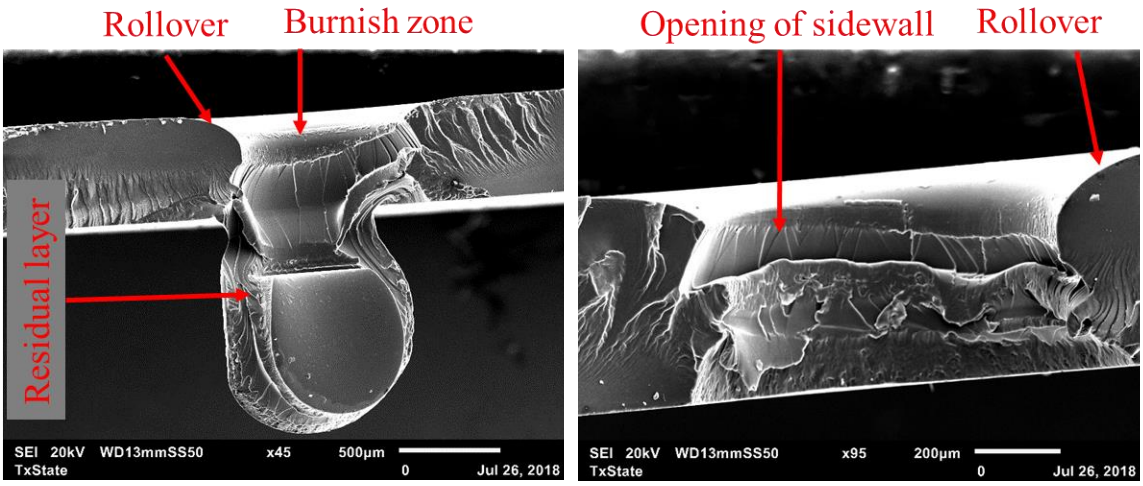

(a) (b)

Figure 4.8. SEM images of a bisected through-hole with the attached residual layer (a) and the opposite circumference (b).

4.3.3 Results with a Clearance of 200 µm

Optical micrographs at 2.5x10 of incomplete through-holes punched with a clearance of 200 µm were shown in Figure 4.9. The residual layers were intact, and they obstructed the bottom diameter. The distribution of machining marks was inconsistent over the three locations of 10 (a), 20 (b) and 30 (c) mm. The machining marks from the primary

mold insert are predominate on the surface adjacent to the bottom portion of the through-holes at all locations. Machining marks from the complementary mold inserts are prevalent adjacent to the top portion of the circumference and the immediate surface area that surrounds the bottom of the through-hole. From the top orientation a fracture can be observed.

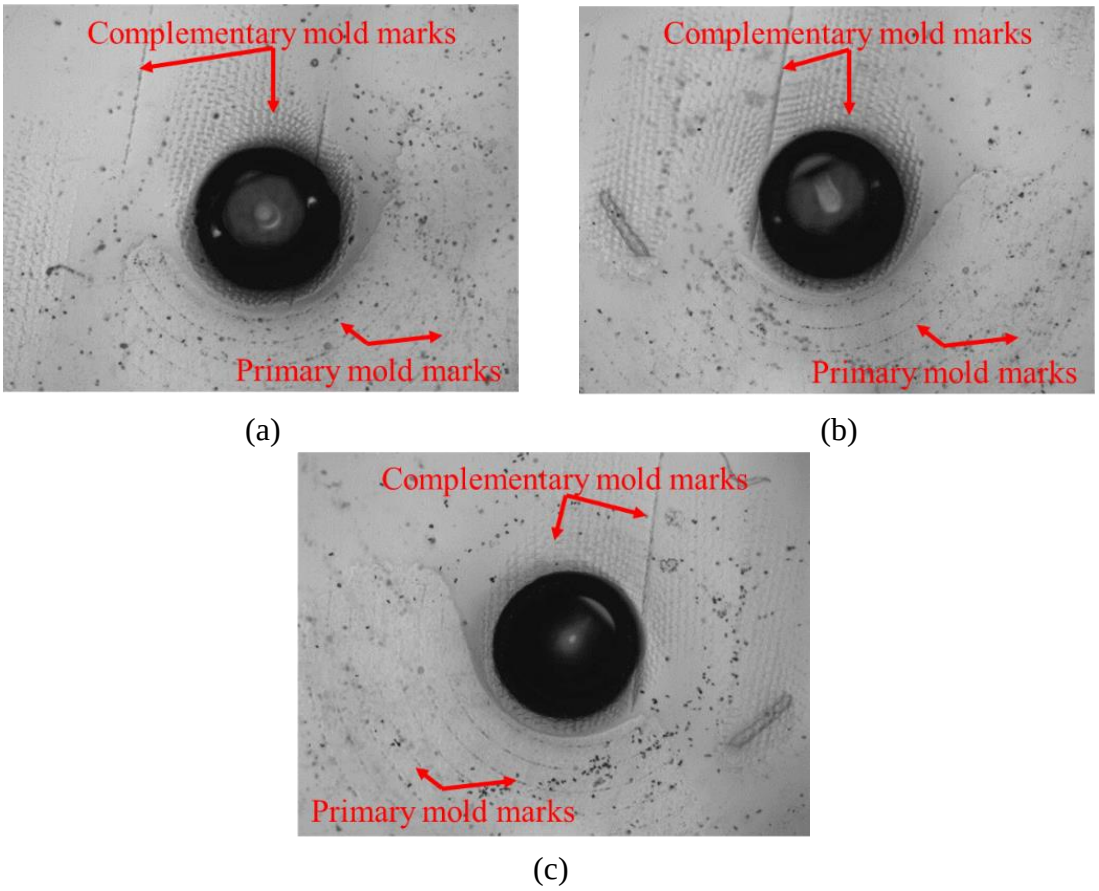

Figure 4.9. Optical micrographs at 2.5x10 of the top diameter of a partially complete through-hole that was fabricated with a clearance of 200 µm at locations of 10 (a), 20 (b), and 30 (c) mm.

SEM images of a typical incomplete through-hole that was punched with a clearance of 200 µm at a location of 30 mm were shown in Figure 4.10. The images showed the top diameter (a), the residual layer (b), and the sidewall of the residual layer (c). A

rollover encircled the top diameter which had a size of 857 µm, and a defect was present on the right-side of the circumference. The remainder of the circumference of the top diameter was uniform with minimal defects. The residual layer could be seen from the top orientation and a section of it was fractured from the substrate.

The sample was inverted to allow observation of the residual layer as shown in Figure 4.10(b). The residual layer was mostly intact, and the fracture was limited to the top-right quadrant. The residual layer protruded from the bottom surface of the substrate and was encircled by the impression left the die. The residual layer was formed into a post with a height of 775 µm and as shown in Figure 4.10(c).

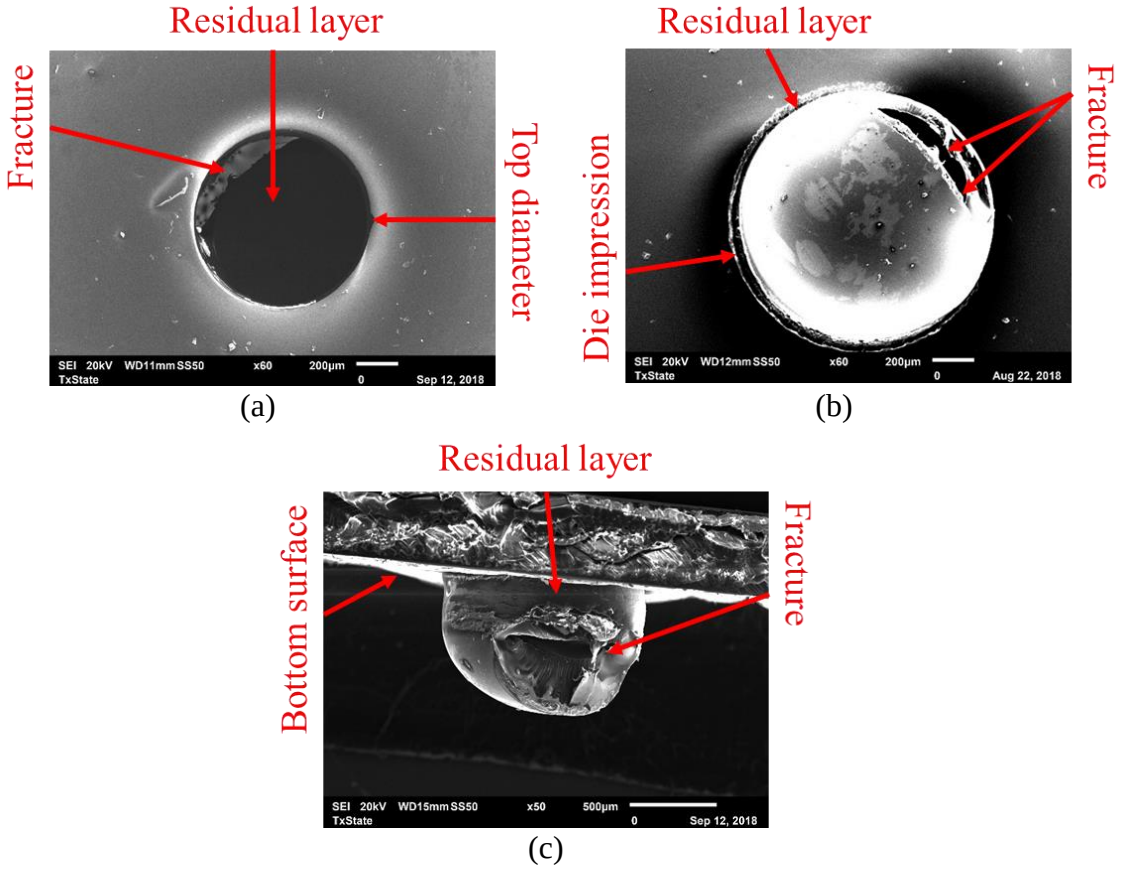

Figure 4.10. SEM images an incomplete through-holes fabricated with a clearance of 200 µm at 30 mm; showing the top diameter (a), bottom diameter (b), and sidewall (c).

4.3.4 Results with a Clearance of 300 µm

Optical micrographs at 2.5x10 of incomplete through-holes punched with a clearance of 300 µm are shown in Figure 4.11 The residual layers were intact, and the bottom diameters were obstructed. At locations of 10, 20 and 30 mm the machining marks from the primary mold insert were distinctive and encircled the top diameter of the through-holes. At 30 mm, the machining marks from the primary and complementary mold insert were distinctive and could be observed from the top orientation. The top diameter was encircled by the spiral machining marks from the primary mold insert. The areas that surrounded the bottom diameter were enveloped by the coarse machining marks.

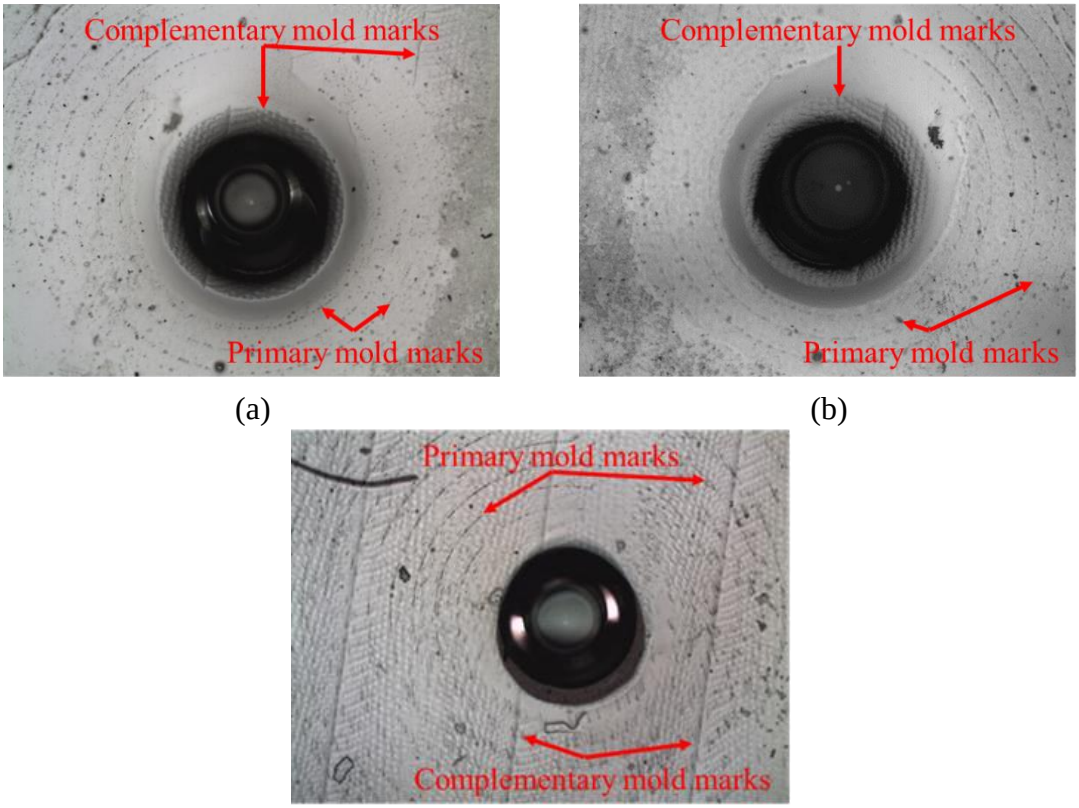

Figure 4.11. Optical micrographs at 2.5x10 of the top diameter of a partially complete through-hole that was fabricated with a clearance of 300 µm at locations of 10 (a), 20 (b), and 30 (c) mm.

Figure 4.12 shows SEM images of the top and bottom diameter of a typical incomplete through-hole fabricated with a clearance of 300 µm at 10 mm. The edge of the top diameter was inconsistent along the circumference. The left side of the circumference was uniform, and the edges had limited defects. On the right side, a portion of the circumference was depressed and formed a sloped edge. This caused two distinct edges to be visible on the top-right quadrant of the top diameter which had an approximate size 890 µm. The residual layer was present and could be seen from the top orientation. From the bottom orientation the residual layer could be described as a hemisphere-tipped post, and no fractures were present on the sidewalls. This post extended from the bottom surface of the substrate with a height of approximately 550 µm. It was surrounded by the impression generated by the die.

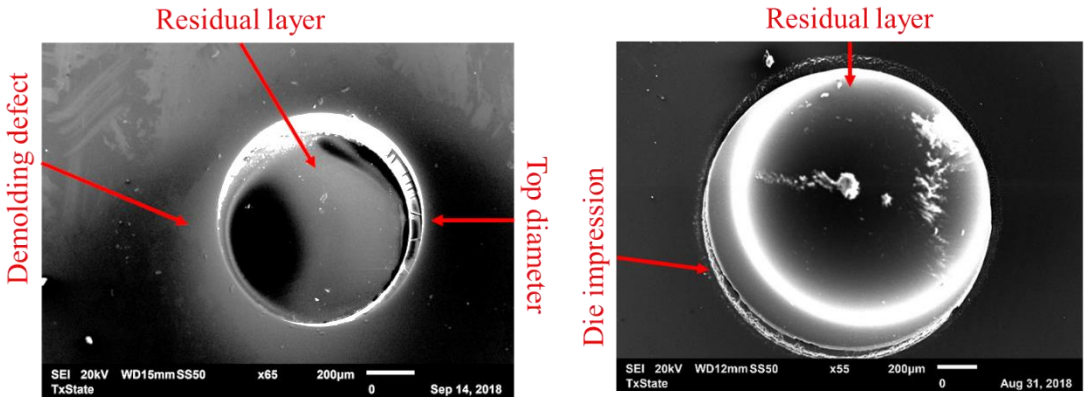

(a) (b)

Figure 4.12. SEM images an incomplete through-hole that was fabricated with a clearance of 300 µm at 10 mm; showing the top diameter (a) and residual layer (b).

4.3.5 Results with a Clearance of 400 µm

Optical micrographs of incomplete through-holes at locations of 10, 20, and 30 mm are shown in Figure 4.13. They were mechanically punched with a clearance of 400 µm. At the three locations the visibility of the transferred machining marks was distinct. At 10

(a) and 30 (b) mm only the spiral machining marks transferred from the primary mold insert were predominate and completely encircled the top diameter. At 30 mm (c) the trace marks from both the primary and complementary mold inserts were visible from the top orientation. This indicated that the pressure from the embossing cycle was more evenly distributed at larger displacements from the center of the mold inserts.

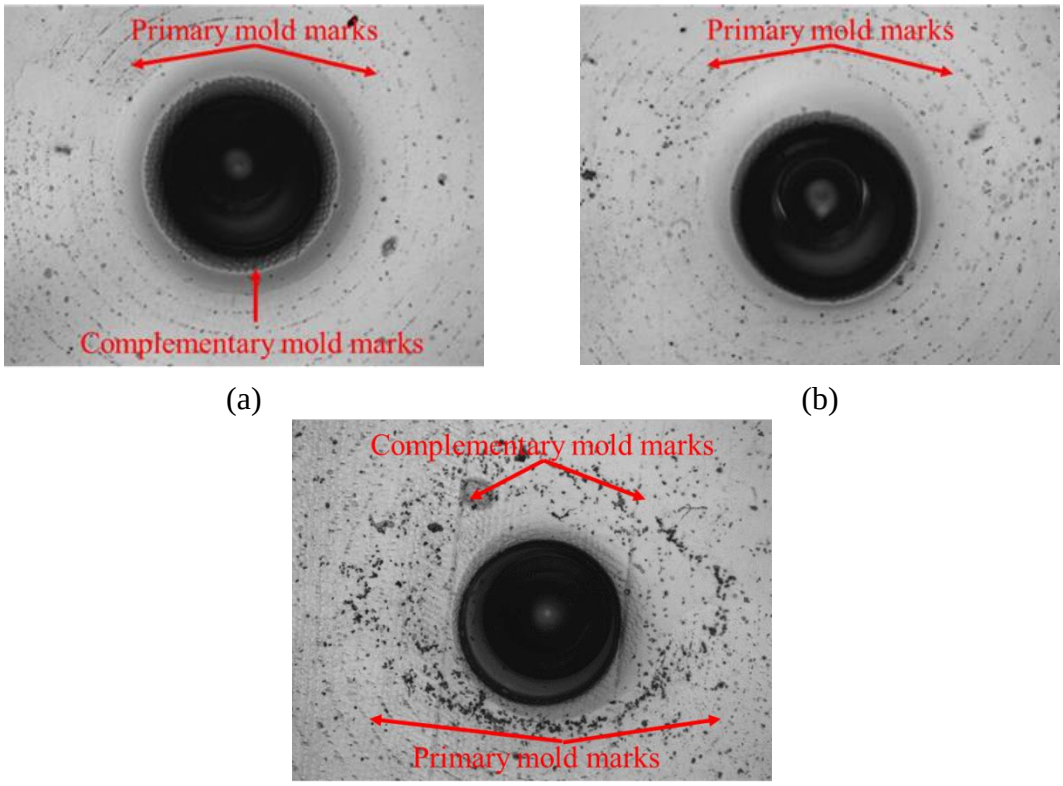

Figure 4.13. Optical micrographs at 2.5x10 of the top diameter of a partially complete through-hole that was fabricated with a clearance of 400 µm at locations of 10 (a), 20 (b), and 30 (c) mm.

An incomplete through-hole fabricated with a clearance of 400 µm at 30 mm was shown in Figure 4.14. The majority of the top diameter was distorted, and the distortion enlarged its circumference as shown in the SEM image of Figure 4.14(a). The distortion also generated two distinct edges of the top diameter, and the residual layer was visible.

The residual layer was drawn into a hemisphere tipped post that extended beyond the bottom surface of the substrate, as shown in Figure 4.14(b). These hemispheres tipped posts were common on the samples at the three locations. The posts tended to be rigid with no fractures present on the sidewalls. The machining marks from the complementary mold insert were visibly located on the peripheral areas that surrounded the post.

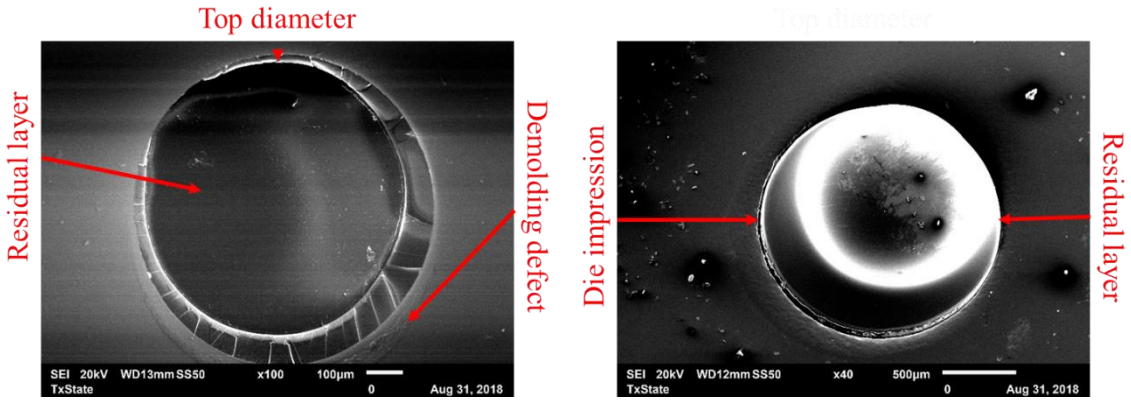

(a) (b)

Figure 4.14. SEM images an incomplete through-hole that was fabricated with a clearance of 400 µm at 30 mm; showing the top diameter (a) and residual layer (b).

4.4 Effect of Clearance

Clearance influenced the ability to generate a complete or a partially complete through-hole. The 50 µm clearance was able to fabricate a complete through-hole over all the samples. When the clearance was increased to 100 µm it produced complete or partially completed through-holes at locations of 10, 20, and 30 mm. Through-holes that were partially completed could be converted to a complete through-hole with a post processing step that was not invasive.

Mechanical punching with clearances of 200, 300, and 400 µm had limited success. When the clearance was 200 µm, only 14 out of the possible 36 through-holes were

partially completed. Only 7% of the through-holes were classified as partially completed after punching with clearance values of 300 and 400 µm. The remaining through-holes were incomplete with no fractures on the sidewalls of the residual layers. The residual layers were rigid, and an invasive post process would have been needed to remove them.

4.4.1 Effect of a 50 µm Clearance

The sidewall of the through-hole that was mechanically punched with a clearance of 50 µm can be used to infer the behavior of the PMMA. SEM images of the sidewall of a through-hole that was completed were shown in Figure 4.15. When the pin impacted the surface, it compressed the PMMA and forced it to flow into the die. This formed the rollover and caused the edge of the top diameter to curve. The pin then penetrated the surface of the PMMA and the friction between the pin and PMMA formed the burnish zone. A shear force separated the residual layer from the top portion of the through-hole and generated a shear zone that was approximately 375 µm in height. Reliefs were seen on the sidewall and could indicate the sections where PMMA was sheared from the substrate.

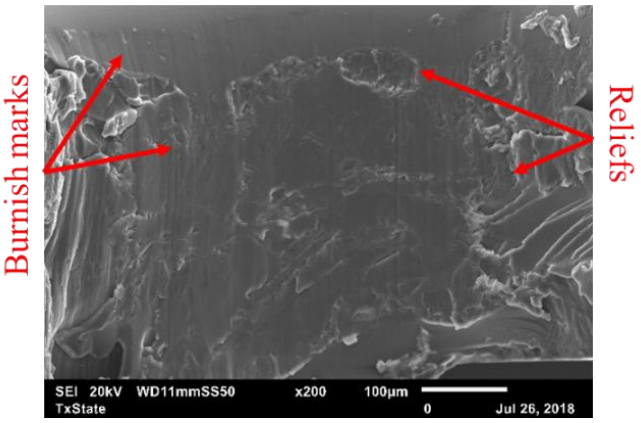

Figure 4.15. SEM image of the sidewall of a completed through-hole fabricated with a clearance of 50 µm at 0 mm, with indications of striations and reliefs.

When observing the bottom diameter of the through-hole its form was not consistent Figure 4.16. On the right side (Fig. 4.16(a)) a fragment of PMMA protruded from the bottom surface. On the left side (Fig. 4.16(b)) the edge of the bottom diameter was visible and had no fragments protruding from the bottom surface. This fracture extended into the through-hole by 81 µm, from the bottom diameter. The inconsistency of the edge was used to infer what occurred during mechanical punching. On the right side, the edge of the die generated a fracture which completely separated a portion of the residual layer from the substrate. This fracture did not progress or occur at all the points along the circumference as a fragment of the residual layer was still present on the left (Fig. 4.16(b)).

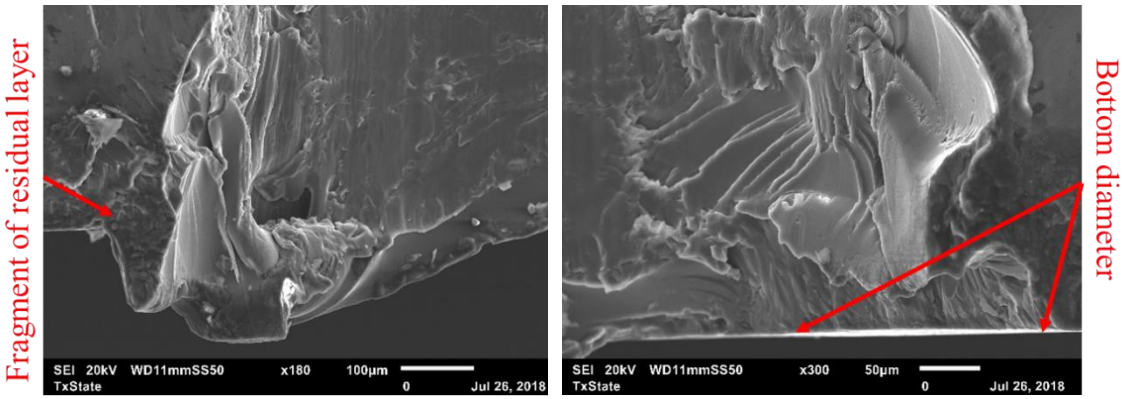

(a) (b)

Figure 4.16. The bottom portion of a complete through-hole fabricated with a clearance of 50 µm with the fragment of the residual layer (a) and the bottom diameter (b).

To the left of the fragment, an indentation created by the edge of the die was visible. This indicated that the die did not generate a fracture and the residual layer was connected to the substrate. The displacement of the pin and the pressure applied during hot embossing caused the residual layer to advance into the die. A fracture could have separated a portion of the residual layer from the substrate, which generated the remaining fragment as the pin continued to translate. Another possibility is that the residual layer did not fracture from

the substrate even after the pin was fully displaced. The residual layer could have been stripped during the demolding step since the fragments tended to be brittle.

4.4.2 Effect of a 100 µm Clearance

Figure 4.17 shows a through-hole that was partially completed with the residual layer still attached. Magnification was increased to better observe the topography of the sidewall. The pin impacted the top surface of the PMMA substrate and forced PMMA to flow into the die. This caused the formation of the rollover that was observable along the top diameter as shown in Figure 4.17(a).

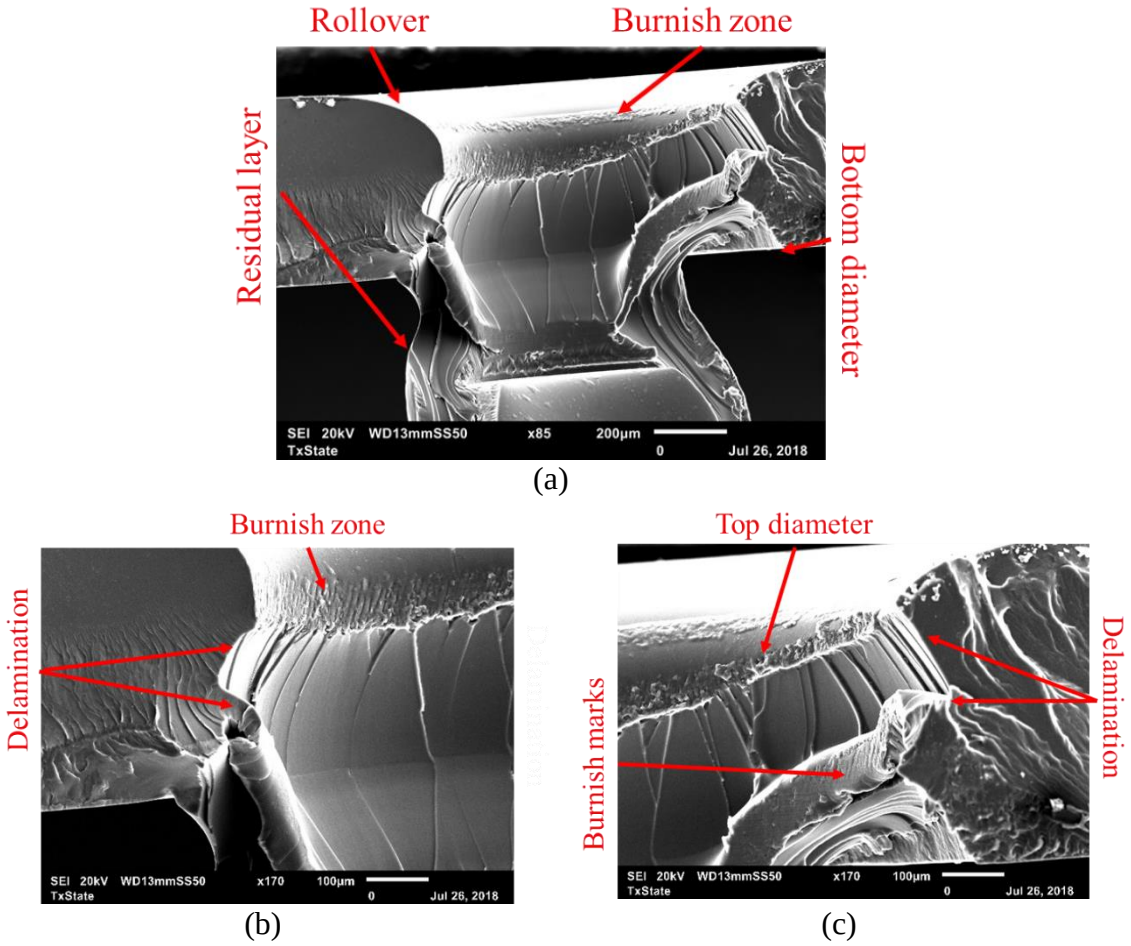

Figure 4.17. SEM images of a partially completed through-hole that was fabricated with a clearance of 100 µm (a), showing the defects of the sidewall along the circumference (b,c).

As the displacement of the pin increased, it penetrated the PMMA. Friction between the sidewalls of the pin and upper portion of the through-hole generated a burnished zone. This caused striations to be present on a portion of the sidewall as shown in Figure 4.17(b). A fracture was then generated, and it began to separate the residual layer from the substrate. As the fracture occurred, it transmitted into the sidewall. The sidewall began to yield which caused it to delaminate and caused it to taper outwards. This can be indicated by the matching fracture lines on the sidewall of the through-hole seen. The delamination formed a recess that was present along the circumference of the sidewall as shown in Figure 4.17(c). SEM images of the opposite portion of the partially complete through-hole and the sidewall near the bottom diameter were visible in Figure 4.18.

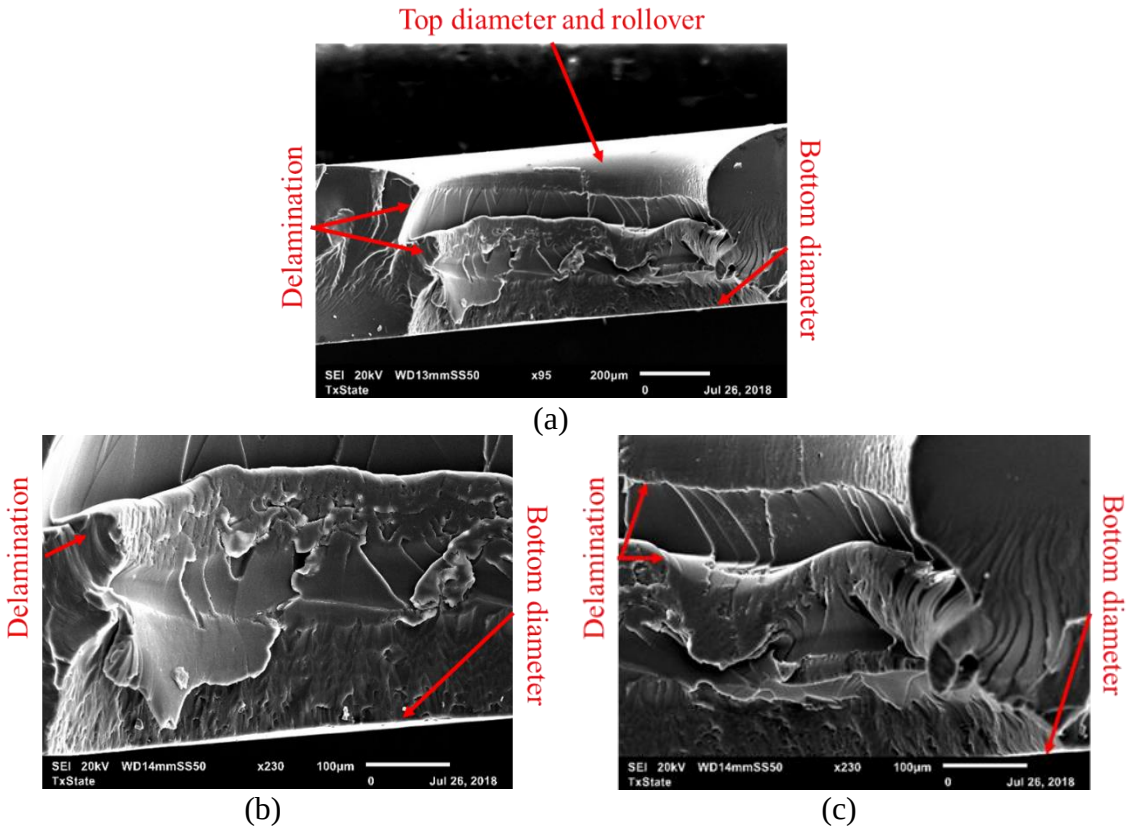

Figure 4.18. SEM images of a partially completed through-hole that was fabricated with a clearance of 100 µm (a), showing the defects of the sidewall (b,c).

The fracture zone showed the delamination of the sidewall and the formation of the pocket that spanned the through-hole. The edge of the ridge that formed the pocket showed the burnish marks and were comparable to the burnish on the top portion of the through-hole. The topography of the sidewall near the bottom diameter showed a different texture than the surfaces of the top portion of the through-hole. The shift in texture of the sidewall was likely the result of the fracture that generated the bottom diameter of the through-hole. The images showed that the fracture generated by the punch and the fracture generated by the die were able to intersect. Since the separate fracture lines were able to converge, the residual layer was removed.

Many of the through-holes generated with a clearance of 100 µm were partially completed with an attached residual layer. The residual layers were not removed by the mechanical punching process or stripped during the demolding step. The residual layers were removed with a post processing step. The inability to fracture and remove the residual layer during a process step may have been related to misalignment between the primary and complementary mold insert. An attached residual layer and the bottom diameter of the through-hole can be seen in the SEM image in Figure 4.19. Misalignment was observable as the top diameter was shifted upwards. Due to this shift, one section the clearance was reduced to approximately 54 µm, while in another section the clearance increased to approximately 125 µm.

During punching, the fracture that created the bottom diameter was initiated at the zone where the clearance was narrow. This caused the PMMA to fracture along the edges of the die. The fracture then prematurely terminated or did not occur at areas with a higher

clearance. In these areas the residual layer could not fracture and it caused the residual layer to remain attached.

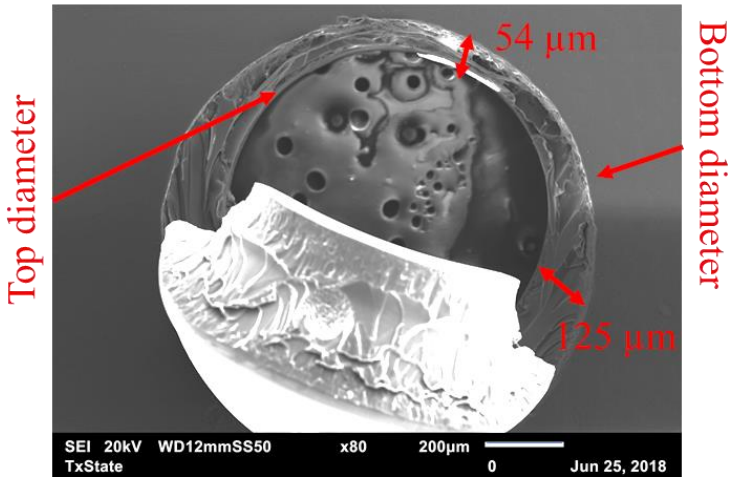

Figure 4.19. SEM images of a partially completed through-hole an attached residual layer that was fabricated with a clearance of 100 µm at 20 mm.

4.4.3 Effects of a 200, 300, and 400 µm Clearance

Figure 4.20 showed an SEM image of a partially completed through-hole that was fabricated with a clearance of 200 µm. It was observable that the residual layer began to separate from the substrate. The fragment that connected the residual layer to the substrate was brittle and could be removed. The bottom diameter of the through-hole was encircled by an impression of the edge of the die. It transitioned into the sidewall of the through-hole which extended into the top diameter of the through-hole.

The fracture of the residual layer, the bottom diameter, and the top diameter can be seen Figure 4.21. In Figure 4.21(a) from the top diameter, the sidewalls began to taper away from the center of the through-hole. The tapering likely occurred when the sidewalls began to delaminate due to increased displacement of the pin. The delamination then reached the bottom surface of the PMMA substrate and generated the fracture of the

residual layer. This behavior could also be seen from the SEM images of the residual layer of the partially completed through-hole as shown in Figure 4.21(b).

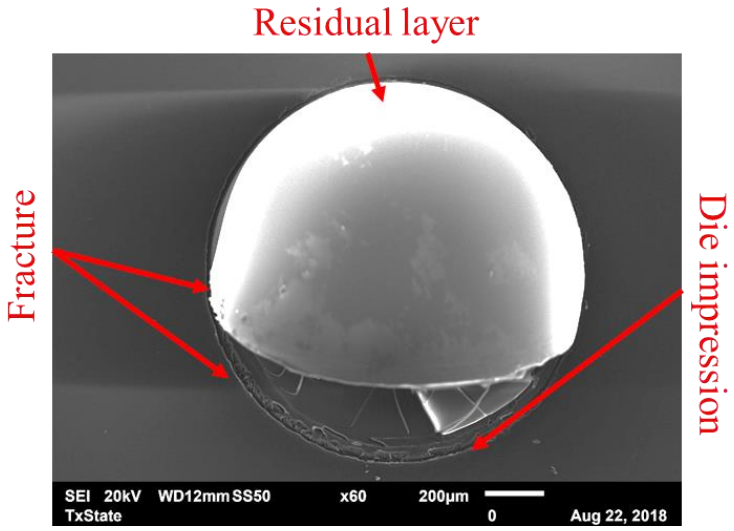

Figure 4.20. SEM images of a partially completed through-hole an attached residual layer that was fabricated with a clearance of 200 µm at 20 mm.

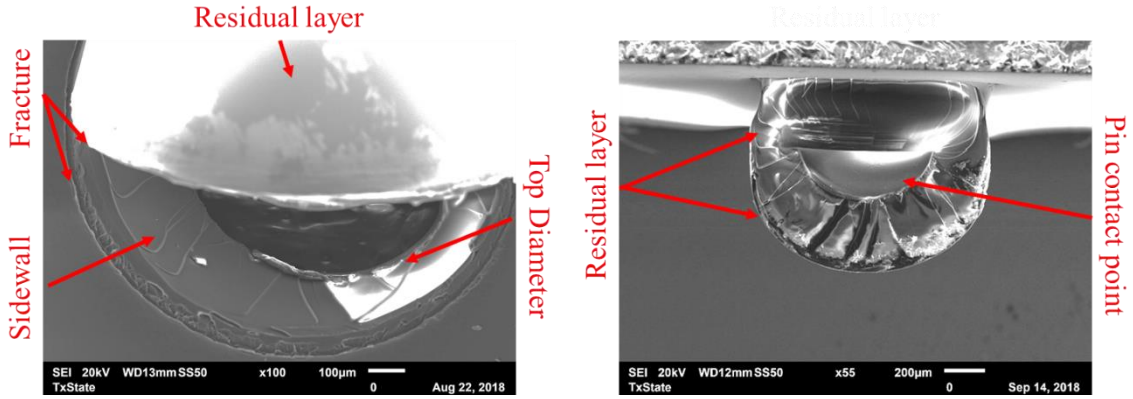

(a) (b)

Figure 4.21. SEM images of a partially completed through-hole an attached residual layer that was fabricated with a clearance of 200 µm at 20 mm showing the through-hole (a) and a perpendicular view of the fracture (b).

The section where the pin impacted the PMMA was visible. Below the point of contact, the sidewall of the residual layer showed a taper that extended to the bottom. The topography of the sidewall that was tapered is comparable to the sidewall of the through-

hole. This indicated that the PMMA delaminated starting at the contact point between the pin and substrate. It travelled on a bias to the bottom of the sample which caused the residual layer to fracture.

4.4.4 Formation of Incomplete Through-Holes

When clearance was above 100 µm the formation of a complete or partially completed through-hole was limited as only 19 partial through-holes were generated. The sidewalls of typical incomplete through-holes that were mechanically punched with clearances of 200 (a), 300 (b), and 400 (c) µm are shown in Figure 4.22.

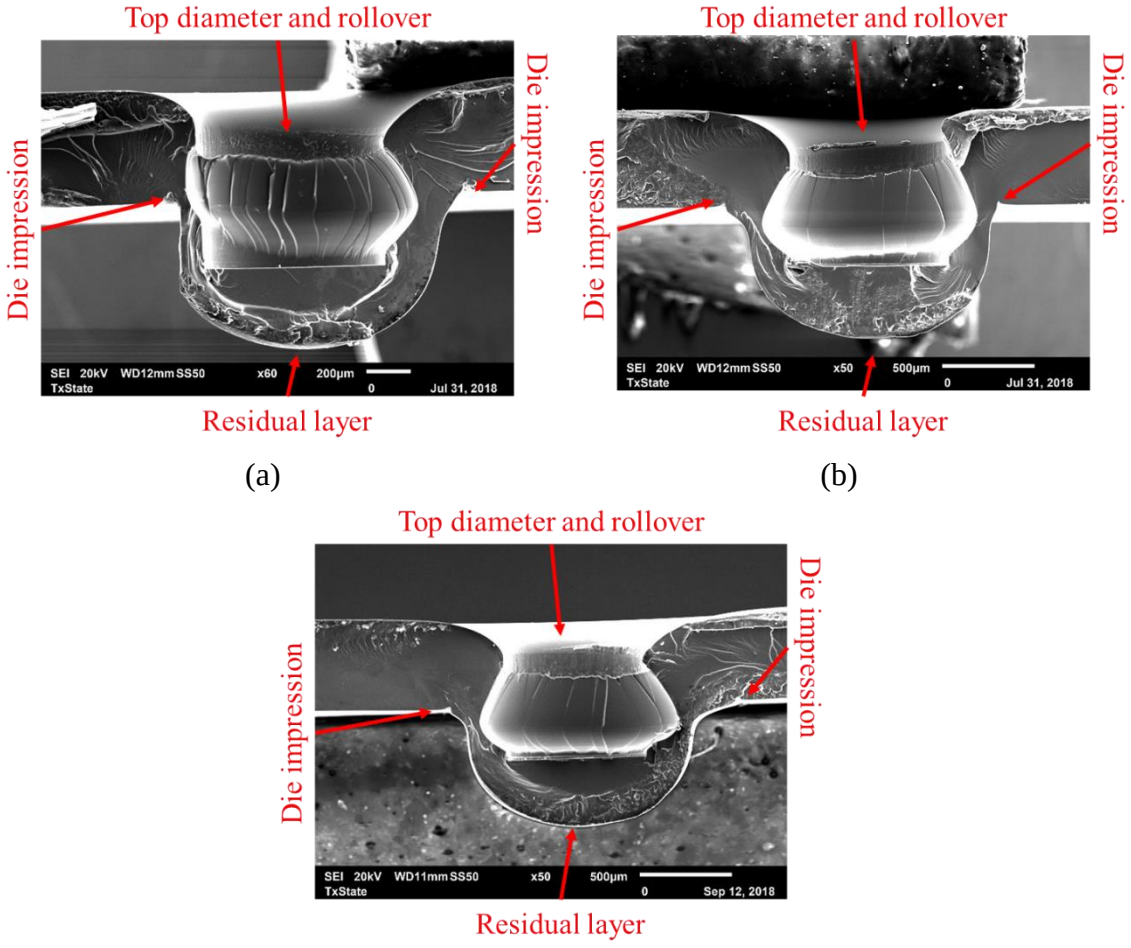

Figure 4.22. SEM images of the sidewalls of incomplete through-holes fabricated with clearance of 200 (a), 300 (b), and 400 (c) µm and the resulting hemisphere tipped post.

The behavior of the PMMA was similar when the three levels of clearance were used. The samples were bisected to allow for better observation of their sidewalls. In a typical sample, the rollover was seen on the circumference of the top diameter and it was formed by the impact of the pin. After the pin penetrated the surface, friction between the PMMA and the sidewall of the pin formed the burnish zone. A fracture generated, and it separated the residual layer from the burnish zone. As the displacement of the pin increased, the sidewall of the through-hole began to delaminate. When the wall delaminated, the sidewall began to taper, and the diameter of the hole increased. The movement of the pin stopped when the primary mold insert contacted the top surface of the PMMA substrate.

At this point the pin displaced 0.8 mm and it should have exited the from the bottom surface of the PMMA. The fracture that would have generated the bottom diameter did not occur when punching clearances of 200, 300, and 400 µm. This was evident as the point of contact between the edge of the die and the PMMA were still visible. Since the fracturing of the bottom diameter did not occur, the residual layer could not be removed, and the hole was incomplete. The pressure from the hot embossing process forced the PMMA to advance into die and displace the residual layer from the substrate. This formed the residual layer into a hemisphere tipped post; the posts in the images were approximately 0.65 (a), 0.70 (b), and 0.66 (c) mm.

4.4.5 Formation of Partial Through-holes with Clearances of 200, 300, and 400 µm

The bottom side of a partial through-hole that was mechanically punched with a clearance of 400 µm was shown in Figure 4.23. In the image, the attached residual layer, the bottom diameter, and the impression that was generated by the edge of the die could be

seen. A significant observation was the location of the bottom diameter with respect to the impression generated by the die. The circumference of the bottom diameter was displaced from the die impression by approximately 200 µm. This indicated that the bottom diameter may have formed independently from the edge of the die. On the sidewall of the through-holes striations were visible and they spanned the length. This meant a delamination traveled to the bottom of the substrate and partially separated the residual layer.

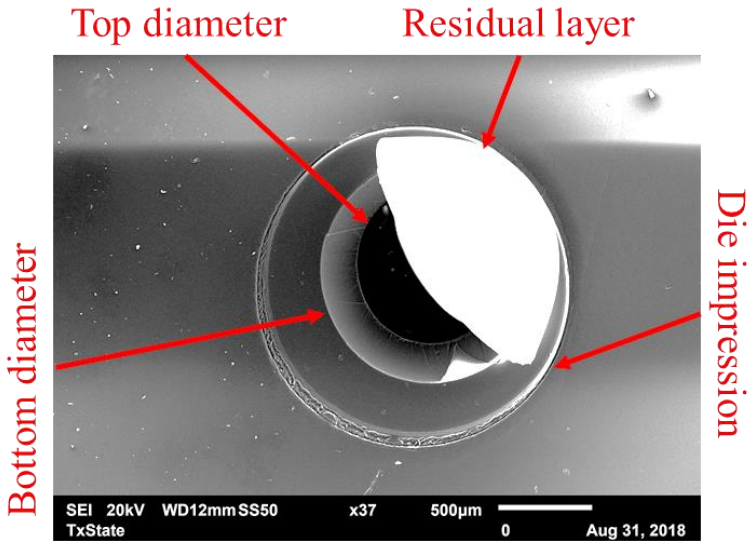

Figure 4.23. SEM images of the sidewalls of partially complete through-holes fabricated with clearance of 400 µm at a location of 30 mm.

One reason that a through-hole could be fabricated at a larger clearance could have been the uneven distribution of the embossing pressure. Partial through-holes generated with clearances of 300 and 400 µm were limited to locations further from the center of the mold. The two partial through-holes generated with a clearance of 300 µm were located at 30 mm from the center of the mold. When clearance was 400 µm, two partial through-holes were located at 30 mm and one was located at 20 mm.

Optical micrographs of the surface areas of through-holes that were located at 20 and 30 mm showed more distinct machining marks that were transferred from the

complementary and primary mold inserts. This indicated that these areas experienced an embossing force that was more consistent than at other areas. The embossing step typically compressed the PMMA substrate by 30 μm. This meant that the pin was able to displace an additional 30 μm into the substrate material. The additional displacement caused by this compression could have allowed the residual layer to fracture from the substrate.

4.4.6 Characterization

To observe the effect of clearance, the top diameter, bottom diameter, rollover diameter, and rollover height of completed through-holes were measured. The top diameter and bottom diameter were measured with the measurescope and the DRO at a magnification of 5x10. The point where the flat surface of the sample transitioned into the rollover were located using the measurescope at magnification 5x10. The distance between two transition points was measured with the DRO. The rollover height was measured with a focus-defocus method. First the measurescope was focused on the flat surface that surrounded a through-hole. The focal distance was lowered until the edge of the top diameter was visible. The change in focal length was recorded by the DRO. The average dimensions were reported with the 95% confidence interval.

4.4.7 Dimensions of Completed Through-Holes

The average top and bottom diameters of through-holes that were completed are summarized in Figure 4.24. The average top diameter was consistent over the five levels of clearance. It ranged from 0.82 to 0.84 mm and the ranges of the confidence intervals were 0.01 to 0.07 mm. The significant confidence level at clearance of 300 μm was caused by the small sample size; only two complete through-holes were generated. The bottom diameter showed more variation in their average size. As the size of the clearance

increased, the size of the bottom diameter increased. After 200 µm the bottom diameters were more consistent and did not show any increases. When clearance was 50 µm the average bottom diameter was 0.99 mm and for a clearance of 100 µm the average measurement was 1.01 mm. With clearances of 200, 300, and 400 µm the bottom diameters were comparable. Their averages were 1.1 to 1.2 mm and varied by 0.02 to 0.03 mm.

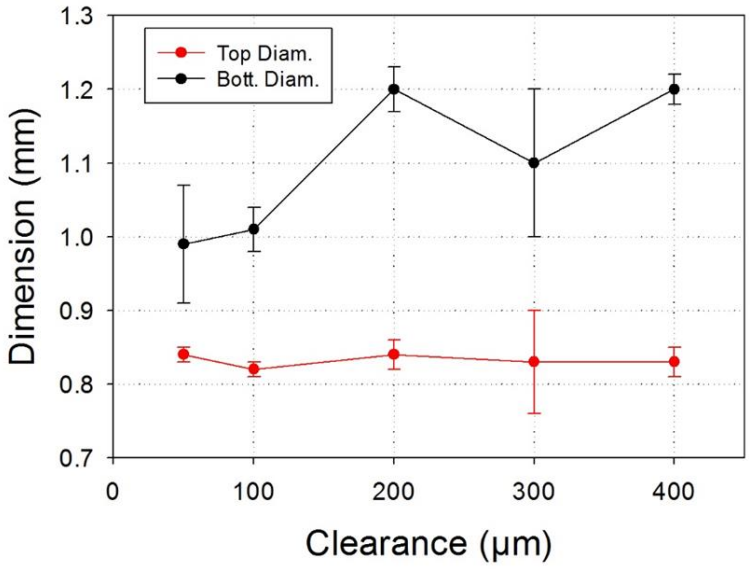

Figure 4.24. The average size of the top and bottom diameter.

The measurements showed that the size of the bottom diameter was greater when compared to the top diameter, typically by 150 to 400 µm. The sizes of the bottom diameters were comparable to the diameter of the die that was applied. For example, the die that provided a clearance of 100 µm had a diameter of 1.0 mm. When it was applied, it generated an average bottom diameter of 1.01 mm. From the SEM images it was observed that the fracture on the bottom surface occurred adjacent to the edge of the die when clearance was 50 and 100 µm. Therefore, the die could impart its physical dimensions to the bottom diameter of the through-hole. Micro mechanically punched through-holes with

variation between the top and bottom diameters have been reported by Joo et al. (2005) and Chern et al. (2006) for metallic foils, Rhim et al (2006) for polymers and ceramics.

An discrepency arises when observing the bottom diameters of the complete through-holes that were fabricated with clearances of 200, 300 and 400 µm. At these levels of clearance, the bottom diameters that were produced had comparable average diameters of 1.2 mm. For clearances of 300 and 400 µm the size of the bottom diameter was anticipated to be in the proximity of 1.4 and 1.6 mm, respectively. Instead, the completed through-holes had bottom diameters that were significantly less than the diameter of their respective dies. Their diameters were typically smaller by 0.3 to 0.4 mm. This can be attributed to the inability of the die to generate a secondary fracture. The SEM images (Fig 4.23) showed that only one fracture of the residual layer occurred, and it was independent of the edge of the die. Since the die could not produce a secondary fracture it could not impart any of its physical dimensions to the bottom diameter of the through-hole.

The generation of the rollover was caused when the substrate material was drawn into the clearances between the sidewalls of the punch and die. When clearances were increased, more material could flow into the die and the height and diameter of the rollover increased. The average diameter and height of the rollovers of completed through-holes are shown in Figure 4.25. The rollover diameter created by clearances of 50 and 100 µm were comparable at 1.1 mm each. As clearances increased from 200 to 400 µm, the diameter of the rollover increased. The through-holes fabricated with a clearance of 400 µm had the largest rollover at 1.8 mm. There was a positive correlation between the rollover height and the size of the clearance. The dimensions of rollover were reported by Rhim et al. (2005) and Xu et al. (2012) to be dependent on the sizes of the clearance.

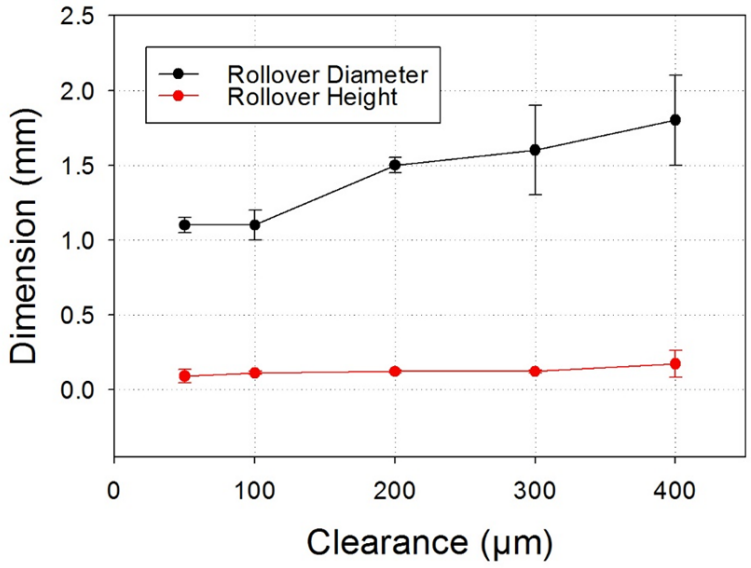

Figure 4.25. The average size of the diameter and height of the rollover.

The depth and diameter of a rollover may not have been consistent over the surface area of the top diameter of the through-hole. A cause of this could have been the misalignment between the pin and die. If misalignment was present, the clearances would have been inconsistent. Quadrants of the through-hole may have had a wider clearance zone, while other quadrants would have had a narrower clearance zone. This would have affected how much substrate material could have been drawn into the die and would ultimately affect the consistency of the rollover. It would present a challenge when accumulating modular devices in a stacked assembly. As devices are interconnected rollover could create an additional gap or cause misalignment between the outlet and inlet of devices. Dead volumes could be generated as fluids become entrapped in between the devices. Insufficient flow of fluids could lead to a less reliable analytical techniques.

4.5 Conclusion

Clearance was shown to have a critical effect on the mechanical punching process. The primary effect in the study was it dictated the generation of the bottom diameter. Which

was generated as the residual layer fractured and was separated from the bottom of the substrate. When clearance was 50 μm, it produced completed through-holes that had a shear zone that spanned most of the sidewall. When clearance was 100 μm, it could produce a through-hole that needed to be post-processed to become complete. The sidewall of these holes was damaged as the mechanical punching process generated different regimes of textures and artifacts. With a clearance of 50 and 100 μm the size of the bottom diameter was comparable to the diameter of the respective die. Mechanical punching with clearance of 200, 300, and 400 μm had limited success in producing complete or partial through-holes. The limited success was due to the inability of the die to generate the fracture which should propagated from the bottom of substrate. Instead, a fracture generated from the top and propagated to the bottom diameter. With one fracture generated it created a bottom diameter with a typical size of 1.2 mm.

The optical micrographs show the embossing force was not consistently applied on the top and bottom surfaces. Machining marks from both the primary and complementary mold inserts were more distinct at locations of 30 mm. The force applied during the embossing process was not evenly distributed over the surface of the polymer substrate. Through-holes at larger radial distances from the center of the mold inserts experienced a consistent force from the mold insert. It indicated that the embossing force was not fully applied until the top surface of the PMMA contacted the top surface of the primary mold. This would mean the pin fully penetrated the substrate. This could mean that a complete or incomplete through-hole was formed before the embossing force was applied.

5. NUMERICAL MODEL OF MICRO- MECHANICAL PUNCHING

5.1 Introduction

In this chapter the micro-mechanical punching process was modeled with the Finite Element Analysis (FEA) software package DEFORM-2D (Scientific Forming Technologies Corp., Columbus, OH). FEA is a useful tool for simulating the interactions between tool geometries, material properties, and process parameters. The micro-punching process was modeled to show the effects of clearances of 50, 100, 200, 300, and 400 μm. The behavior of the PMMA was observed at different stages of the mechanical punching process and during the hot embossing phase. The predicted through-holes were compared to the experimental results.

5.2 Numerical Modeling of PMMA Behavior

During thermoforming processes, PMMA is generally treated at a temperature above its T_g of 105 °C. As it surpasses its T_g, PMMA will transition from a rigid, brittle solid to a viscoelastic plastic. In this softened state the polymer will become malleable and will begin to flow as pressure is applied to it using master molds. Agrawal et al. (2010) investigated and defined the thermo-mechanical properties of PMMA. When temperature is elevated mechanical properties such as Young's Modulus and Ultimate tensile strength will decrease. When those mechanical properties are reduced, the PMMA can experience greater strain before fracturing. This change in mechanical properties and behavior with respect to temperature needs to be defined for reliable numerical modeling.

Flow stress is defined as the stress needed to keep a unit of viscoelastic material in a state of steady, plastic deformation (Bowden, 1972). In ductile materials, the flow stress is a significant parameter for fatigue failures. Previous work by Gomez (2015) and Juang

(2008) defined the flow stress of PMMA in a temperature range of 25 to 250 °C. When PMMA was at an ambient temperature the flow stress was approximately 85 MPa. This means the fluidic resistance is high thus more significant force is needed to cause it to flow. When its temperature increased to 95 °C the flow stress of PMMA drop significantly to approximately 5.5 MPa. When T_g is surpassed the flow stress of PMMA was less than 1 MPa. As the temperature is increased, the fluidic resistance of PMMA will reduce. It will be more susceptible to pressure which could cause it to flow if the pressure is constant.

5.3 Fracture Criteria in Numerical Models

Damage in a simulation is the probability that a ductile fracture will occur, and its model is selected during the pre-processing stage of the simulation (STFC, 2014). The damage factor (D_f) during a simulation can be calculated by Equation 5.1, where σ^* is the maximum principal tensile strength, σ is the effective stress, and $d\varepsilon$ is the effective strain increment. The routines of the simulations will compare the values of D_f to the user-defined critical damage value of the numerically modeled substrate material. Damage or a fracture is predicted when the calculated values of D_f surpasses the user-defined critical value of damage. When the critical damage value is surpassed, the fractured material can be deleted from the environment by the software.

$$D_f = \int {\sigma^*}/{\sigma}\, d\epsilon \tag{5.1}$$

Cockcroft and Latham (CL) is the default model for calculating fracture in a numerical environment and is suitable for materials under tension (SFTC, 2014). Damage is a function of the accumulated values of the maximum principal stress and the differential plastic strain of the material (Mirghasemi, 2018). The routine version of CL is defined by Equation 5.2, where σ^T is the maximum principal stress, and $d\varepsilon^P$ is the differential of the

plastic strain. When CL exceeds the critical value of the substrate material, a fracture will be predicted. CL is particularly used for the prediction of tensile ductile fractures but may not be applicable to modeling fracture caused by compression (Comaneci et al., 2012; STFC, 2012)

$$CL = \int \sigma^T d\varepsilon^p \tag{5.2}$$

The Normalized Cockcroft and Latham (NCL) is shown in Equation 5.3 where σ^T is the maximum principal stress, $\bar{\sigma}$ is the effective stress, and $d\varepsilon^P$ is the differential of the plastic strain. Dividing the maximum principal stress by the effective stress will normalize the damage value. When the NCL value surpasses the defined critical value, a fracture can be predicted by utilizing the numerical model. The NCL model is suitable for estimating fracture behavior caused by shearing (Mahesh). It was selected as the fracture criteria to numerically simulate the micro-punching process of a PMMA substrate.

$$NCL = \int {\sigma^T}/{\bar{\sigma}}\, d\varepsilon^p \tag{5.3}$$

5.4 Simulation of Micro-Mechanical Punching

Figure 5.1 shows a punch, die, and PMMA substrate modeled along an axisymmetric boundary. The 2D model was generated with the pre-processer in DEFORM-2D. Modeling with an axisymmetric boundary is possible for environments where the geometries are symmetrical. By doing so, it will reduce the computational loads and solution time by limiting the densities of the elements. The punch was modeled as 0.4 x 0.8 mm, and the PMMA substrate was 0.5 x 10 mm. The dimensions of the pin and PMMA substrate were constant for all simulations. To generate five levels of clearances, the die

was varied; the sidewall of the die was displaced from the axisymmetric boundary by 0.45, 0.5, 0.6, 0.7, and 0.8 mm. The depth of the die was constant at 2 mm.

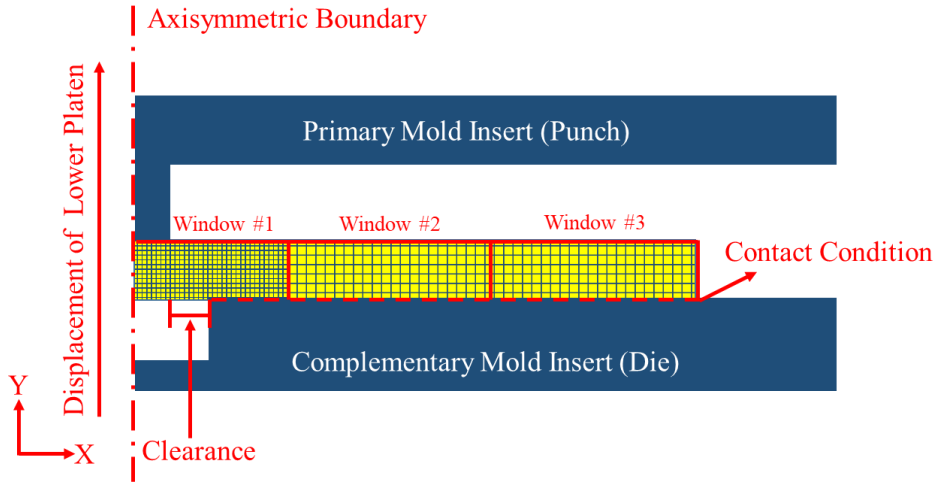

Figure 5.1. Axisymmetric model of the micro-mechanical punching process showing geometries and mesh windows.

Since the proposed model only considers a single pin and die, the portion of PMMA closest to the axisymmetric boundary is of most interest. The PMMA substrate was divided into three sections with different element sizes. The 15 µm element size was applied to the portion of PMMA that interacted with punch and die features (Soderberg, 2006). When progressing away from this area the elements were increased to 30 and 45 µm, The PMMA was divided into a total of 6846 square-elements. The number of elements per mesh window is summarized in Table 5.1. The critical value was set to 0.45 (Gomez, 2015).

Table 5.1. Distribution of elements.

Mesh Window	Window Length (mm)	Element Size (µm)	Total Elements
#1	1.7	15	3778
#2	3.3	30	1833
#3	5.0	45	1235

The complementary mold insert was set to translate in the positive Y-direction at a rate of 0.0084 mm/sec. It was assumed that the molding process was isothermal; the temperatures of the PMMA, and the punching tools was set to 120 °C. A sticking condition was applied to between the PMMA and the complementary mold insert, to prevent separation.

5.5 Results of the Simulations

5.5.1 Flow Behavior of PMMA

The distribution of stress during the impact phase of a mechanical punching step is shown in Figure 5.2. The pin displaced 0.05 mm into the top surface of the PMMA with the five different levels of clearance.

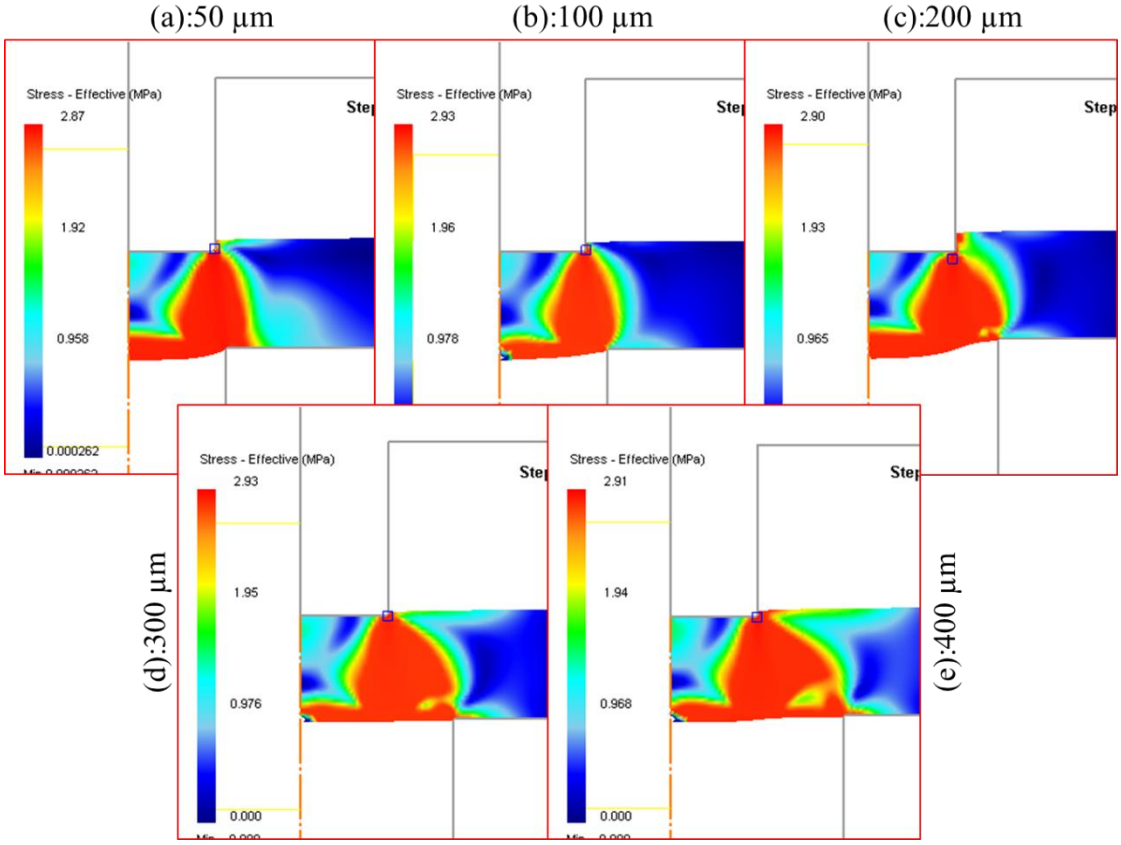

Figure 5.2. The evolution of effective stress at a die displacement of approximately 0.05 mm with clearances of (a) 50, (b) 100, (c) 200, (d) 300, and (e) 400 µm.

The impact of the pin compressed the PMMA at the initial point of contact. This caused PMMA on the bottom side to flow into the die, which caused its surface to become round. Clearance was observed to influence the distribution of the effective stress. At clearances of 50 (a), 100 (b), 200 (c), 300 (d), and 400 (e) µm, the effective stress was localized in between the edges of the pin and die (Achouri et al., 2014). The width of the stress band increased with clearances and it approximately 3 MPa.

Figure 5.3 shows pins that displaced approximately 0.10 mm into the surface of the polymer. The pin penetrated the surface of the PMMA and formed the top diameter with rollover present on its edge.

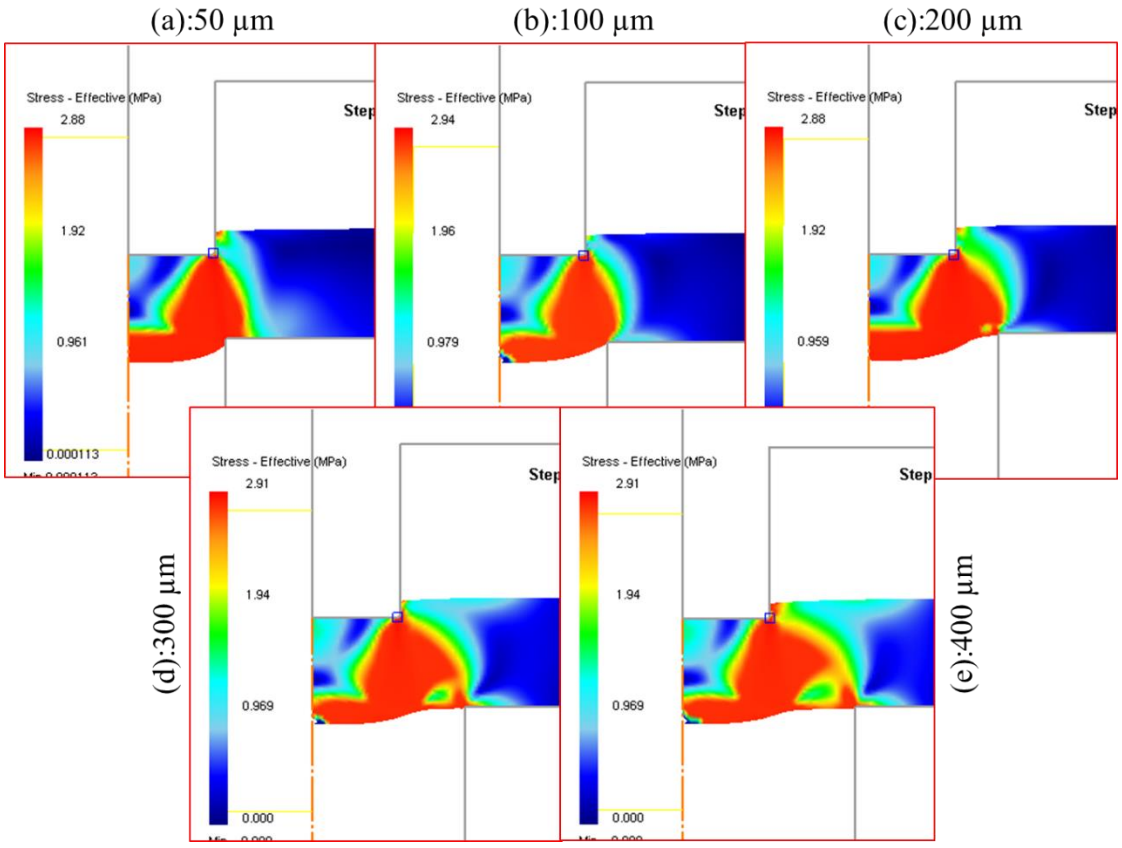

Figure 5.3. The evolution of effective stress at a die displacement of approximately 0.1 mm with clearances of (a) 50, (b) 100, (c) 200, (d) 300, and (e) 400 µm.

The vertical displacement of the die and substrate caused the PMMA to advance up the sidewall of the pin and into the die. The friction between the sidewall of the pin and the PMMA generated stress. The increased stress on the PMMA could indicate the formation of the burnish zone. The stress then propagated into the surfaces areas that surrounded the edge of the top diameter. The areas of the substrate were placed under tension which was caused by the bulk displacement of the PMMA substrate and the friction between the sidewall of the pin and the PMMA. The clearance allowed this portion of PMMA to flex around the edge of the die and began to increase the dimensions of the rollover. Damage values in these simulation steps ranged from 0 to 0.26 which is below the critical damage value of 0.45.

Figure 5.4 shows the effective stress after the substrate had displaced approximately 0.25 mm, 50% of the thickness of the sheet. At clearance of 50 (a) and 100 (b) μm it was observed that effective stress on the PMMA in the clearance zone relaxed. The stress than began to evolve in the residual layer and in the side walls of the through-hole. For clearances of 200 (c), 300 (d), and 400 (e) μm the stress was maximized in the areas below the edge of the pin and adjacent to the edge of the die. In the areas where stress was relaxed, the damage factors when clearance was 50 and 100 μm were approximately 8.8 and 7.2, respectively. By comparison at clearances of 200, 300, and 400 μm the damage factor was 0. This indicated that PMMA mechanically punched with clearances of 50 and 100 μm were fracturing during these steps. This can be observed in the model as reliefs were formed in the sidewalls of the through-holes and the bottom diameter of the through-holes were generated (Soderberg, 2006). Under the larger clearances the PMMA was still flowing into the die and no fracture was predicted.

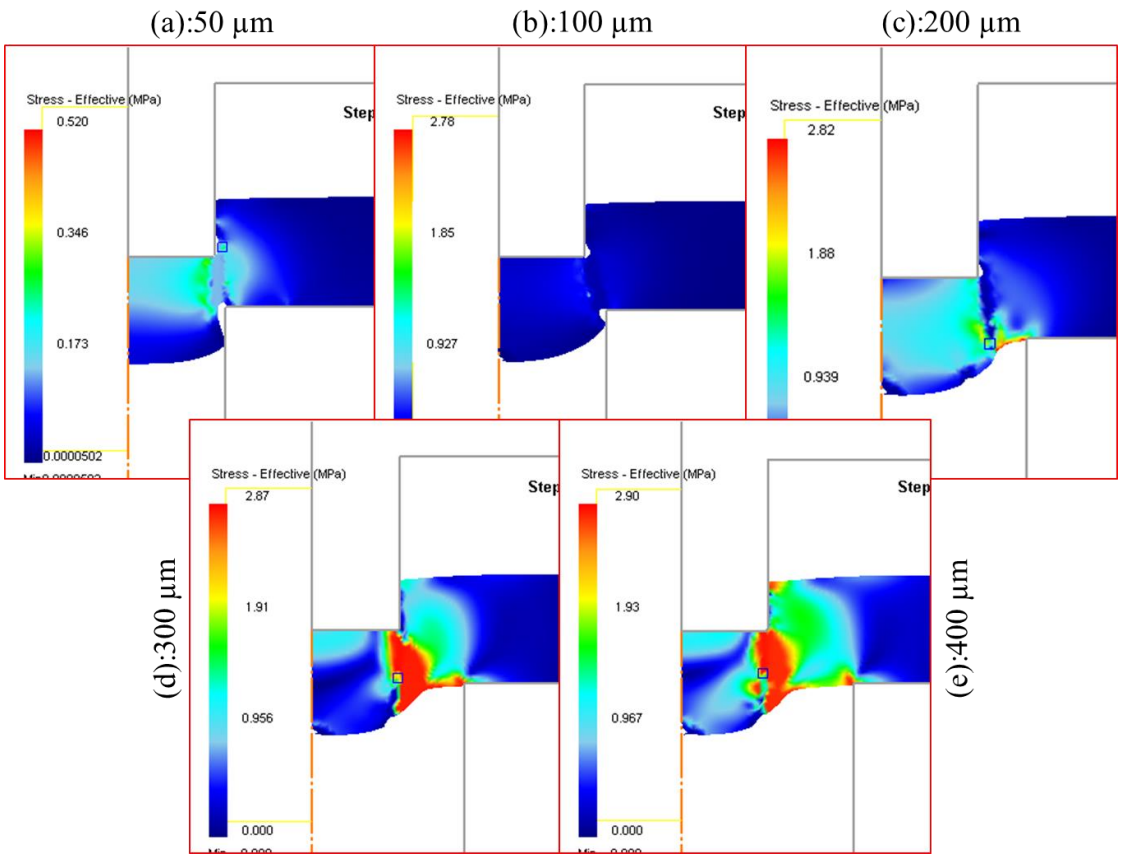

Figure 5.4. The evolution of effective stress at a die displacement of approximately 0.25 mm with clearances of (a) 50, (b) 100, (c) 200, (d) 300, and (e) 400 µm.

Figure 5.5 shows the model after the pin has displaced approximately 0.35 mm into the surface of the PMMA. With clearances of 50 (a), 100 (b), 200 (c), 300 (d), and 400 (e) µm, stress was predominant in the portions of the residual layer that contacted the pins and the portions of PMMA that were adjacent to the dies. These sections of PMMA were likely under tension since the substrate was displacing upwards and the movement of the residual layer was constrained by the pins (Achouri et al, 2014). In areas near the pin and die, fractures were predicted since the damage factors for clearances of 50, 100, and 200 µm ranged from 7 to 8, and for clearances of 300 and 400 µm the damage factors were 4 to 6. The through-hole fabricated with a clearance of 50 µm shows a long shear zone that

extended from the top diameter Its sidewall showed minimal tapering. The fracture for a 100 µm clearance was more significant as it caused the size of the relief to increase. For 200 µm a relief was generated on the sidewall. A long shear zone was also observed when clearance was 300 and 400 µm and no reliefs on the sidewall were observed.

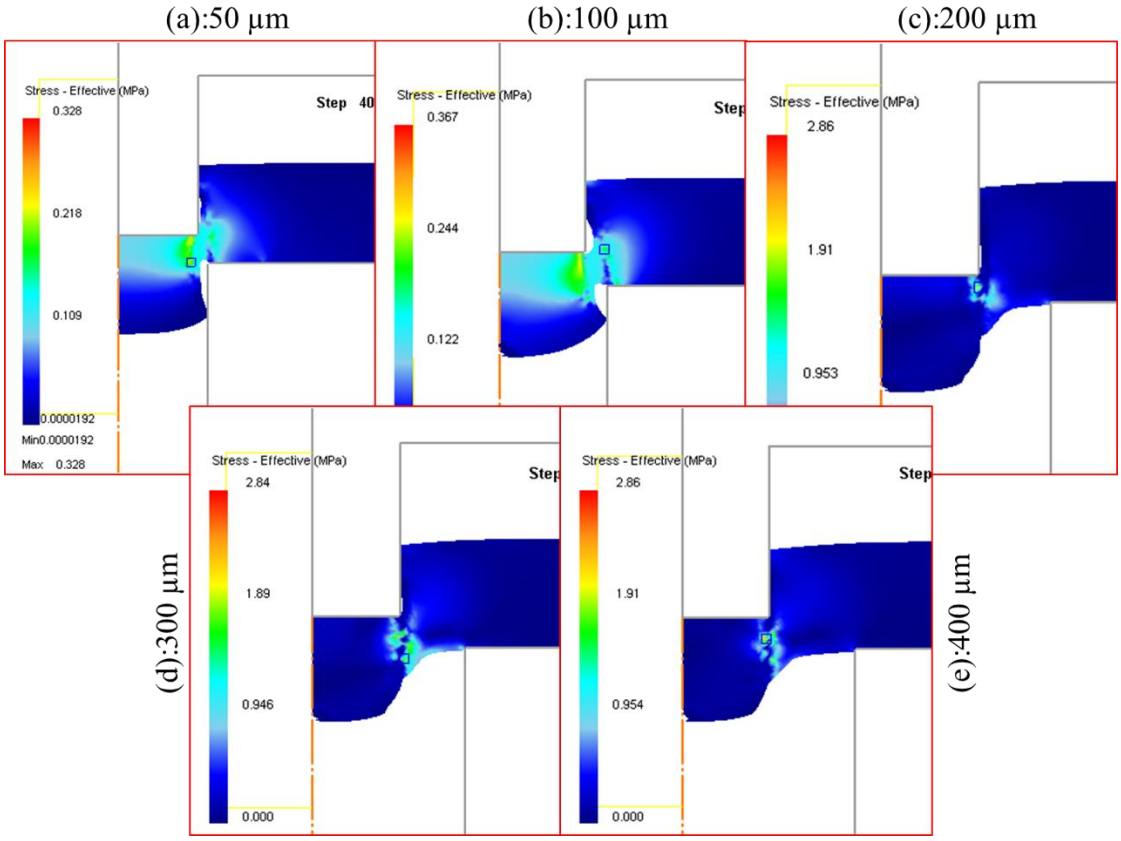

Figure 5.5. The evolution of effective stress at a die displacement of approximately 0.35 mm with clearances of (a) 50, (b) 100, (c) 200, (d) 300, and (e) 400 µm.

Figure 5.6 shows the models after the pin had displaced approximately 0.50 mm into the surface of the PMMA. With clearances of 50 (a), 100 (b), 200 (c), 300 (d) and 400 (e) µm, the residual layers were still intact and had not been separated from the substrate. Stress was predominantly in the fragments that connect the residual layer to the substrate. It was likely generated by tension. The diameters of the residual layers punched with

clearances of 50, 100 and 200 µm are not consistent over their lengths. The bottom portions of the residual layers extend outward and had a larger diameter which decreased when progressing to the top diameter.

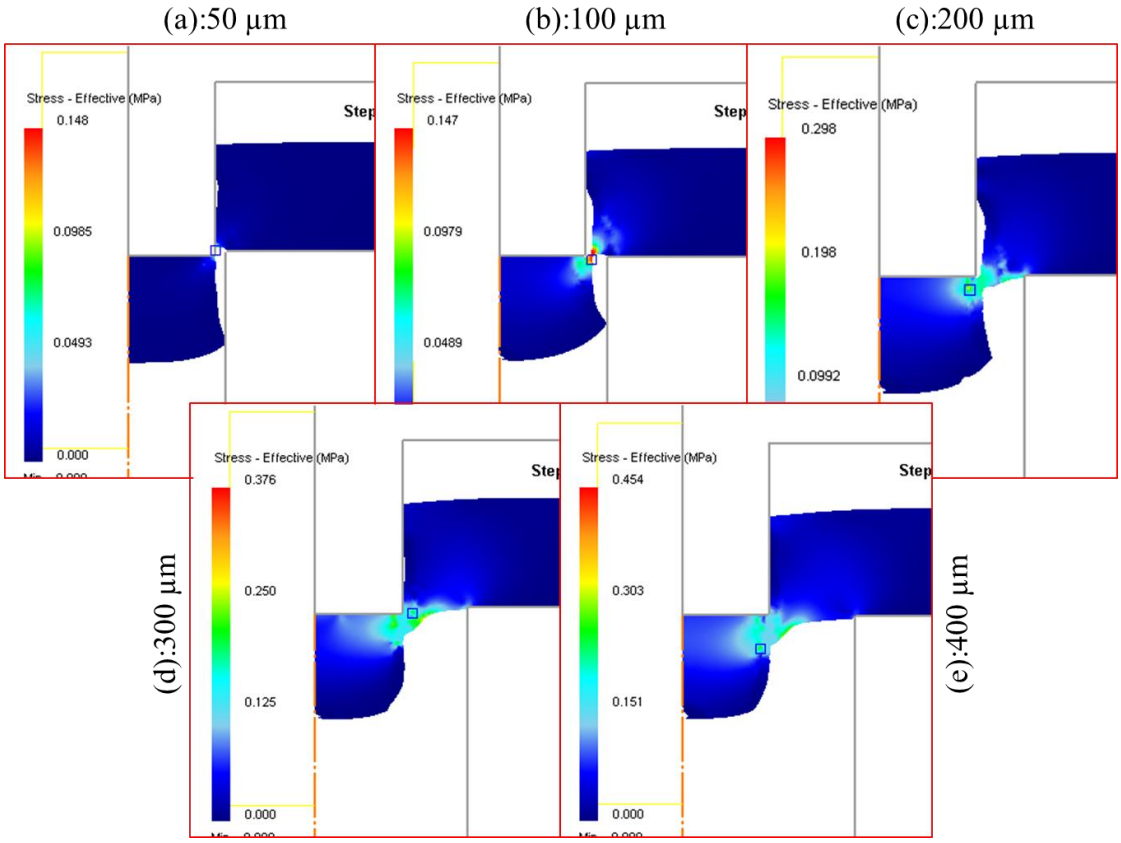

Figure 5.6. The evolution of effective stress at a die displacement of approximately 0.50 mm with clearances of (a) 50, (b) 100, (c) 200, (d) 300, and (e) 400 µm.

Figure 5.7 shows the model after the pins had displaced by 0.56 mm and exited the bottom surface of the substrate. For clearances of 50 and 100 µm, the residual layers were separated from the substrate and deleted by the software. The top diameter of both completed through-holes (Fig. 5.7(a) and (b)) are contacting the sidewall of the pin. As the substrate displaces vertically, friction is generated and spreads into the substrate material. This friction forces the PMMA to flex about the edge of the die. This explains why stress

is observed in the PMMA that is adjacent to the edge of the die. When clearance was 200 (c), 300 (d), and 400 (e) µm, the residual layer was still intact and connected to the substrate.

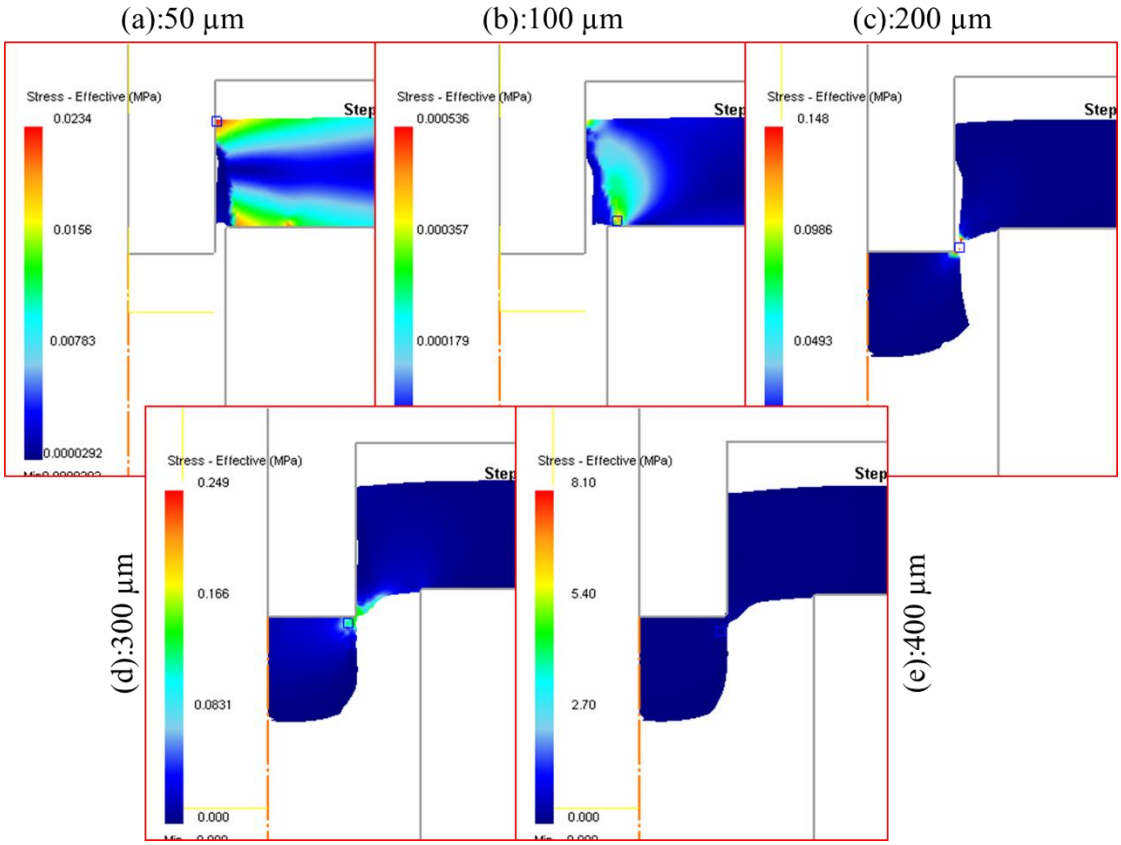

Figure 5.7. The evolution of effective stress at a die displacement of approximately 0.56 mm with clearances of (a) 50, (b) 100, (c) 200, (d) 300, and (e) 400 µm.

The fragment that connected the residual layer to the substrate material was still under tension. This tension caused the fragment to begin necking, where its cross section began to reduce in width. The damage in the necked part of the fragments ranged from 14 to 23.5, which indicated that fracture in these areas were predicted.

Figure 5.8 shows the models after the pins has displaced 0.8 mm and extended from the bottom surface by 0.3 mm. The residual layers were removed for the through-holes that

were punched with clearances of 200, 300, and 400 µm. The software deleted the elements that were fractured from the substrate. The displacement of the pins caused the PMMA to flex around the edges of the die.

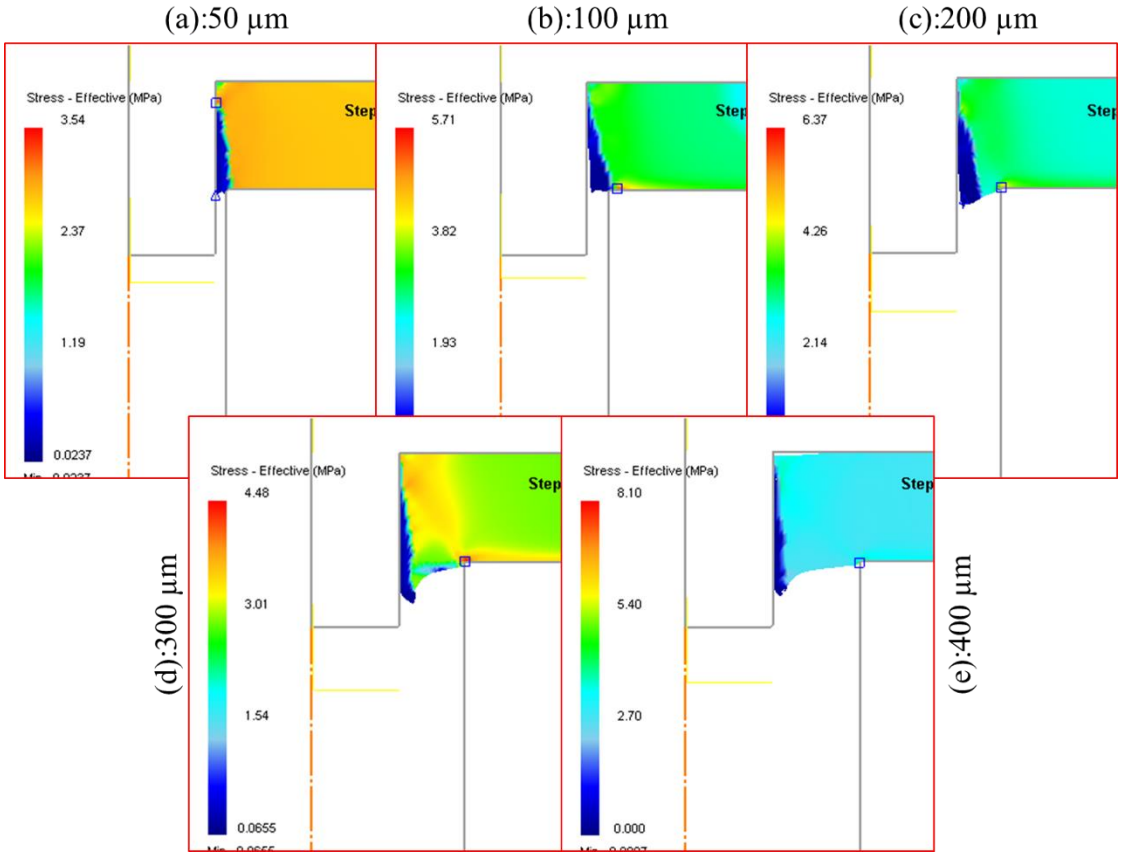

Figure 5.8. The evolution of effective stress at a die displacement of approximately 0.80 mm with clearances of (a) 50, (b) 100, (c) 200, (d) 300, and (e) 400 µm.

The surface area that surrounded the pins was in contact with the top surface of the PMMA. At this displacement the hot embossing process had begun. The substrate was being compressed in between both molds inserts as indicated by the generation of stress in the substrate. The compression then squeezed the PMMA which flowed into the clearance zones in between the sidewalls of the pins and dies. This created a sharp profile on the edge of the top diameter and consistent profile on the sidewall. In subsequent simulation steps

the substrate was further compressed by the displacement of the die. This caused the flow of the PMMA to continue and advance further into the dies.

5.6 Effect of Clearance

A significant observation from the model was the distribution of stress as the pins passed through the material. The stress was typically localized to the portions of PMMA that spanned the clearance zones. It transmitted outward and into the residual layers and the remaining substrate. When clearance increased, the width of the stress band also increased. The prediction of fracture also varied by the size of the clearance. The evolution of damage was tracked at two distinct points; point 1 was located at the edge of the pin and point 2 was located at the edge of the die as shown in Figure 5.9. Additionally, other state variables such as stress were recorded for all steps in the simulation for all clearances.

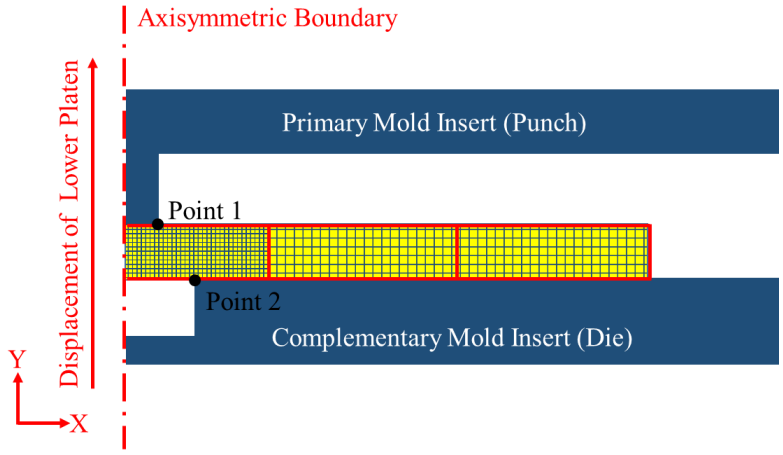

Figure 5.9. Location of point tracking in Deform-2D.

5.6.1 Evolution of Damage Factors and Effective Stress

Figure 5.10 showed the evolution of damage at point 1. It showed a stable increase in the calculated damage values for all clearances. This indicated that at all clearances, the displacement of the pin was able to generate a fracture which defined the top diameters of

the through-holes. The displacement needed to generate a fracture also increased as clearance was increased (Quazi and Shaikh, 2012). For example, with 50 and 400 µm, fracture was predicted at displacements of 0.17 and 0.32 mm, respectively. A positive relationship between clearance and the penetration needed to generate a facture was also observed by Achouri et al. (2014). The damage factor at point 1 eventually relaxed to 0 for all clearances. This indicated that the residual layer was separated and deleted by the software. Since it was deleted, no substrate material was at point 1 and no damage values were recorded.

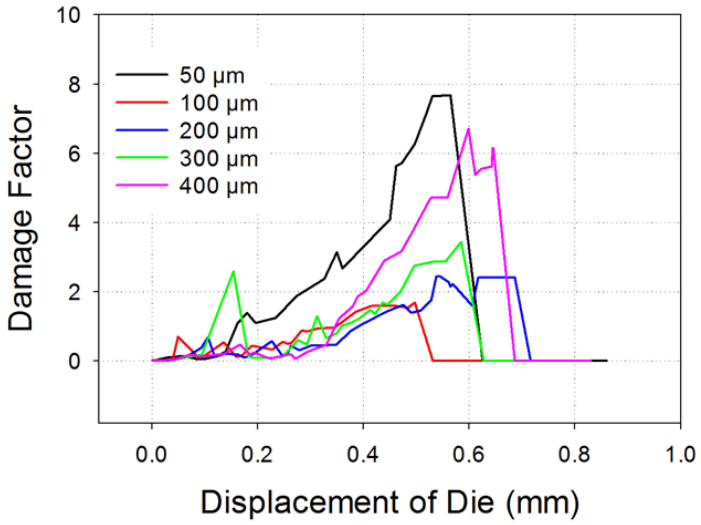

Figure 5.10. Tracking of the damage factor at the edge of the pin (point 1).

At point 2 only clearances of 50 and 100 µm displayed an evolution of damage as shown in Figure 5.11. These clearances generated fractures at approximate displacements of 0.13 and 0.22 mm, respectively. The damage factors created by the dies were relatively consistent which indicated that the dies propagated the fracture into the substrate. The fractures created by the die were able to converge with the fractures generated by their pins (Soderberg, 2006; Achouri et al., 2014). When clearances were 200 µm and above, the

damage values were approximately 0 until the dies had fully displaced. This indicated that the dies did not generate fractures on the bottom side of the substrate. The fractures that generated the bottom diameter of the through-holes were displaced from the dies. The damage that propagated after the full displacement was related to the application of the molding force. Point 2 did not have a relaxation in damage, since the hot embossing process caused PMMA to flow around the edges of the dies. Both graphs showed that when clearance was decreased, it localized the damage in areas adjacent to the edge of the pin and die. This would increase the probability of fractures being predicted in the models

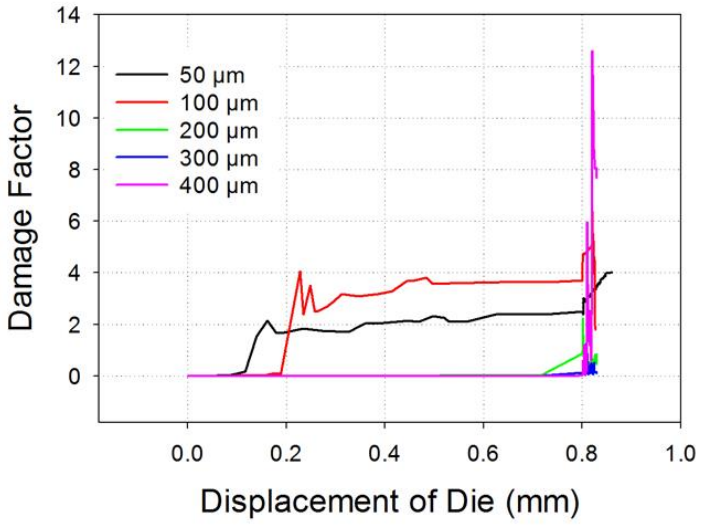

Figure 5.11. Tracking of the damage factor at edge of the die (point 2).

The evolution of effective stress at point 1 with respect to the displacement of the dies is seen in Figure 5.12. Effective stress is suitable to examine the behavior of a polymer at a temperature above its T_g and it is a criterion for the fracture of ductile materials. At point 1 it showed that the maximum stress was approximately 3 MPa which was consistent among the clearances. The magnitude of effective stress was not significantly affected by the size of the clearance. Point 1 shows stress relaxed to 0 MPa at varying displacements

for each level of clearance. This was caused by the deletion of the residual layer due to fracture and no polymer was contacting the edge of the pin (Kwak et al., 2002; Soderberg, 2006; Quazi and Shaikh, 2012). Since residual layers fractured at different displacements the relaxation points varied.

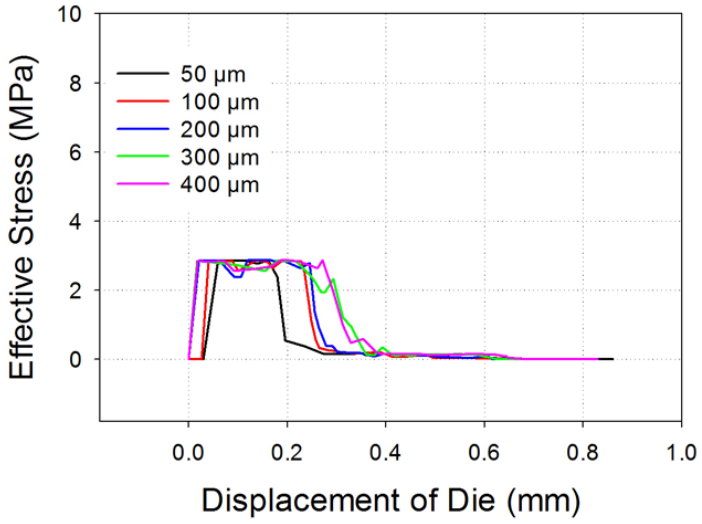

Figure 5.12. Tracking of the effective stress at the edge of the pin (point 1).

For point 2, the graphs show that stress relaxed for all levels of clearance as shown in Figure 5.13. For clearances of 50 and 100 µm the relaxation was related to the facture and deletion of the residual layer. When clearance was 200 µm and above, the stress caused at point 2 was related to the tension between the residual layer and substrate as seen in Figure 5.4 to Figure 5.5. When the residual layer was removed it relieved tension and caused stress to relax as seen in Figure 5.7. After a full displacement of the pin, point 2 showed a dramatic increase in effective stress.

This was a representation of the effect of hot embossing, where the PMMA was being compressed and flowing into the dies. As it flowed into the cavities it rubbed against the corners of the dies and generated stress. Clearance did not appear to influence the

magnitude of the effective stress, only its distribution. The stress was being generated by the movement of the dies and not the hot embossing process. As the die displaced more, it caused more PMMA to flow into the die and partially fill it.

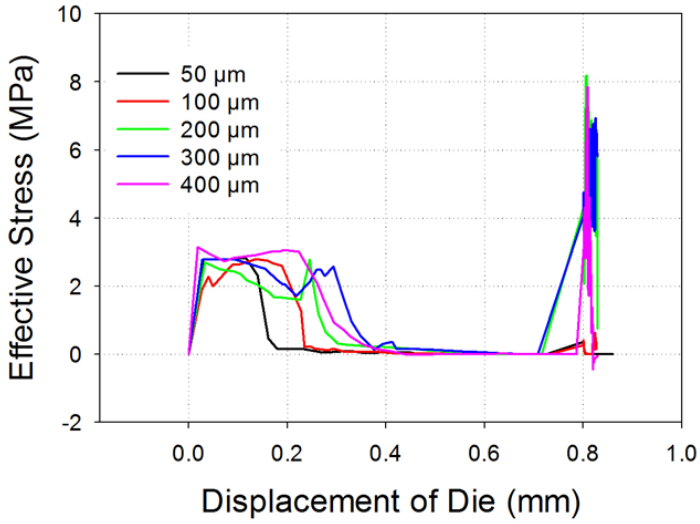

Figure 5.13. Tracking of the effective stress at edge of the die (point 2).

5.6.2 Dimensions of the Predicted Through-Holes

The dimensions of the numerically generated through-holes were compared to the average dimensions of the experimental through-holes. In the simulations, the hot embossing process affected the profiles of the top diameter and the sidewall. Therefore, measurements of the numerical through-holes were taken at the step after the residual layer was removed. An exact match was not expected but relationships between dimensions and clearances can be inferred and discussed.

Figure 5.14 compares the top diameters of the experimental through-holes to the simulated through-holes. The simulated through-holes were predicted to be significantly smaller and ranged from 0.800 to 0.806 mm. The top diameters of the experimental through-holes had a larger size and ranged from 0.820 to 0.840 mm. The top diameters

were relatively consistent over the clearances for both the simulations and experiments. This indicated that clearance did not have a significant effect on the size of the top diameter.

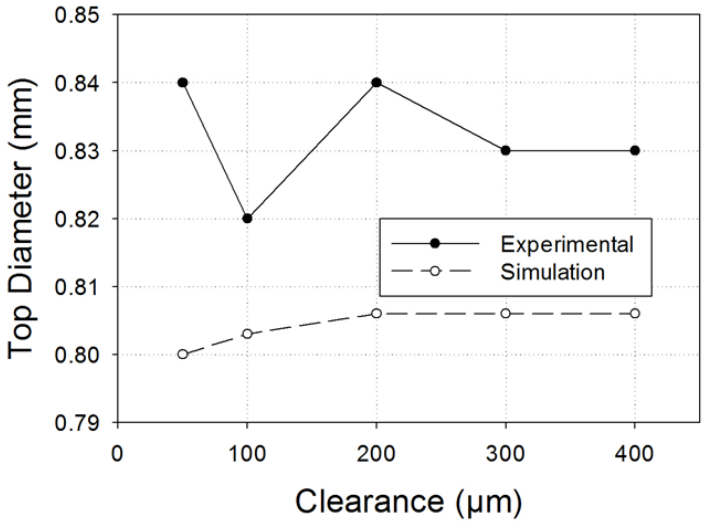

Figure 5.14. Comparison of the top diameter of the simulations and experiments.

Figure 5.15 compares the bottom diameter of the numerical and experimental through-holes. At 50 and 100 μm a slight trend was shown where the bottom diameter increased in size as the clearances was increased. For the simulation the bottom diameters increased from 0.94 to 1.05 mm when clearance was increased to 100 μm. The same behavior was seen in the experiments, the bottom diameter increased from 0.99 to 1.02 mm. This is a typical variation in mechanical punching (Joo et al., 2005, Chern et al. 2006; Rhim et al, 2006). When clearance was 200, 300 and 400 μm, there was slight agreement with respect to the size of bottom diameters. The experimental work showed that the bottom diameter ranged from 1.1 to 1.2 mm, the simulations predicted a smaller bottom diameter where the range was from 0.820 to 0.860 mm. The simulation and experiment agreed that the size of the bottom diameter was consistent with the three clearances. This indicates that the simulations and the experiments agreed that a single fracture occurred.

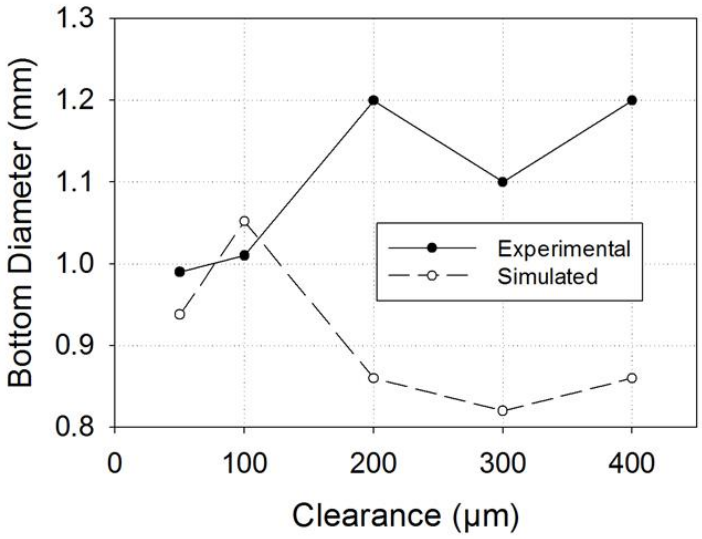

Figure 5.15. Comparison of the bottom diameter of the simulations and experiments.

Figure 5.16 compares the height of the rollover of the numerical and experimental through-holes. In the experimental values, a positive trend can be observed. The height of the rollover increased as higher clearances were used. When clearance was 50 µm the height was 0.990 and it increased to 1.20 mm when clearance was 400 µm. The simulations did not fully agree with this trend seen in the experiment. The simulation predicted smaller rollover values with a slightly positive increase in the size as clearance was increased (Kwak et al., 2002). Among the clearances it ranged only from 0.20 to 0.30 mm. When clearances were 200 µm and larger the dimensions of height ranged from 0.27 to 0.30 mm. At 50 and 100 µm the height was consistent at 0.20 mm.

Figure 5.17 compares the diameter of the rollover of the numerical and experimental through-holes. The diameters of the rollover increased from 1.1 to 1.8 mm in the experimental results. The simulations predicted a larger rollover diameter that increased from 1.40 mm to 2.06 mm when clearance was increased from 50 to 400 µm. Both the

experiments and simulations showed a similar trend. A positive relationship between rollover diameter and an increase in clearance was observed by Kwak et al. (2002).

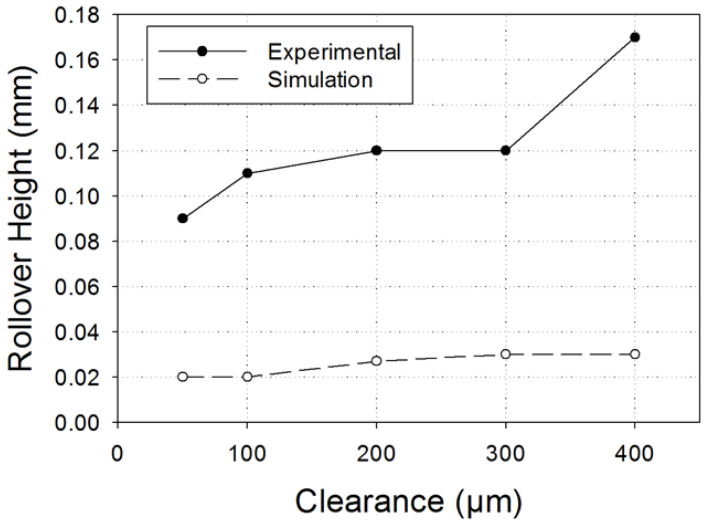

Figure 5.16. Comparison of the rollover height of the simulations and experiments

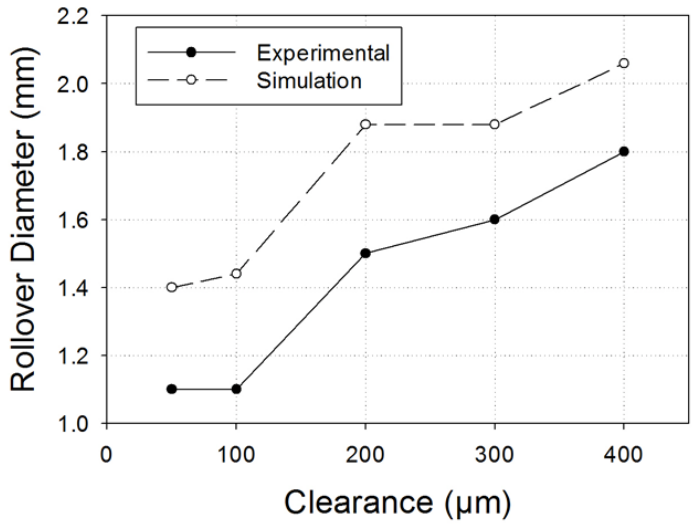

Figure 5.17. Comparison of the rollover diameter of the simulations and experiments.

5.6.3 Clearance of 50 μm

Figure 5.18 shows a comparison of the profiles of an experimental and numerical through-holes that were completed. The SEM images showed a more distinct rollover that

was present on the top diameter. The edge was more rounded, and its depth was more significant. On the numerical model the depth of the rollover was diminutive, and the edge appeared to be a sharp point with less rounding. In the simulation, the rollover transitioned into a burnish zone which was approximately 110 µm in length, the subsequent fracture zone was 370 µm long, with a bottom fracture length of 25 µm. The sidewalls of experimental and numerical through-holes were comparable. Both sidewalls showed a long shear zone that extended to the bottom diameter. The experimental profile had a burnish length of 132 µm, fracture length of 243 µm, and a bottom fracture length of 58 µm.

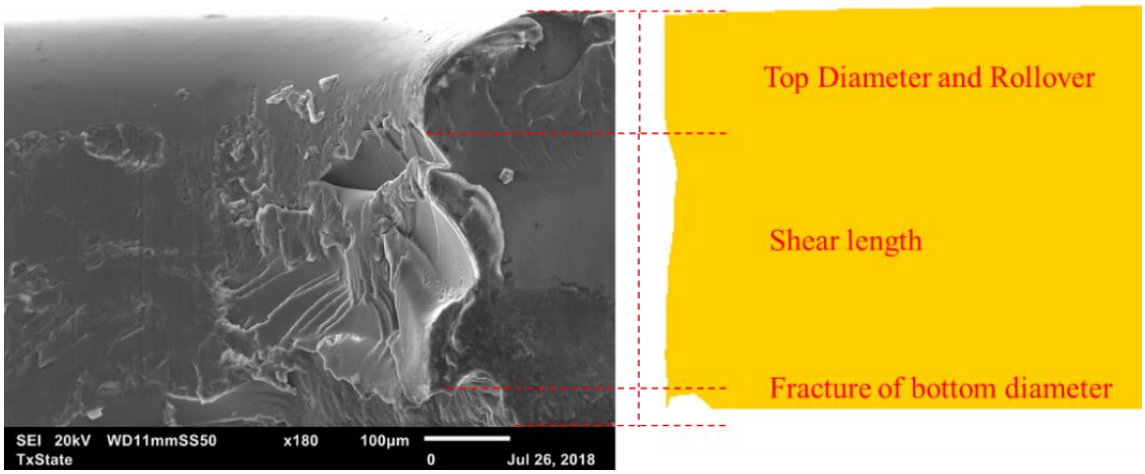

Figure 5.18. Profiles of an experimental through-hole compared to the profile of the numerically predicted through-hole fabricated with a clearance of 50 µm.

The formation of the bottom diameter was comparable between the simulation and the experiment. The location of the bottom diameter was displaced from the location of the top diameter. This was due to the fracture that generated the edge of the bottom diameter extending into the substrate. The simulation reaffirmed that the fracture was generated in the proximity of the edge of the die (Soderberg et al., 2006; Achouri et al., 2014).

5.6.4 Clearance of 100 µm

Figure 5.19 compares the profile of through-holes that were produced experimentally and numerically. Both the numerical and experimental through-holes were generated with a clearance of 100 um. The presence of the rollover was observed in the profiles of the numerical and experimental through-holes. In the simulation, the rollover was less distinct, and the edge of the top diameter had a sharp profile. The simulation showed that the burnish zone transitioned into the fracture zone which extended to the bottom diameter. In the simulation, the rollover transitioned into a burnish zone which was approximately 160 µm in length. The subsequent fracture zone was 310 µm long and had a bottom fracture length of 25 µm. The fracture generated a relief of the sidewall and increased the diameter of the through-hole.

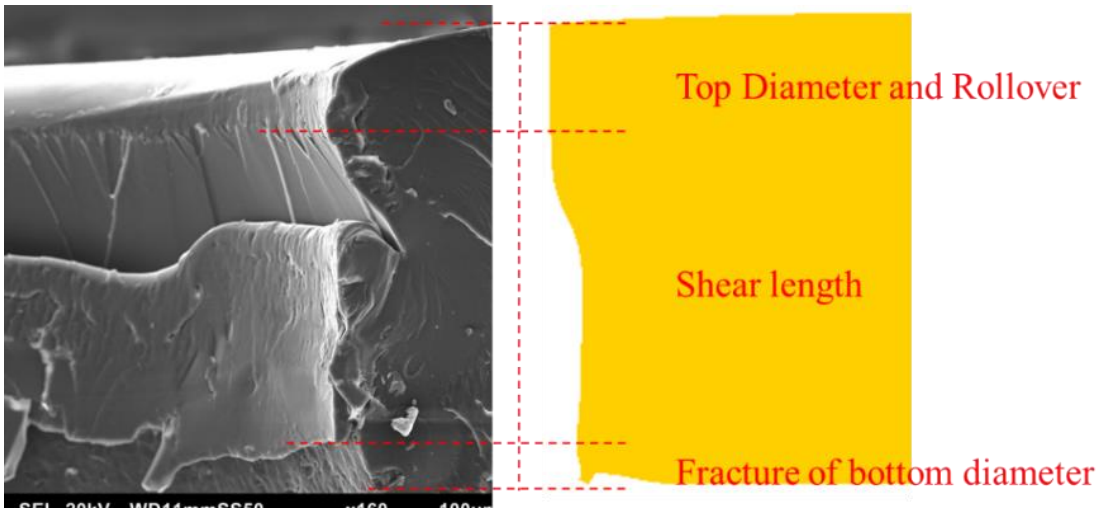

Figure 5.19. Profiles of an experimental through-hole compared to the profile of the numerically predicted through-hole fabricated with a clearance of 100 µm.

The experimental results showed a less consistent sidewall because a delamination occurred. The experimental profile had a burnish length of 73 µm, fracture length of 325 µm, and a bottom fracture length of 75 µm. Aside from the delamination, the size of the

diameter was relatively consistent where a relief was not generated. The simulation and the experimental model agree that when the bottom of the residual layer was fractured it extended into substrate.

Figure 5.20 compares the profiles of the residual layer of an experiment and the residual layer of the numerical model. Both results showed the effect of the impact of the pin which forced the PMMA to flow into the die. As it flowed into the die it generated a round profile on the bottom of the residual layer. The diameters of the residual layers are inconsistent, they increased when progressing from the top to the bottom portion. Both the experiment and simulation show agreement that the residual layer was separated from the substrate by two different fractures. One fracture generated the top diameter and the second fracture generated the bottom diameter.

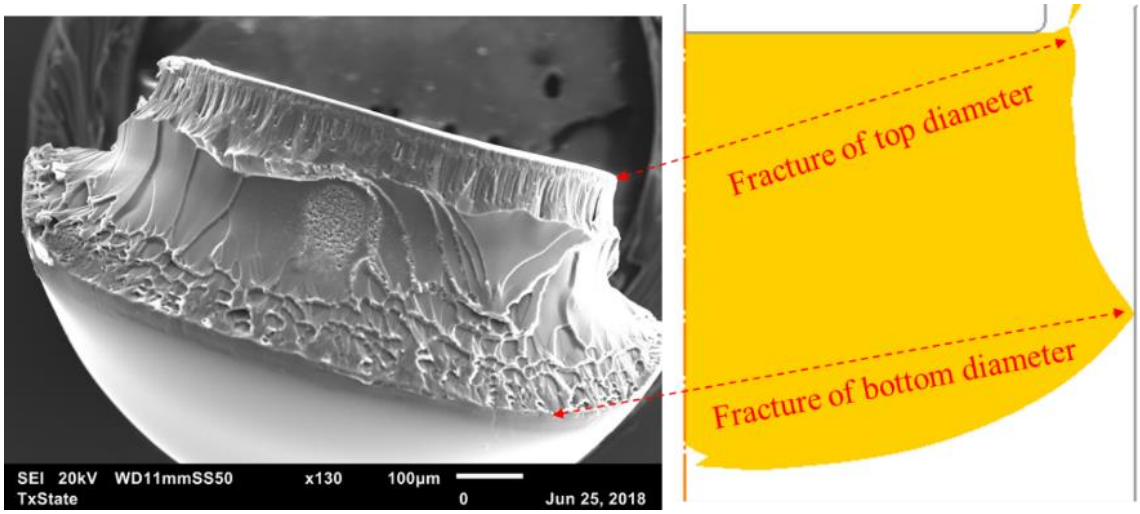

Figure 5.20. Profiles of an experimental residual layer compared to the profile of the numerically predicted residual layer fabricated with a clearance of 100 µm.

5.6.5 Clearance of 200, 300, 400 µm

The numerical models predicted that a through-hole could be generated even when clearance was increased beyond 100 µm. However, the experimental results for clearances

of 200, 300, and 400 µm were limited, where only 19 partial through-holes were generated. Experiments showed that the bottom diameter significantly increased and varied from the top diameter. Imaging showed that the through-holes were generated with a single fracture that progressed from the top to the bottom of the substrate. This fracture caused the sidewall to taper outward which increased the bottom diameter of the through-hole. On completed through-holes the average bottom diameter for all clearances was approximately 1200 µm.

Figure 5.21 compares the top and bottom diameters of an experimental through-hole to the profile of a numerically generated through-hole. The through-holes were produced with a clearance of 400 µm. Both show that the top diameter was uniform, and it was surrounded by the rollover.

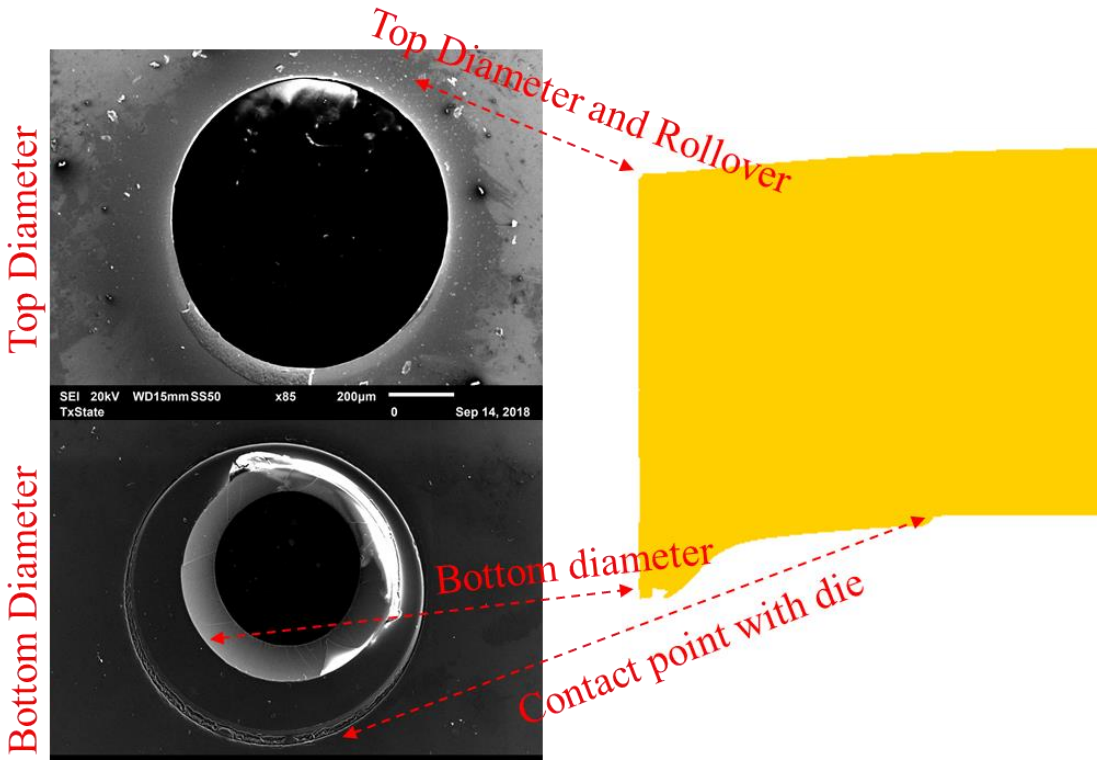

Figure 5.21. Comparison of the top and bottom diameter of an experiment through-hole to the profile of a numerically predicted through-hole that was generated with a clearance of 400 µm.

The simulation showed a long shear zone that extended 460 µm, a top diameter of 802 µm, and a bottom diameter of 850 µm but showed no burnish zone. The simulation agreed that a single fracture traveled from the top of the substrate to the bottom side and removed the residual layer. A contrast between the numerical model and experimental results was the size of the bottom diameter and the profile of the sidewall. The experimental through-hole had a top diameter of 840 µm, a bottom diameter of 1200 µm, a burnish zone of 105 µm and the length of the shear zone was 220 µm. The sidewall of the experimental through-hole had a taper and was not linear like the sidewall of the simulation. This was attributed to the difference in the propagation of the fracture of the residual layer.

5.7 Conclusion

The simulation predicted a complete through-hole could be fabricated at all levels of prescribed clearances. It also predicted that the residual layers were removed before the hot embossing process became dominant. They varied with respect to the generation of the fractures that generated the through-hole. For clearances of 50 and 100 µm it predicted that both the pin and the die generated a fracture. Therefore, the bottom diameter of the through-hole was related to the size of the respective die. When clearance was increased, it showed that only the pin generated a fracture. This fracture started at the top of the substrate and propagated to the to bottom surface of the substrate.

When comparing the experiment to the numerical models, it was observed that the simulation overestimated the effects of the hot embossing process. The simulations predicted that the compressive force would cause the PMMA to flow into the pin and generate a top diameter with a sharp profile. It also predicted that PMMA from the substrate

would flow into the die and partially fill the cavity. By comparison, the experiments showed that hot embossing had minimal effects on the edge quality of the through-holes.

6. CONCLUSIONS AND FUTURE WORK

6.1 Conclusions

The fabrication of microfluidic interconnection through a micro-mechanical punching process was investigated. Passive alignment was used to align two complementing mold inserts in a double-sided hot embossing. Features for micro-mechanical punching were integrated with the double-sided hot embossing process and through-holes could be generated. Through-holes could be reproduced by the incorporation of the two micro-forming processes. The through-holes were characterized to determine the effect of clearances and infer the behavior of the PMMA. Numerical simulations were used to study the behavior of the PMMA during a punching step. Micro-mechanical punching via double-sided hot embossing shows potential for creating microfluidic interconnection structures. This work can be used as a groundwork to optimize the micro-mechanical punching process on thermoplastic polymers.

6.1.1 Passive Alignment for Double-Sided Molding

A classic design for a kinematic coupling was modified to allow its joints to be detachable. This design was integrated to two complementing mold inserts for double-sided hot embossing. Experimental setup could be assembled in a short period of time, their subsequent alignment was accurate and precise. This allowed the primary mold insert to be mounted to the thermal press with minimal steps, no machine vision, and no adjustments to its relative location. However, mounting the primary mold insert to the thermal press created an under-constrained assembly. This meant motions could have occurred before or during the embossing step. This was represented by the misalignment that was observed in the experimental results.

6.1.2 Micro-Mechanical Punching

The two mold inserts were applied to micro-mechanically punch through-holes on a PMMA substrate. This experiment replicated complete, partially complete, and incomplete through-holes. The through-holes were characterized to determine their dimensional quality and observe the effect of the selected clearance values.

The success of micro-mechanically punching a substrate of thermoplastic polymer was significantly dependent on the selection of clearance. When clearance was 50 and 100 μm the success rate of producing a partial or complete through-holes was 100%. Through-holes punched with a clearance of 50 μm showed a consistent sidewall while through-holes punched with a clearance of 100 μm showed more defects on the sidewall. At clearances 200 μm and above the PMMA behaved differently and punching was less successful. The main difference was the generation of a single fracture by the pins. A partial through-hole could only be completed if the fracture could travel to the bottom of the substrate.

6.1.3 Numerical Models of Micro-Mechanical Punching

The numerical simulations showed that clearance had a significant effect on the behavior of the PMMA during processing. The simulations were able to reasonably predict the fracture that occurred during fabrication. The numerical analysis showed that two fractures could generate and converge at clearances of 50 and 100 μm. It was also observed that the size of the bottom diameter correlated to the size of the die. When clearance was above 200 μm or above, the model only predicted one fracture. This fracture initiated at the top and propagated to the bottom of the substrate.

The profile of the sidewall were affected by the increased molding pressure as seen in the simulations. The molding pressure also caused PMMA to flow into and fill the die

cavity. The experimental results did not fully agree with the numerical analysis as rollover was observed and no significant flow of polymer was seen.

6.2 Future Work

6.2.1 Further Study of the Alignment Process

The proposed alignment system has potential and should be further developed for more robust application. The mechanical joints that were designed were presumed to provide a kinematically constrained assembly. This was concluded by observing the assembly of the two mold inserts. It is recommended that constraint and motion of the proposed mold inserts be analyzed mathematically. A limitation of the alignment process was the detachment of the primary mold insert from the vacuum platen. This meant the primary mold insert had to be realigned and remounted before each micro-punching trial. An improvement would be to redesign the bolting holes. This could allow the primary mold insert to be fastened to the vacuum platen. This could improve the repeatability of the experiments and be beneficial for double-sided molding applications.

6.2.2 Further Development of Micro-Mechanical Punching

In this study the process parameters were limited to one set of values. This allowed for the characterization of the behavior of PMMA. It would be valuable to increase the breadth of the process parameters and equipment design to move towards a parametric study. This would allow for the optimization of certain design factors such as pin size, pin geometries, die sizes, and thermal press conditions. For examples, clearances between 50 and 100 μm were the most successful, it would be a helpful to determine the optimal clearance value. A process to remove the attached residual layers could be useful for more successful micro-mechanical punching with non-optimal clearances.

6.2.3 Expanding Numerical Modeling

The numerical models provided reliable insights into the behavior of PMMA during punching. However, the simulations considered an ideal condition where misalignment was not present. This meant that the clearance was always assumed to be consistent at all points on the circumference. It would be beneficial to move from an axisymmetric model to a plane stress model. The misalignment between the pin and the die to can be modeled which would generate a more informative simulation model. Additionally, the effects of cooling and demolding could also be investigated.

APPENDIX SECTION

APPENDIX A PERFORMANCE OF THE MEASURESCOPE

The performance of the measurescope was determined and represented by the accuracy and precision. A gauge block (Mitutoyo Corp., Kawasaki, Japan) with a length of 2 inches were measured. The length was measured in the X- and Y-Axis nine times with a magnification of 20x10. The gauge block was left in the same position for all nine measurements and both directions.

Table A.1. Performance of measurescope

	X-Axis (in)	Y-Axis (in)
Maximum Value	2.00028	2.00011
Minimum Value	2.00008	1.99983
Mean Value	2.0005	1.99973
Standard Deviation	0.00006	0.0001
95% Confidence interval	± 0.0006	± 0.0001

Table A.2. Magnifications of measurescope

Available magnifications
2.5x10
5x10
10x10
20x10

REFERENCES

Achouri M., Germain G., Dal Santo P., Saidane D. 2017. Experimental and numerical analysis of micromechanical damage in the punching process high-stress low-alloy steel. *Material and Design.* 56 657-670.

Agrawal S., Patidar D., Dixit M., Sharma K., Saxena N.S. 2010. Investigation of thermo-mecchanical properties of PMMA. *Nat. Con. Of Thermophysical Properties.* 09 79-82.

Arlon Electronic Materials. 2012. Drilling defects: causes and solutions Retrieved from URL.http://www.arlonemd.com/wp-content/uploads/2016/05/Drilling-Defects-Causes-and-Solutions-v1.1-2016.pdf.

Biermann D., Heilmann G. 2009. Burr minimization strategies in machining operations. *Proceedings of the CIRP International Conference on Burr.s* 2nd-3rd 13-20.

Bobak M., Agarwal M., Torisawa YS., Takayama S. 2010. Simultaneous fabrication of PDMS through-holes for three-dimensional microfluidic alications. *Lab on a Chip.* 10 1983-1986.

Bowden P.B., Jukes J.A. 1972. The plastic flow of isotropic polymers. *Journals of Materials Science.* 7(1) 52-63.

Bottger G., Schroder H. Jordan R. 2013. Active or passive fiber-chip-alignment: approaches to efficient solutions. *Proceedings of SPIE.* 8630 863006-1-17.

Chen Y., Zhang L., Chen G. 2008. Fabrication, modification, and application of poly (methyl methacrylate) microfluidic chips. *Electrophoresis.* 42 1801-1814.

Chern G.L., Engin Y.J., Liu S.F. 2006. Development of a micro-punching machine and study on the influence of vibration machining in micro-EDM. *J. of Mat. Proc. Tech.* 125-126, 102-109.

Chou J., Du N., Floriano P., Christodoulides N., McDevitt J. 2012. Hot embossing polyethylene through-hole chips for bead based microfluidic devices. *Biosens. Bielectron.* 42 653-660.

Chowdhury M.K., Sun L. Cunningham S., Malshe A. 2010. Investigation of chemical de-burring and subsequent plasma cleaning of mechanically punched micro via array fabricated in LCP substrate. *Electronic Components and Technology Conference.* 2010 998-1003.

Comaneci R., Zharia L., Chelariu R., 2011. Damaging prediction of difficult-to-work aluminum alloys during equal channel angular pressing. *J. Mat. Eng. Per.* 21(3) 287-291.

Conner G., Song I.H., Park T., You B.H. 2014. Method of mold alignment for double-sided hot embossing of micro fluidic devices using kinematic constraints. *Micro & Nano Letters.* 9 741-745.

DeGarmo E. P., Black, J. T., Kohser R. A. 2012. Materials and processes in manufacturing. New York: Macmillan Pub. Co.

Dyer P.E., Srinivasan R., 1986. Nanosecond photoacoustic studies on ultraviolet laser ablation of organic polymers. *A. Phys. Lett.* 48(6) 445-447.

Eriksson M., Goossens H., Peijs T. 2015. Influence of drying procedure on glass transition temperature of PMMA based nanocomposites. *Nanocomposites.* 8 36-45.

Evonik Industries. 2009. Machining plexiglass® guidelines for workshop practice manual.

Faura F., Garcia A., Esterms M. 1998. Finite element analysis of optimum clearance in the blanking process. *Journal of Materials Processing Technology.* 80-81 121-125.

Florian J. 1996. Practical thermoforming principles and applications. 2nd ed 319-360.

Ghatak A., Dupaix R. 2010. Material characterization and continuum modeling of poly (methyl methacrylate) (PMMA) above the glass transition. *Intl. J. Structural Changes in Solids.* 1 53-63.

Gomez J. 2015. Fabrication of through-holes for the interconnections of polymer microfluidic devices. Doctoral Dissertation Texas State University, San Marcos, TX.

Gurung. 2007. Passive alignment of micro-fluidic chips using the principle of elastic averaging. Master Dissertation Louisiana State University, Baton Rouge, LA.

Hart A.J., Slocum A., Willoughby P. 2004. Kinematic coupling interchangeability. *Precision Engineering.* 28(1) 1-15.

He Y., Fu J.Z., Chen Z.C. 2007. Research on optimization of the hot embossing process. *J. Micromech. Microeng.* 17 2420-2425.

Heckele M., Bacher W., Muller K.D. 1998. Hot embossing – the molding technique for plastic microstructures. *Microsystems Technologies.* 4 122-124.

Henann D.L., Srivasta V., Taylor H.K., Hale M.R., Hardt D.E., Anand, L. 2009. Metallic glasses: viable tool materials for the production of surface microstructures in amorphous polymers by micro-hot-embossing. *J. Micromechanics and Microengineering.* 19(11) 1-10.

Horng RH., Han P., Chen H.Y., Lin K.W., Tsai T.M., Zen J.M. 2005. PMMA-based capillary electrophoresis electrochemical detection microchip fabrication. *J. Micromech. Microeng*. 15 6-10.

Huang, E. S., O'Grady M., Basu A., Winn A., John P. Lee J. 2010. The juvenile diabetes research foundation continuous glucose monitoring study group. the cost-effectiveness of continuous glucose monitoring in type 1 diabetes. *Diabetes Care*. 33(6), 1269–1274.

Islam R., Wieder B., Lindner P., Glinser S., C. 2002. One micron precision optically aligned method for hot Eembossing and nanoimprinting. *Proceedings of IEEE Sensors.* 2 931-935.

Juang Y.J., Lee L.J., and Koelling K. 2002. Hot Embossing in microfabrication. part I: experimental polymer. *Engineering and Science.* 42 539-550.

Juang Y.J., Lee L.J., and Koelling K. 2002. Hot embossing in microfabrication. part II: rheological characterization and process analysis polymer. *Eng. and Sci.* 42 551-566.

Karioja P., Ollila J., Putila V.P., Keranen K., Hakkila J. Kopola H. 2000. Comparison of active and passive fiber alignment techniques for multimode laser pigtailing. *2000 Proceedings. 50th Electronic Components and Technology Conference. 244*-249.

Kalpakjian S. 2014. *Manufacturing engineering and technology*. Reading, Mass: Addison Wesley.

Kiew C.M., Lin W.J., Teo T.J., Tan J.L., Lin W., Yang G. 2009. Finite element analysis of PMMA pattern formation during hot embossing process. *IEEE/ASME Intl. Con. On Adv. Intelligent Mechatronics.* 314-317.

Kim J.T., Yoon B.Y., Choi C.G. 2004. Passive alignment method of polymer PLC devices by using a hot embossing technique. *IEEE Photonics Technology Letters.* 16 1664-1666.

Kurtz S., Foulds J., Jewett C., Srivastas S., Edidin A. 1997. Validation of a small punch testing technique to characterize the mechanical behavior of ultra-high-molecular-weight polyethylene. *Biomaterials.* 16 1659-1663.

Kuppan P., Narayanan R., Oyyaravelu R., Balan A., Ballan S.A. 2016. Performance evaluation of electrode materials in electric discharge deep hole drilling of inconel 718 superalloy. *Procedia Engineering.* 174 53-59.

Kwak T.S., Kim Y.J., Bae W.B. 2002. Finite elements analysis on the effect of die clearance on shear planes in fine blanking. *J. Mat. Proc. Tech.* 130-131 462-468.

Joo B.Y., Oh S.I., and Jeon B.H. 2001. Development of micro punching system. *CIRP Annual.* 50 191-4.

Joo B.Y., Rhim S.H., Oh S.I. 2005. Micro-hole fabrication by mechanical punching process. *Journal of Materials Processing Technology*. 170 593-601.

Lay D. Stade E. 2003 Linear algebra and its applications 3rd ed.

Liu X., Mwangi M., Li X.J., O'Brien M., Whitesides G. 2011. Paper-based piezoresistive MEMS sensors. *Lab on a Chip.* 11 2189-2196.

Mazzeo A., Dirckx M., Hardt D., 2007. Single-step through-hole punching by hot embossing. *ANTEC 2007.* 2977-2981.

Mahesh J.U. Chapter 4 finite modeling and simulation.

Mathur A., Roy S.S., Tweedie M., Mukhopadhyay S., Mitra S.K., McLaughlin J.A. 2009. Characterization of PMMA microfluidic channels and devices fabricated by hot embossing and sealed by direct bonding. *Current Applied Physics.* 9 119-1202.

Mirghasemi S.M., Eivani A.R., Seyedein S.H., Jafarian H.R. 2018. A comparison between routine vs. normalized Cockroft-Latham fracture criteria for prediction of fracture during equal channel angular pressing. *Eng. Frac. Mech.* 199 721-729.

Mohammadi M., Davoodi J., Javanbakht M., Rezaei H. 2017 Glass transition temperature of PMMA/modified alumina nanocomposite: molecular dynamic study *Materials Science.* 1-11.

Pan C.T., Wu T.T., Chen M.F., Chang Y.C., Lee C.J., Huang J.C. 2008. Hot embossing of micro-lens array on bulk metal glass. *Sensors and Actuators.* 141 422-431.

Peng L., Deng Y., Yi P., Lai X. 2014 Micro hot embossing of thermoplastic polymers: a review. *J. Micromech. Microeng.* 24 013001.

Petersen R., Mashid R., Andersen N., Keller S., Hansen H., Boisen A. 2015. Hot embossing and mechanical punching of biodegradable microcontainers for oral drug delivery. *Microelectronic Engineering.* 133 104-109.

Puntambekar A., Ahn C.H. 2002. Self-aligning microfluidic interconnects for glass- and plastic-based microfluidic systems. *Journal of Micromechanics and Microengineering.* 12 35-40.

Quazi T.Z., Shaikh R.S., 2012. An overview of clearance optimization in sheet metal blanking process. *Intl. J. Modern Eng. Res.* 2(6) 4547-4558.

Reynaerts D., Heere P.H., Van Brussel H. 1997. Microstructuring of silicon by electro-discharge machining (EDM) — part I: theory. *Sensors and Actuators.* 60 212-218.

Rani, S., Park, T., You, B., Soper, S., Murphy, M., & Nikitopoulos, D. 2010. Numerical Simulations of Misalignment Effects in Microfluidic Interconnects. *MRS Proceedings*. 1272, 1272-KK09-04.

Rhim S.H., Oh S.I., Jeon B.H. 2001. Development of micro punching system *CRIP Annals* 50(1) 191-194.

Rhim S.H., Son Y.K., Oh S.I. 2005. Punching of ultra-small size hole array *CRIP Annals* 54(1) 261-264.

Rossen S.G. 2008. An analysis of through-hole punching in PMMA with varied process parameters Undergraduate Thesis Massachusetts Institute of Technology, Cambridge, MA.

Scientific Thermal Forming Company (STFC) 2014 DEFORM-2D manual.

Schnabl M. 2010. Deburring machine for round billets – equipment for efficient removal of burrs from billets. *Proceedings of the CIRP International Conference on Burrs.* 2nd-3rd 221-226.

Shan X., Maeda R., Murakoshi Y. 2003. Micro Hot Embossing Replication of Microstructures. *Japanese J. of Alied Physics.* 3859-3862.

Slocum A.H., 2003. Kinematic couplings: a review of design principles and applications. *Journal of Microelectromechanical Systems*. 12, no. 6, 1-35.

Slocum A.H., Braunstein D. 1999. Kinematic coupling system for thin plates and sheets and the like U.S. Patent. 5,915,678 issued Jun. 29, 1999.

Soderberg M. 2006. Finite element simulation of punching Master Dissertation Lulea University of Technology, Lulea, Sweden.

Subramonian S., Atlan T. Ciocirlan B., Campbell C. 2013. Optimum selection of variable punch-die clearance to improve tool life in blanking non-symmetric shapes. *Intl. J. of Mach. Tools & Manu.* 75 63-71.

Spence-Parson A. 2006. The formula for successful punching manual.

Tahk D. Paik S.M. Lim J. Bang S. Oh S. Ryu H. Jeon N.L. 2017. Rapid large area fabrication of multiscale through-hole membranes. *Lab on a Chip.* 11 1817-1825.

Trinkle C., Lee L. 2011. High-precision microcontact printing of interchangeable stamps using kinematic coupling. *Lab on a Chip.* 17 455-459.

Wang G., Folk E., Barlow F., Elshabini A. 2006. Fabrication of microvias for multilayer LTCC substrates. *IEEE Transactions on Electronics Packaging Manufacturing*. 29 32-21.

Weinhold M., Powell D. 1996. High speed laser ablation of microbial holes in non-woven aramid reinforced printed wiring boards to reduce cost. *Circuit World.* 22(3) 16-22.

Werner J. 2005 Hot Embossing of Through-holes in cyclo-olefin copolymer (TOPAS®) *Diploma Thesis* University of Allied Sciences Oldenburg.

Wu C.H., Hung C.H., Hu Y.Z. 2009. Parametric study hot embossing on micro-holes. *Advanced materials Research.* 74 251-254.

Xiong Y. Shafer S.A. 1993. Depth from focusing and defocusing. *IEEE* 68-73.

Xu J., Guo B., Shan D., Wang C., Li J., Liu Y., Qu D. 2012. Development of a micro-forming system for micro-punching process of micro-hole arrays in brass foil. *J. of Mat. Proc. Tech.* 212(11) 2238-2246.

Yi S.M., Joo B.M., Park M.S., Chu C.N. Oh S.I. 2006. Mechanical punching of 15μm size hole. *Microsystem Technologies.* 12 877-882.

You B.H., Chen P.C., Park D.S., Park S., Nikitopoulos D.E., Soper S., Murphy M 2009. Passive micro-assembly of modular embossed, polymer microfluidic devices using exact constraint design. *J. Micromech. Microeng.* 19 1-11.

Yuen P.K. 2008. SmartBuild–A truly plug-n-play modular microfluidic system. *Lab on a Chip* 8 1374-1378.

Zhu X., Cui T. 2011. Fabrication of polymer via holes by a combination of hot embossing and indentation processes. *J. Micromech. Microeng.* 21 045032.